Adaptive Second-Order Fast Nonsingular Terminal Sliding Mode Tracking Control for Fully Actuated Autonomous Underwater Vehicles

Lei Qiao and Weidong Zhang, *Senior Member, IEEE*

***Abstract*—This paper focuses on the design of an adaptive second-order fast nonsingular terminal sliding mode control (ASOFNTSMC) scheme for the trajectory tracking of fully actuated autonomous underwater vehicles (AUVs) in the presence of dynamic uncertainties and time-varying external disturbances. First, a second-order fast nonsingular terminal sliding mode (SOFNTSM) manifold is designed to achieve a faster convergence rate than the existing second-order nonsingular terminal sliding mode (SONTSM) manifold. Then, by using this SOFNTSM manifold, an ASOFNTSMC scheme is developed for the fully actuated AUVs to track the desired trajectory. The designed SOFNTSM manifold yields local exponential convergence of the position and attitude tracking errors to zero, and the developed ASOFNTSMC scheme ensures that the error trajectories always move toward the SOFNTSM manifold and once they hit the manifold, remain on it in the presence of dynamic uncertainties and time-varying external disturbances. By deriving the expression of the bounding function of the system uncertainty and using adaptive technique to estimate the unknown parameters of the system uncertainty bounds, the ASOFNTSMC scheme does not require the prior knowledge of the upper bound of the system uncertainty. Meanwhile, through involving the discontinuous sign function into the time derivative of the control input, the ASOFNTSMC scheme eliminates the chattering without reducing the tracking precision. Compared with the existing adaptive SONTSM control (ASONTSMC) scheme, the proposed ASOFNTSMC scheme offers a faster convergence rate for the trajectory tracking control of fully actuated AUVs. Two comparative simulation cases performed respectively on two fully actuated AUVs demonstrate the superiority of the ASOFNTSMC scheme over the ASONTSMC scheme.**

***Index Terms*—Adaptive second-order fast nonsingular terminal sliding mode control (ASOFNTSMC), autonomous underwater vehicles (AUVs), fully actuated, trajectory tracking.**

I. Introduction

AUTONOMOUS underwater vehicles (AUVs) are becoming the main tools for executing a great number of undersea missions such as search, rescue, exploration, surveillance, monitoring, reconnaissance, oceanographic mapping, geological sampling, minesweeping, ocean floor survey, and deep sea archaeology [1]–[5]. During the execution of the above undersea missions, AUVs are often expected to track some reference trajectories. To achieve this goal, efficient controller that can provide fast and accurate position and attitude tracking is required. However, it is a very challenging task to design proper trajectory tracking controller for AUVs due to the notable difficulties such as strongly coupled, highly nonlinear, and uncertain properties of the AUV dynamics as well as the time-varying external disturbances, which are hard to measure or estimate in undersea environments [5]–[9].

Among the existing control methodologies, sliding mode control (SMC) has found wide acceptance and continues to draw particular attention from the research community due to its strong robustness with respect to both modeling uncertainties and external disturbances [10]. Owing to the above attractive features, SMC has been widely used in the tracking control of underwater vehicles; see, for example, [11]–[16]. However, these SMC approaches are designed by using linear sliding mode (LSM), which can only guarantee the asymptotical convergence of the tracking errors to zero because of the asymptotical convergence of the LSM manifolds. For the trajectory tracking control of underwater vehicles, fast convergence is a high priority. Nevertheless, this can be achieved only at the price of a large control input by using the above SMC approaches. Large control input may result in the saturation of the thrusters, which is highly undesirable in practical applications. In addition, although different methods are adopted by the above SMC approaches to solve the chattering problem in the LSM due to the discontinuous switching term, e.g., in [11], [14], and [16], saturation function is utilized to replace the sign function to smooth the switching term, in [12], sliding mode switch gain adjustment method based on exponential function is presented to replace the discontinuous switching term to reduce the undesired chattering phenomenon, and in [13] and [15], sigmoid function is used to replace the sign function to weaken the chattering, these replacement methods result in the reduction of the tracking precision, that is, the tracking errors cannot converge to zero. In our previous work [17], a double-loop chattering-free adaptive integral sliding mode controller is proposed for the trajectory tracking of underwater vehicles. With respect to the above SMC approaches, this controller can eliminate the chattering without

Manuscript received December 10, 2016; revised June 18, 2017 and November 30, 2017; accepted February 17, 2018. This work was supported by the National Natural Science Foundation of China under Grant 61473183 and Grant U1509211; and in part by the China Scholarship Council Foundation. *(Corresponding author: Weidong Zhang.)*

Associate Editor: F. Zhang.

The authors are with the Department of Automation, Shanghai Jiao Tong University, Shanghai 200240, China (e-mail: qiaolei2008114106@gmail.com; wdzhang@sjtu.edu.cn).

Digital Object Identifier 10.1109/JOE.2018.2809018

reducing the tracking precision. However, like the above SMC approaches, the design of this controller is also based on the LSM and therefore the convergence of the tracking errors is also asymptotical.

Terminal SMC (TSMC) is designed to achieve the finite-time convergence of the system dynamics by using a nonlinear sliding mode manifold called terminal sliding mode (TSM) manifold [18], [19]. Compared with the conventional SMC, TSMC can offer a faster convergence rate without spending a large control effort [20]. Because of this superiority, TSMC has recently been applied to the tracking control of underwater vehicles. Based on the TSM and fast TSM (FTSM) presented respectively in [19] and [21], Elmokadem *et al.* [22] proposes the TSMC and fast TSMC (FTSMC) methods for horizontal trajectory tracking of underactuated AUVs. The two control methods guarantee fast convergence of the tracking errors to zero meanwhile eliminate the chattering without reducing the tracking precision by replacing the sign function by a saturation function. However, both control methods suffer from the singularity problem. Moreover, to suppress the effects of the uncertainties and disturbances, the upper bounds of them must be known in the two control methods design, which are almost impossible to obtain in many practical applications. Based on the nonsingular TSM (NTSM) developed in [23], Elmokadem *et al.* [22] also proposes a nonsingular TSMC (NTSMC) method for horizontal trajectory tracking of underactuated AUVs. In comparison with the TSMC and FTSMC schemes [22], this control method not only yields fast convergence of the tracking errors to zero and eliminates the chattering without reducing the tracking precision, but also avoids the singularity problem completely. Nevertheless, to suppress the effects of the uncertainties and disturbances, the upper bounds of them are also needed in the control method design. By combining the NTSM presented in [24] and adaptive technology, Wang *et al*. [25] proposes a multivariable output feedback adaptive NTSMC (ANTSMC) approach for 3-D trajectory tracking of underwater vehicles with parameter uncertainties and external disturbances. This control approach ensures the local finite-time convergence of the position and attitude tracking errors to small bounded fields. In contrast to the NTSMC scheme [22], this control approach does not require the bound information of the parameter uncertainties and external disturbances. Therefore, the system robustness is enhanced. However, the position and attitude tracking errors cannot be ensured to converge to zero. Moreover, although the saturation function is used to replace the discontinuous sign function to reduce the chattering phenomenon, the tracking precision is harmed. By using the NTSM [23] together with adaptive algorithm, Zhang *et al*. [26] proposes a different ANTSMC method for 3-D trajectory tracking of underwater vehicles in time-varying ocean currents. Compared with the ANTSMC scheme [25], this control method not only avoids the requirement of the bound information of the uncertainties and disturbances, but also guarantees the local finite-time convergence of the position and attitude tracking errors to zero. Nevertheless, although a continuous switching term based on fractional power is adopted in place of the discontinuous sign function to eliminate the chattering, the tracking precision is also harmed.

Second-order SMC (SOSMC) is a more recent and efficient method for chattering elimination [27]. Compared with the first-order SMC, the SOSMC has the advantage that it provides a smooth control and better performance in the control implementation yielding less chattering and better convergence accuracy while preserving the robustness properties [28]. Based on the NTSM [23], Feng *et al*. [29] proposes a second-order NTSMC (SONTSMC) scheme for uncertain linear multivariable systems. This controller utilizes a second-order NTSM (SONTSM) manifold, which consists of a NTSM manifold and a proportional-integral sliding mode (PISM) manifold for the input–output subsystem to realize fast convergence of the states. Meanwhile, chattering is eliminated without reducing the tracking precision. Nevertheless, the bound information of the uncertainties and their derivatives is required in the control scheme design. In practical applications, the above bound information is often difficult to know, which therefore limits the application of this SONTSMC scheme. Based on the SONTSM [29], Mondal and Mahanta [30] proposes an adaptive SONTSMC (ASONTSMC) scheme for robot manipulators. The SONTSM manifold used in this control scheme is composed of a NTSM manifold and a proportional-derivative sliding mode (PDSM) manifold so that fast convergence of the tracking errors to zero is achieved. Also, chattering is eliminated without reducing the tracking precision. In comparison with the SONTSMC scheme [29], this ASONTSMC scheme avoids the requirement of the bound information of the system uncertainty by using an adaptive tuning method to estimate the unknown bound parameters of the system uncertainty.

From above, the ASONTSMC scheme [30] holds at least one of the following advantages compared with the TSMC, FTSMC, and NTSMC schemes [22], ANTSMC scheme [25], ANTSMC scheme [26], and SONTSMC scheme [29]:

1) it avoids the singularity problem completely;
2) it does not require the bound information of the system uncertainty;
3) it guarantees the tracking errors to converge to zero;
4) it eliminates the chattering without reducing the tracking precision.

Although exciting results are obtained by the ASONTSMC scheme [30], it still has one main aspect to be improved. That is, on the SONTSM manifold, when the PDSM variable is far from the equilibrium point, the absolute value of its derivative is much smaller than that on the LSM manifold under the same sliding mode coefficients, which leads to that the convergence rate of the PDSM variable is slow and is much slower than the exponential convergence rate.

To overcome the aforementioned shortcoming of the ASONTSMC scheme [30], a second-order fast NTSM (SOFNTSM) manifold, which is composed of a fast NTSM (FNTSM) manifold and a PDSM manifold is proposed in this paper. It yields that on the SOFNTSM manifold, when the PDSM variable is far from the equilibrium point, its convergence rate is faster than that on the SONTSM manifold, and when the PDSM variable is close to the equilibrium point, its convergence rate is similar to that on the SONTSM manifold. Therefore, the designed SOFNTSM manifold ensures a faster

convergence rate than the SONTSM manifold [30]. Next, by employing this SOFNTSM manifold, an adaptive SOFNTSM control (ASOFNTSMC) scheme is designed for the trajectory tracking of fully actuated AUVs with dynamic uncertainties and time-varying external disturbances. The designed SOFNTSM manifold guarantees that the PDSM variable vector fast converges to zero in finite time and then the position and attitude tracking errors locally converge to zero exponentially, and the developed ASOFNTSMC scheme drives the error trajectories to the SOFNTSM manifold to realize the sliding mode motion in spite of dynamic uncertainties and time-varying external disturbances. The prior knowledge of the upper bound of the system uncertainty is not required by deriving the expression of the bounding function of the system uncertainty and using an adaptive mechanism to estimate the unknown parameters of the system uncertainty bounds. Meanwhile, chattering is eliminated without reducing the tracking precision through involving the discontinuous sign function into the time derivative of the control input. In contrast to the ASONTSMC scheme [30], the proposed ASOFNTSMC scheme provides a faster convergence rate for the trajectory tracking control of fully actuated AUVs. The improved performance of the ASOFNTSMC scheme over the ASONTSMC scheme is illustrated through two comparative simulation cases performed respectively on two fully actuated AUVs.

The rest of this paper is organized as follows. The SOFNTSM manifold is developed and its superiority over the SONTSM manifold [30] is exhibited in Section II. In Section III, an ASOFNTSMC scheme is designed and analyzed for the trajectory tracking of fully actuated AUVs with dynamic uncertainties and time-varying external disturbances. Two comparative numerical simulations performed respectively on two fully actuated AUVs are given to demonstrate the superiority of the proposed ASOFNTSMC scheme over the ASONTSMC scheme [30] in Section IV. Finally, conclusions are drawn in Section V.

Notations: Throughout this paper, we use the normal math fonts for scalars, bold math fonts for vectors and bold (upper case) math fonts for matrices. For a vector $\boldsymbol{\zeta} \in R^n$, denote $\boldsymbol{\zeta}^{\gamma_1/\gamma_2} = [|\zeta_1|^{\gamma_1/\gamma_2}\mathrm{sgn}(\zeta_1), \ldots, |\zeta_n|^{\gamma_1/\gamma_2}\mathrm{sgn}(\zeta_n)]^T$, where γ_1, γ_2 are positive odd integers and $\mathrm{sgn}(\cdot)$ is the standard sign function, denote $\mathrm{diag}(\boldsymbol{\zeta}) = \mathrm{diag}(\zeta_1, \ldots, \zeta_n)$, where $\mathrm{diag}(\cdot)$ is the diagonal matrix, $\max_{i=1,\ldots,n}(\zeta_i)$ denotes the largest element in $\boldsymbol{\zeta}$, the norm of vector $\boldsymbol{\zeta}$ is defined as the Euclidean norm, i.e., $\|\boldsymbol{\zeta}\| = \sqrt{\boldsymbol{\zeta}^T\boldsymbol{\zeta}}$. For a matrix $\boldsymbol{\Lambda} \in R^{n\times n}$, $\lambda_{\max}(\boldsymbol{\Lambda})$ and $\lambda_{\min}(\boldsymbol{\Lambda})$ denote the largest and smallest eigenvalues of $\boldsymbol{\Lambda}$, respectively, the norm of matrix $\boldsymbol{\Lambda}$ is defined as the induced 2-norm, i.e., $\|\boldsymbol{\Lambda}\| = \sqrt{\lambda_{\max}(\boldsymbol{\Lambda}^T\boldsymbol{\Lambda})}$.

II. SOFNTSM Manifold

In this section, a SOFNTSM manifold is designed and its superiority over the SONTSM manifold [30] is analyzed for its application in the trajectory tracking control of fully actuated AUVs. Before the SOFNTSM manifold design, let us review the SONTSM manifold presented in [30].

A. SONTSM Manifold

The SONTSM manifold presented in [30] is composed of a PDSM manifold s_1 and a NTSM manifold s_2 and is described as follows:

$$s_1 = \dot{e} + k_1 e, s_2 = s_1 + k_3 \dot{s}_1^{a/b} \tag{1}$$

where $e \in R$ is the tracking error, k_1, k_3 are positive constants, and a, b are positive odd integers satisfying $1 < a/b < 2$.

On the SONTSM manifold $s_2 = 0$, there is

$$\dot{s}_1 = -\left(\frac{s_1}{k_3}\right)^{b/a}. \tag{2}$$

Due to that $b/a < 1$, when s_1 is far from the equilibrium point, $|\dot{s}_1|$ is much smaller than that on the LSM manifold under the same sliding mode coefficients (note that on the LSM manifold, there is $\dot{s}_1 = -s_1/k_3$), which leads to that the convergence rate of s_1 is slow and is much slower than the exponential convergence rate.

B. SOFNTSM Manifold

To increase the convergence rate of the SONTSM manifold [30] when the PDSM variable is far from the equilibrium point on it, a SOFNTSM manifold is developed based on the FNTSM presented in [31]. The designed SOFNTSM manifold consists of a PDSM manifold s_1 and a FNTSM manifold s_2 and is described as follows:

$$s_1 = \dot{e} + k_1 e, s_2 = s_1 + k_2 s_1^{g/h} + k_3 \dot{s}_1^{a/b} \tag{3}$$

where e, k_1, k_3, a, b are defined as in the SONTSM manifold, k_2 is a positive constant, and g, h are positive odd integers satisfying $g/h > a/b$.

On the SOFNTSM manifold $s_2 = 0$, there is

$$\dot{s}_1 = -\left(\frac{s_1 + k_2 s_1^{g/h}}{k_3}\right)^{b/a}. \tag{4}$$

Because $g/h > 1$, when s_1 is far from the equilibrium point, the high-order term of s_1 plays a major role in the convergence rate of s_1, then (4) can be approximated by

$$\dot{s}_1 = -\left(\frac{k_2 s_1^{g/h}}{k_3}\right)^{b/a}. \tag{5}$$

Since $g/h > a/b$, (5) guarantees a faster convergence rate for s_1 than (2).

On the other hand, due to $g/h > 1$, when s_1 is close to the equilibrium point, the first-order term of s_1 plays a major role in the convergence rate of s_1, then (4) can be approximated by

$$\dot{s}_1 = -\left(\frac{s_1}{k_3}\right)^{b/a}. \tag{6}$$

Compared with (2), (6) provides a similar convergence rate for s_1.

From above, the SOFNTSM manifold ensures a faster convergence rate than the SONTSM manifold [30].

Remark 1: The SONTSM manifold $s_2(t)=0$ and the SOFNTSM manifold $s_2(t)=0$ guarantee the finite-time convergence of the PDSM variable s_1 to the equilibrium point $s_1=0$, and the exact convergent time can be determined by

$$t'_r = \int_0^{|s_1(0)|} \frac{k_3^{b/a}}{s_1^{b/a}} ds_1 = \frac{a}{a-b} k_3^{b/a} |s_1(0)|^{1-b/a} \tag{7}$$

and

$$t_r = \int_0^{|s_1(0)|} \frac{k_3^{b/a}}{\left(s_1 + k_2 s_1^{g/h}\right)^{b/a}} ds_1 = \frac{a}{a-b} k_3^{b/a} |s_1(0)|^{1-b/a} \times F\left(\frac{b}{a}, \frac{(a-b)h}{a(g-h)}, \frac{ag-bh}{a(g-h)}, -k_2|s_1(0)|^{g/h-1}\right) \tag{8}$$

respectively, where $F(\cdot)$ denotes Gauss' Hypergeometric function [32].

Remark 2: The convergent time of s_1 on the SOFNTSM manifold $s_2(t)=0$ is shorter than that on the SONTSM manifold $s_2(t)=0$, i.e., $t_r < t'_r$. This can be proved as follows.

On the SONTSM manifold $s_2(t)=0$, the convergent time t'_r taken from $s_1(0)$ to $s_1(t'_r)=0$ can be obtained from (7) as

$$t'_r = \int_0^{|s_1(0)|} \frac{k_3^{b/a}}{s_1^{b/a}} ds_1 \tag{9}$$

and on the SOFNTSM manifold $s_2(t)=0$, the convergent time t_r taken from $s_1(0)$ to $s_1(t_r)=0$ can be obtained from (8) as

$$t_r = \int_0^{|s_1(0)|} \frac{k_3^{b/a}}{\left(s_1 + k_2 s_1^{g/h}\right)^{b/a}} ds_1. \tag{10}$$

It is obvious that

$$\left(s_1 + k_2 s_1^{g/h}\right)^{b/a} > s_1^{b/a}, \qquad s_1 > 0 \tag{11}$$

which follows that

$$t_r < t'_r. \tag{12}$$

This completes the proof.

III. ASOFNTSMC for Fully Actuated AUVs

In this section, by using the SOFNTSM manifold presented in Section II together with adaptive technology, an ASOFNTSMC scheme is proposed for the trajectory tracking of fully actuated AUVs in the presence of dynamic uncertainties and time-varying external disturbances. First, the kinematic and dynamic models of an AUV are presented. Subsequently, the ASOFNTSMC scheme design is provided. Finally, the stability analysis is given.

A. Kinematic and Dynamic Models of an AUV

As shown in Fig. 1, there are two commonly used coordinate frames, namely, the inertial frame and body-fixed frame to describe the motion of an AUV. Let $\boldsymbol{\eta} = [x, \quad y, \quad z, \quad \phi, \quad \theta, \quad \psi]^T$ be the position and attitude of the vehicle in the inertial frame, where $x, y, z \in R$ represent the position and $\phi, \theta, \psi \in R$ represent the attitude (roll, pitch, and yaw). Let $\boldsymbol{\vartheta} = [u, \quad v, \quad w, \quad p, \quad q, \quad r]^T$ be the linear and angular velocities of the vehicle in the body-fixed frame, where $u, v, w \in R$ represent the surge, sway, and heave velocities and $p, q, r \in R$ represent the angular velocities. By using a Jacobian matrix $\boldsymbol{J}(\boldsymbol{\eta}) \in R^{6\times 6}$ to relate the two frames, the kinematic model of an AUV can be obtained as [33]

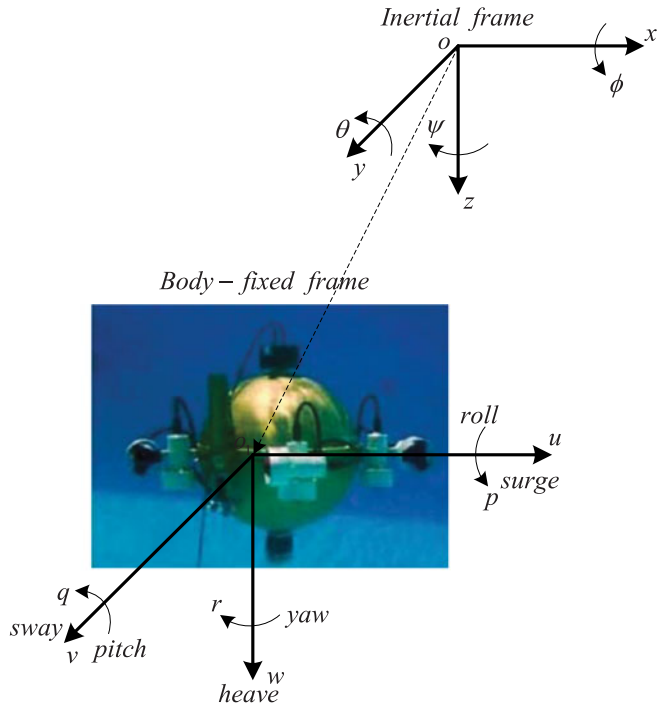

Fig. 1. Inertial and body-fixed coordinate frames.

$$\dot{\boldsymbol{\eta}} = \boldsymbol{J}(\boldsymbol{\eta})\boldsymbol{\vartheta} \tag{13}$$

where $\boldsymbol{J}(\boldsymbol{\eta})$ is defined as

$$\boldsymbol{J}(\boldsymbol{\eta}) = \begin{bmatrix} \boldsymbol{J}_1(\boldsymbol{\eta}) & \mathbf{0}_{3\times 3} \\ \mathbf{0}_{3\times 3} & \boldsymbol{J}_2(\boldsymbol{\eta}) \end{bmatrix}. \tag{14}$$

In (14), $\boldsymbol{J}_1 : R^6 \to R^{3\times 3}$ and $\boldsymbol{J}_2 : R^6 \to R^{3\times 3}$ are defined as

$$\boldsymbol{J}_1(\boldsymbol{\eta}) = \begin{bmatrix} c\psi c\theta & -s\psi c\phi + c\psi s\theta s\phi & s\psi s\phi + c\psi c\phi s\theta \\ s\psi c\theta & c\psi c\phi + s\psi s\theta s\phi & -c\psi s\phi + s\psi c\phi s\theta \\ -s\theta & c\theta s\phi & c\theta c\phi \end{bmatrix}$$

$$\boldsymbol{J}_2(\boldsymbol{\eta}) = \begin{bmatrix} 1 & s\phi t\theta & c\phi t\theta \\ 0 & c\phi & -s\phi \\ 0 & s\phi/c\theta & c\phi/c\theta \end{bmatrix}$$

in which $s\cdot$, $c\cdot$, and $t\cdot$ denote $\sin(\cdot)$, $\cos(\cdot)$, and $\tan(\cdot)$, respectively, and $\mathbf{0}_{3\times 3} \in R^{3\times 3}$ represents a matrix of zeros.

Remark 3: For guidance and control applications, it is common to use *xyz*-convention in terms of Euler angles [34]. Using

this convention, $\boldsymbol{J}_2(\boldsymbol{\eta})$ suffers from an Euler angle singularity when the pitch angle $\theta = \pm\pi/2$ rad. For routine operations of fully actuated AUVs, the singularity can be avoided by designing the vehicle with metacentric restoring forces to help to regulate the pitch angle or by choosing a desired trajectory that remains sufficiently far from pitch angle of $\theta = \pm\pi/2$ rad [34]. For the operations, which need the vehicle to go straight up or down, the singularity can be avoided by setting the desired pitch angle to $0\ rad$ and letting the fully actuated AUVs use only vertical thrusters to accomplish such operations. However, to handle the situations when operation near $\theta = \pm\pi/2$ rad is required, unit quarternions used in [5] can be adopted to represent the orientation without representation singularities. In this study, we only consider the first two types of operations of fully actuated AUVs. Thus, the pitch angle θ is bounded such that $|\theta| \leq \theta_{\max} < \pi/2$ rad, where $\theta_{\max}$ is a known positive constant.

Based on Remark 3, the following assumption can be made.

Assumption 1: The Jacobian matrix $\boldsymbol{J}(\boldsymbol{\eta})$ and its inverse $\boldsymbol{J}^{-1}(\boldsymbol{\eta})$ exist and are bounded, i.e., there exists a known positive constant $\bar{J}_1$ such that $\sup_{\boldsymbol{\eta}}\|\boldsymbol{J}(\boldsymbol{\eta})\| \leq \bar{J}_1$ and $\sup_{\boldsymbol{\eta}}\|\boldsymbol{J}^{-1}(\boldsymbol{\eta})\| \leq \bar{J}_1$ [34]. Furthermore, the first time derivatives of $\boldsymbol{J}(\boldsymbol{\eta})$ and $\boldsymbol{J}^{-1}(\boldsymbol{\eta})$ are bounded such that $\sup_{\boldsymbol{\eta}}\|\dot{\boldsymbol{J}}(\boldsymbol{\eta})\| \leq \bar{J}_2\|\dot{\boldsymbol{\eta}}\|$ and $\sup_{\boldsymbol{\eta}}\| \overbrace{\boldsymbol{J}^{-1}(\boldsymbol{\eta})}^{\cdot} \| \leq \bar{J}_2\|\dot{\boldsymbol{\eta}}\|$, where $\bar{J}_2$ is a known positive constant.

The dynamic model of an AUV with parameter uncertainties and external disturbances can be expressed by a body-fixed vector representation as [33]

$$\underbrace{(\hat{\boldsymbol{M}}+\tilde{\boldsymbol{M}})}_{\boldsymbol{M}}\dot{\boldsymbol{\vartheta}} + \underbrace{(\hat{\boldsymbol{C}}(\boldsymbol{\vartheta})+\tilde{\boldsymbol{C}}(\boldsymbol{\vartheta}))}_{\boldsymbol{C}(\boldsymbol{\vartheta})}\boldsymbol{\vartheta} + \underbrace{(\hat{\boldsymbol{D}}(\boldsymbol{\vartheta})+\tilde{\boldsymbol{D}}(\boldsymbol{\vartheta}))}_{\boldsymbol{D}(\boldsymbol{\vartheta})}\boldsymbol{\vartheta} + \underbrace{(\hat{\boldsymbol{g}}(\boldsymbol{\eta})+\tilde{\boldsymbol{g}}(\boldsymbol{\eta}))}_{\boldsymbol{g}(\boldsymbol{\eta})} + \boldsymbol{\tau}_{d\vartheta} = \boldsymbol{\tau}_{\vartheta} \tag{15}$$

where $\boldsymbol{M} = (\hat{\boldsymbol{M}}+\tilde{\boldsymbol{M}}) \in R^{6\times6}$ is the inertia matrix including the added mass, $\boldsymbol{C}(\boldsymbol{\vartheta}) = (\hat{\boldsymbol{C}}(\boldsymbol{\vartheta})+\tilde{\boldsymbol{C}}(\boldsymbol{\vartheta})) \in R^{6\times6}$ groups the centripetal and Coriolis forces, $\boldsymbol{D}(\boldsymbol{\vartheta}) = (\hat{\boldsymbol{D}}(\boldsymbol{\vartheta})+\tilde{\boldsymbol{D}}(\boldsymbol{\vartheta})) \in R^{6\times6}$ describes the hydrodynamic damping terms, $\boldsymbol{g}(\boldsymbol{\eta}) = (\hat{\boldsymbol{g}}(\boldsymbol{\eta})+\tilde{\boldsymbol{g}}(\boldsymbol{\eta})) \in R^6$ stands for the vector of restoring forces (gravity and buoyancy), $\hat{\boldsymbol{M}}$, $\hat{\boldsymbol{C}}(\boldsymbol{\vartheta})$, $\hat{\boldsymbol{D}}(\boldsymbol{\vartheta})$, and $\hat{\boldsymbol{g}}(\boldsymbol{\eta})$ are the nominal terms, $\tilde{\boldsymbol{M}}$, $\tilde{\boldsymbol{C}}(\boldsymbol{\vartheta})$, $\tilde{\boldsymbol{D}}(\boldsymbol{\vartheta})$, and $\tilde{\boldsymbol{g}}(\boldsymbol{\eta})$ are the uncertain terms, $\boldsymbol{\tau}_{d\vartheta} \in R^6$ is the vector collecting the time-varying external disturbances, and $\boldsymbol{\tau}_{\vartheta} \in R^6$ is the vector of the control input.

In general, the hydrodynamic damping of AUV moving in 6 DOF at high speed will be highly nonlinear and coupled. Nevertheless, according to [33], a common simplification can be made is that only the linear and quadratic damping terms are considered. This makes sense to the following assumption.

Assumption 2: The model parameter terms $\boldsymbol{M}$, $\boldsymbol{C}(\boldsymbol{\vartheta})$, $\boldsymbol{D}(\boldsymbol{\vartheta})$, and $\boldsymbol{g}(\boldsymbol{\eta})$ are bounded such that

$$\|\boldsymbol{M}\| \leq b_0, \qquad \|\boldsymbol{C}(\boldsymbol{\vartheta})\| \leq b_1\|\boldsymbol{\vartheta}\|$$
$$\|\boldsymbol{D}(\boldsymbol{\vartheta})\| \leq b_2 + b_3\|\boldsymbol{\vartheta}\|, \qquad \|\boldsymbol{g}(\boldsymbol{\eta})\| \leq b_4$$

where b_i $(i = 0, \ldots, 4)$ are unknown positive constants.

Remark 4: According to the expression of $\boldsymbol{g}(\boldsymbol{\eta})$ given in [33], $\boldsymbol{g}(\boldsymbol{\eta})$ is associated with $\boldsymbol{\eta}$ only in the form of trigonometric functions of Euler angles. Thus, it is reasonable to assume that $\boldsymbol{g}(\boldsymbol{\eta})$ is upper bounded by an unknown positive constant.

Assumption 3: The time-varying external disturbances vector $\boldsymbol{\tau}_{d\vartheta}$ is once differentiable in time. Moreover, $\boldsymbol{\tau}_{d\vartheta}$ and $\dot{\boldsymbol{\tau}}_{d\vartheta}$ are bounded, i.e., there exist unknown positive constants α_0 and α_1 such that $\|\boldsymbol{\tau}_{d\vartheta}\| \leq \alpha_0$ and $\|\dot{\boldsymbol{\tau}}_{d\vartheta}\| \leq \alpha_1$.

An inertial representation of the AUV dynamics (15) can be generated by applying the kinematic transformations (13) to (15) as [33]

$$\underbrace{(\hat{\boldsymbol{M}}(\boldsymbol{\eta})+\tilde{\boldsymbol{M}}(\boldsymbol{\eta}))}_{\boldsymbol{M}(\boldsymbol{\eta})}\ddot{\boldsymbol{\eta}} + \underbrace{(\hat{\boldsymbol{C}}(\boldsymbol{\vartheta},\boldsymbol{\eta})+\tilde{\boldsymbol{C}}(\boldsymbol{\vartheta},\boldsymbol{\eta}))}_{\boldsymbol{C}(\boldsymbol{\vartheta},\boldsymbol{\eta})}\dot{\boldsymbol{\eta}} + \underbrace{(\hat{\boldsymbol{D}}(\boldsymbol{\vartheta},\boldsymbol{\eta})+\tilde{\boldsymbol{D}}(\boldsymbol{\vartheta},\boldsymbol{\eta}))}_{\boldsymbol{D}(\boldsymbol{\vartheta},\boldsymbol{\eta})}\dot{\boldsymbol{\eta}} + \underbrace{(\hat{\boldsymbol{G}}(\boldsymbol{\eta})+\tilde{\boldsymbol{G}}(\boldsymbol{\eta}))}_{\boldsymbol{G}(\boldsymbol{\eta})} + \boldsymbol{\tau}_{d\eta} = \boldsymbol{\tau}_{\eta} \tag{16}$$

where $\boldsymbol{M}(\boldsymbol{\eta}) = \boldsymbol{J}^{-T}\boldsymbol{M}\boldsymbol{J}^{-1} = \hat{\boldsymbol{M}}(\boldsymbol{\eta}) + \tilde{\boldsymbol{M}}(\boldsymbol{\eta})$, $\boldsymbol{C}(\boldsymbol{\vartheta},\boldsymbol{\eta}) = \boldsymbol{J}^{-T}(\boldsymbol{C}(\boldsymbol{\vartheta}) - \boldsymbol{M}\boldsymbol{J}^{-1}\dot{\boldsymbol{J}})\boldsymbol{J}^{-1} = \hat{\boldsymbol{C}}(\boldsymbol{\vartheta},\boldsymbol{\eta}) + \tilde{\boldsymbol{C}}(\boldsymbol{\vartheta},\boldsymbol{\eta})$, $\boldsymbol{D}(\boldsymbol{\vartheta},\boldsymbol{\eta}) = \boldsymbol{J}^{-T}\boldsymbol{D}(\boldsymbol{\vartheta})\boldsymbol{J}^{-1} = \hat{\boldsymbol{D}}(\boldsymbol{\vartheta},\boldsymbol{\eta}) + \tilde{\boldsymbol{D}}(\boldsymbol{\vartheta},\boldsymbol{\eta})$, $\boldsymbol{G}(\boldsymbol{\eta}) = \boldsymbol{J}^{-T}\boldsymbol{g}(\boldsymbol{\eta}) = \hat{\boldsymbol{G}}(\boldsymbol{\eta}) + \tilde{\boldsymbol{G}}(\boldsymbol{\eta})$. $\hat{\boldsymbol{M}}(\boldsymbol{\eta})$, $\hat{\boldsymbol{C}}(\boldsymbol{\vartheta},\boldsymbol{\eta})$, $\hat{\boldsymbol{D}}(\boldsymbol{\vartheta},\boldsymbol{\eta})$, and $\hat{\boldsymbol{G}}(\boldsymbol{\eta})$ are the corresponding nominal terms and they are described as

$$\begin{aligned}
\hat{\boldsymbol{M}}(\boldsymbol{\eta}) &= \boldsymbol{J}^{-T}\hat{\boldsymbol{M}}\boldsymbol{J}^{-1} \\
\hat{\boldsymbol{C}}(\boldsymbol{\vartheta},\boldsymbol{\eta}) &= \boldsymbol{J}^{-T}(\hat{\boldsymbol{C}}(\boldsymbol{\vartheta}) - \hat{\boldsymbol{M}}\boldsymbol{J}^{-1}\dot{\boldsymbol{J}})\boldsymbol{J}^{-1} \\
\hat{\boldsymbol{D}}(\boldsymbol{\vartheta},\boldsymbol{\eta}) &= \boldsymbol{J}^{-T}\hat{\boldsymbol{D}}(\boldsymbol{\vartheta})\boldsymbol{J}^{-1} \\
\hat{\boldsymbol{G}}(\boldsymbol{\eta}) &= \boldsymbol{J}^{-T}\hat{\boldsymbol{g}}(\boldsymbol{\eta}).
\end{aligned} \tag{17}$$

$\tilde{\boldsymbol{M}}(\boldsymbol{\eta})$, $\tilde{\boldsymbol{C}}(\boldsymbol{\vartheta},\boldsymbol{\eta})$, $\tilde{\boldsymbol{D}}(\boldsymbol{\vartheta},\boldsymbol{\eta})$, and $\tilde{\boldsymbol{G}}(\boldsymbol{\eta})$ are the corresponding uncertain terms and they are given by

$$\begin{aligned}
\tilde{\boldsymbol{M}}(\boldsymbol{\eta}) &= \boldsymbol{J}^{-T}\tilde{\boldsymbol{M}}\boldsymbol{J}^{-1} \\
\tilde{\boldsymbol{C}}(\boldsymbol{\vartheta},\boldsymbol{\eta}) &= \boldsymbol{J}^{-T}(\tilde{\boldsymbol{C}}(\boldsymbol{\vartheta}) - \tilde{\boldsymbol{M}}\boldsymbol{J}^{-1}\dot{\boldsymbol{J}})\boldsymbol{J}^{-1} \\
\tilde{\boldsymbol{D}}(\boldsymbol{\vartheta},\boldsymbol{\eta}) &= \boldsymbol{J}^{-T}\tilde{\boldsymbol{D}}(\boldsymbol{\vartheta})\boldsymbol{J}^{-1} \\
\tilde{\boldsymbol{G}}(\boldsymbol{\eta}) &= \boldsymbol{J}^{-T}\tilde{\boldsymbol{g}}(\boldsymbol{\eta}).
\end{aligned} \tag{18}$$

$\boldsymbol{\tau}_{d\eta}$ is the corresponding time-varying external disturbances term and it is obtained as $\boldsymbol{\tau}_{d\eta} = \boldsymbol{J}^{-T}\boldsymbol{\tau}_{d\vartheta}$, and $\boldsymbol{\tau}_{\eta}$ is the corresponding control input term with $\boldsymbol{\tau}_{\eta} = \boldsymbol{J}^{-T}\boldsymbol{\tau}_{\vartheta}$.

Assumption 4: According to Assumptions 1 and 2, the following inequalities hold:

$$\begin{aligned}
\|\boldsymbol{M}(\boldsymbol{\eta})\| &= \left\|\boldsymbol{J}^{-T}\boldsymbol{M}\boldsymbol{J}^{-1}\right\| \leq \left\|\boldsymbol{J}^{-T}\right\|\|\boldsymbol{M}\|\left\|\boldsymbol{J}^{-1}\right\| \leq \bar{J}_1^2 b_0 \\
&\|\boldsymbol{C}(\boldsymbol{\vartheta},\boldsymbol{\eta})\dot{\boldsymbol{\eta}} + \boldsymbol{D}(\boldsymbol{\vartheta},\boldsymbol{\eta})\dot{\boldsymbol{\eta}} + \boldsymbol{G}(\boldsymbol{\eta})\| \\
&\quad \leq \|\boldsymbol{C}(\boldsymbol{\vartheta},\boldsymbol{\eta})\|\|\dot{\boldsymbol{\eta}}\| + \|\boldsymbol{D}(\boldsymbol{\vartheta},\boldsymbol{\eta})\|\|\dot{\boldsymbol{\eta}}\| + \|\boldsymbol{G}(\boldsymbol{\eta})\| \\
&\quad = \left\|\boldsymbol{J}^{-T}(\boldsymbol{C}(\boldsymbol{\vartheta}) - \boldsymbol{M}\boldsymbol{J}^{-1}\dot{\boldsymbol{J}})\boldsymbol{J}^{-1}\right\|\|\dot{\boldsymbol{\eta}}\| \\
&\qquad + \left\|\boldsymbol{J}^{-T}\boldsymbol{D}(\boldsymbol{\vartheta})\boldsymbol{J}^{-1}\right\|\|\dot{\boldsymbol{\eta}}\| + \left\|\boldsymbol{J}^{-T}\boldsymbol{g}(\boldsymbol{\eta})\right\| \\
&\quad \leq \left(\left\|\boldsymbol{J}^{-T}\boldsymbol{C}(\boldsymbol{\vartheta})\boldsymbol{J}^{-1}\right\| + \left\|\boldsymbol{J}^{-T}\boldsymbol{M}\boldsymbol{J}^{-1}\dot{\boldsymbol{J}}\boldsymbol{J}^{-1}\right\|\right)\|\dot{\boldsymbol{\eta}}\| \\
&\qquad + \left\|\boldsymbol{J}^{-T}\boldsymbol{D}(\boldsymbol{\vartheta})\boldsymbol{J}^{-1}\right\|\|\dot{\boldsymbol{\eta}}\| + \left\|\boldsymbol{J}^{-T}\boldsymbol{g}(\boldsymbol{\eta})\right\|
\end{aligned}$$

$$\begin{aligned}
&\leq \left\|\boldsymbol{J}^{-T}\right\| \|\boldsymbol{C}(\boldsymbol{\vartheta})\| \left\|\boldsymbol{J}^{-1}\right\| \|\dot{\boldsymbol{\eta}}\| \\
&\quad + \left\|\boldsymbol{J}^{-T}\right\| \|\boldsymbol{M}\| \left\|\boldsymbol{J}^{-1}\right\|^2 \left\|\dot{\boldsymbol{J}}\right\| \|\dot{\boldsymbol{\eta}}\| \\
&\quad + \left\|\boldsymbol{J}^{-T}\right\| \|\boldsymbol{D}(\boldsymbol{\vartheta})\| \left\|\boldsymbol{J}^{-1}\right\| \|\dot{\boldsymbol{\eta}}\| + \left\|\boldsymbol{J}^{-T}\right\| \|\boldsymbol{g}(\boldsymbol{\eta})\| \\
&= \bar{J}_1 b_4 + \bar{J}_1^2 b_2 \|\dot{\boldsymbol{\eta}}\| + (\bar{J}_1^2 b_1 + \bar{J}_1^2 b_3) \|\boldsymbol{\vartheta}\| \|\dot{\boldsymbol{\eta}}\| \\
&\quad + \bar{J}_1^3 b_0 \bar{J}_2 \|\dot{\boldsymbol{\eta}}\|^2.
\end{aligned}$$

By incorporating the uncertainty parts and external disturbances into a vector $\boldsymbol{\tau}_{\rho\eta}$, the dynamic model of the AUV given in (16) can be transformed to the following form:

$$\hat{\boldsymbol{M}}(\boldsymbol{\eta})\ddot{\boldsymbol{\eta}} + \hat{\boldsymbol{C}}(\boldsymbol{\vartheta},\boldsymbol{\eta})\dot{\boldsymbol{\eta}} + \hat{\boldsymbol{D}}(\boldsymbol{\vartheta},\boldsymbol{\eta})\dot{\boldsymbol{\eta}} + \hat{\boldsymbol{G}}(\boldsymbol{\eta}) = \boldsymbol{\tau}_\eta + \boldsymbol{\tau}_{\rho\eta} \tag{19}$$

where $\boldsymbol{\tau}_{\rho\eta}$ is the lumped uncertainty and it is defined as

$$\boldsymbol{\tau}_{\rho\eta} = -\tilde{\boldsymbol{M}}(\boldsymbol{\eta})\ddot{\boldsymbol{\eta}} - \tilde{\boldsymbol{C}}(\boldsymbol{\vartheta},\boldsymbol{\eta})\dot{\boldsymbol{\eta}} - \tilde{\boldsymbol{D}}(\boldsymbol{\vartheta},\boldsymbol{\eta})\dot{\boldsymbol{\eta}} - \tilde{\boldsymbol{G}}(\boldsymbol{\eta}) - \boldsymbol{\tau}_{d\eta}. \tag{20}$$

Based on (17)–(20), Assumptions 1–4 and [26, Assumption (11)] about the upper bound of the lumped uncertainty of underwater vehicles, the following assumption can be made.

Assumption 5: If the required thrust forces do not always exceed the thruster saturation limits, the lumped uncertainty $\boldsymbol{\tau}_{\rho\eta}$ can be bounded by the following form:

$$\|\boldsymbol{\tau}_{\rho\eta}\| \leq \beta_0 + \beta_1 \|\dot{\boldsymbol{\eta}}\| + \beta_2 \|\boldsymbol{\vartheta}\| \|\dot{\boldsymbol{\eta}}\| + \beta_3 \|\dot{\boldsymbol{\eta}}\|^2 \tag{21}$$

where β_i $(i = 0, \ldots, 3)$ are unknown positive constants. The details about this assumption can be seen in the Appendix A.

Remark 5: In fact, the upper bound of the lumped uncertainty $\boldsymbol{\tau}_{\rho\eta}$ is input related due to containing the acceleration signal $\ddot{\boldsymbol{\eta}}$, which is related to the control input $\boldsymbol{\tau}_\eta$. However, it has been pointed out in [26] that when the thrust saturation effect is not serious, it is reasonable to assume that the control input $\boldsymbol{\tau}_\eta$ is bounded. Thus, if the thrust saturation effect is not serious, there always exist some unknown positive constants β_i $(i = 0, \ldots, 3)$ such that the inequality (21) holds (see the Appendix A for the detailed analysis). Generally, there are two main factors that can cause thruster saturation. One is the uncertainties and disturbances existing in the vehicle dynamics. Hence, the above assumption is a limitation on the uncertainties and disturbances that can be tolerated by the AUV system. In this paper, we consider the uncertainties and disturbances that are not very serious and can be tolerated by the vehicle (see the chosen uncertainties and disturbances for simulations and the response curves of the thrust forces, as shown in Section IV). The other one is the desired trajectory chosen for the vehicle to track. If the trajectory that always needs more thrust forces than the thruster saturation limits, adaptive modification of target trajectory or pseudocontrol hedging strategy as suggested in [26] can be applied into the controller design to resolve the thruster saturation problem. In this paper, such as in [26], we choose simple trajectories, which only require the thrust forces to very briefly violate the thruster saturation limits in the beginning phase (see the chosen desired trajectories for simulations and the response curves of the thrust forces, as shown in Section IV). Therefore, from the above mentioned, the inequality (21) can be satisfied.

B. ASOFNTSMC Scheme Design

In this section, an ASOFNTSMC scheme is designed for the trajectory tracking of fully actuated AUVs with the SOFNTSM manifold introduced in Section II. As a result, a faster convergence rate is obtained compared with the ASONTSMC scheme [30]. The control scheme design consists of two steps. First, the desired dynamics are defined in the form of a SOFNTSM manifold. Second, a control law is designed such that the error trajectories always move toward the SOFNTSM manifold, and once they hit the manifold, remain on it in the presence of dynamic uncertainties and time-varying external disturbances. The expression of the bounding function of the system uncertainty is derived and adaptive tuning laws are used to estimate the unknown parameters of the system uncertainty bounds so that the prior knowledge of the upper bound of the system uncertainty is not required. Meanwhile, the discontinuous sign function is involved in the time derivative of the control input and hence chattering is eliminated without reducing the tracking precision.

By using the SOFNTSM manifold introduced in Section II, the PDSM manifold can be defined as

$$\boldsymbol{s}_1 = \dot{\tilde{\boldsymbol{\eta}}} + \boldsymbol{K}_1 \tilde{\boldsymbol{\eta}} \tag{22}$$

where $\tilde{\boldsymbol{\eta}} = \boldsymbol{\eta} - \boldsymbol{\eta}_d$ are the position and attitude tracking errors, $\boldsymbol{\eta}_d \in R^6$ are the desired position and attitude trajectories, and $\boldsymbol{K}_1 = \text{diag}(k_{11}, \ldots, k_{16})$, k_{1i} $(i = 1, \ldots, 6)$ are positive constants.

Assumption 6 [34]: The desired trajectories $\boldsymbol{\eta}_d$ are designed such that $\dot{\boldsymbol{\eta}}_d$, $\ddot{\boldsymbol{\eta}}_d$, and $(d/dt)\ddot{\boldsymbol{\eta}}_d$ exist and are bounded.

Remark 6: It should be noted that the above PDSM manifold can also be chosen as proportional-integral-derivative sliding mode (PIDSM) or PISM manifold. The choice of the PIDSM or PISM manifold does not affect the convergence results obtained subsequently. In this paper, we choose the PDSM manifold, such as in [30], to fairly compare the convergence rate between the proposed ASOFNTSMC scheme and the ASONTSMC scheme [30].

The FNTSM manifold can be defined as

$$\boldsymbol{s}_2 = \boldsymbol{s}_1 + \boldsymbol{K}_2 \boldsymbol{s}_1^{g/h} + \boldsymbol{K}_3 \dot{\boldsymbol{s}}_1^{a/b} \tag{23}$$

where $\boldsymbol{K}_2 = \text{diag}(k_{21}, \ldots, k_{26})$, $\boldsymbol{K}_3 = \text{diag}(k_{31}, \ldots, k_{36})$, k_{2i}, k_{3i} $(i = 1, \ldots, 6)$ are positive constants, and a, b, g, h are positive odd integers satisfying $1 < a/b < 2$ and $g/h > a/b$.

Suppose that t_{r1} (given in Section III-C) is the convergent time of $\boldsymbol{s}_2$ from $\boldsymbol{s}_2(0) \neq \boldsymbol{0}$ to $\boldsymbol{s}_2(t_{r1}) = \boldsymbol{0}$. When $t \geq t_{r1}$, the SOFNTSM manifold $\boldsymbol{s}_2 = \boldsymbol{0}$ is reached, then there is

$$\boldsymbol{s}_1 + \boldsymbol{K}_2 \boldsymbol{s}_1^{g/h} + \boldsymbol{K}_3 \dot{\boldsymbol{s}}_1^{a/b} = \boldsymbol{0} \tag{24}$$

namely

$$s_{1i} + k_{2i} s_{1i}^{g/h} + k_{3i} \dot{s}_{1i}^{a/b} = 0, \quad i = 1, \ldots, 6. \tag{25}$$

According to Remark 1 of Section II-B, the convergent time t_{r2i} taken from $s_{1i}(t_{r1})$ to $s_{1i}(t_{r1} + t_{r2i}) = 0$ for $i = 1, \ldots, 6$

can be obtained as

$$t_{r2i} = \frac{a}{a-b} k_{3i}^{b/a} |s_{1i}(t_{r1})|^{1-b/a} \times F\left(\frac{b}{a}, \frac{(a-b)h}{a(g-h)}, \frac{ag-bh}{a(g-h)}, -k_{2i}|s_{1i}(t_{r1})|^{g/h-1}\right), \quad i = 1, \ldots, 6. \tag{26}$$

Then the convergent time t_s taken from $\boldsymbol{s}_1(t_{r1})$ to $\boldsymbol{s}_1(t_{r1} + t_s) = \boldsymbol{0}$ can be obtained as

$$t_s = \max_{i=1,\ldots,6}(t_{r2i}) \tag{27}$$

and the total convergent time spent from $\boldsymbol{s}_1(0)$ to $\boldsymbol{s}_1 = \boldsymbol{0}$ will be $t_{r1} + t_s$.

When the PDSM manifold $\boldsymbol{s}_1 = \boldsymbol{0}$ is reached for $t \geq t_{r1} + t_s$, there is $\dot{\tilde{\boldsymbol{\eta}}} + \boldsymbol{K}_1\tilde{\boldsymbol{\eta}} = \boldsymbol{0}$. Then the position and attitude tracking errors $\tilde{\boldsymbol{\eta}}$ will converge to zero exponentially.

Thus, the next step is to design a suitable control law such that $\boldsymbol{s}_1$ and $\dot{\boldsymbol{s}}_1$ can be driven to reach the SOFNTSM manifold $\boldsymbol{s}_2 = \boldsymbol{0}$ in finite time and then remain on the manifold $\boldsymbol{s}_2 = \boldsymbol{0}$ to realize the sliding mode motion.

To determine the control law, we first take the time derivative on both sides of (23). Then we have

$$\dot{\boldsymbol{s}}_2 = \dot{\boldsymbol{s}}_1 + \frac{g}{h}\boldsymbol{K}_2\mathrm{diag}(|\boldsymbol{s}_1|^{g/h-1})\dot{\boldsymbol{s}}_1 + \frac{a}{b}\boldsymbol{K}_3\mathrm{diag}(|\dot{\boldsymbol{s}}_1|^{a/b-1})\ddot{\boldsymbol{s}}_1. \tag{28}$$

Substituting (19) and (22) into (28) yields

$$\begin{aligned}\dot{\boldsymbol{s}}_2 = \dot{\boldsymbol{s}}_1 &+ \frac{g}{h}\boldsymbol{K}_2\mathrm{diag}(|\boldsymbol{s}_1|^{g/h-1})\dot{\boldsymbol{s}}_1 + \frac{a}{b}\boldsymbol{K}_3\mathrm{diag}(|\dot{\boldsymbol{s}}_1|^{a/b-1}) \\ &\times \left\{\hat{\boldsymbol{M}}^{-1}(\boldsymbol{\eta})\left[\dot{\boldsymbol{\tau}}_\eta - \frac{d}{dt}(\hat{\boldsymbol{C}}(\boldsymbol{\vartheta},\boldsymbol{\eta})\dot{\boldsymbol{\eta}} + \hat{\boldsymbol{D}}(\boldsymbol{\vartheta},\boldsymbol{\eta})\dot{\boldsymbol{\eta}} + \hat{\boldsymbol{G}}(\boldsymbol{\eta}))\right]\right. \\ &+ \left(\dot{\overbrace{\hat{\boldsymbol{M}}^{-1}(\boldsymbol{\eta})}} + \boldsymbol{K}_1\hat{\boldsymbol{M}}^{-1}(\boldsymbol{\eta})\right) \\ &\times (\boldsymbol{\tau}_\eta - \hat{\boldsymbol{C}}(\boldsymbol{\vartheta},\boldsymbol{\eta})\dot{\boldsymbol{\eta}} - \hat{\boldsymbol{D}}(\boldsymbol{\vartheta},\boldsymbol{\eta})\dot{\boldsymbol{\eta}} - \hat{\boldsymbol{G}}(\boldsymbol{\eta})) \\ &\left. - \frac{d}{dt}\ddot{\boldsymbol{\eta}}_d - \boldsymbol{K}_1\ddot{\boldsymbol{\eta}}_d + \boldsymbol{\tau}_{F\eta}\right\}\end{aligned} \tag{29}$$

where $\boldsymbol{\tau}_{F\eta}$ is the system uncertainty and it is defined as

$$\boldsymbol{\tau}_{F\eta} = \left(\dot{\overbrace{\hat{\boldsymbol{M}}^{-1}(\boldsymbol{\eta})}} + \boldsymbol{K}_1\hat{\boldsymbol{M}}^{-1}(\boldsymbol{\eta})\right)\boldsymbol{\tau}_{\rho\eta} + \hat{\boldsymbol{M}}^{-1}(\boldsymbol{\eta})\dot{\boldsymbol{\tau}}_{\rho\eta}. \tag{30}$$

Based on (17)–(20), Assumptions 1–5, and the knowledge of the AUV dynamics given in [33], the following assumption can be made.

Assumption 7: The system uncertainty $\boldsymbol{\tau}_{F\eta}$ can be bounded by the following form:

$$\begin{aligned}\|\boldsymbol{\tau}_{F\eta}\| \leq{}& \lambda_0 + \lambda_1\|\boldsymbol{\vartheta}\| + \lambda_2\|\dot{\boldsymbol{\eta}}\| + \lambda_3\|\boldsymbol{\vartheta}\|\|\dot{\boldsymbol{\eta}}\| \\ &+ \lambda_4\|\boldsymbol{\vartheta}\|^2\|\dot{\boldsymbol{\eta}}\| + \lambda_5\|\dot{\boldsymbol{\eta}}\|^2 + \lambda_6\|\boldsymbol{\vartheta}\|\|\dot{\boldsymbol{\eta}}\|^2 + \lambda_7\|\dot{\boldsymbol{\eta}}\|^3\end{aligned} \tag{31}$$

in which λ_i $(i = 0, \ldots, 7)$ are unknown positive constants. The details about this assumption can be seen in the Appendix B.

Remark 7: Note that the expressions of the bounding functions of the lumped uncertainty $\boldsymbol{\tau}_{\rho\eta}$ and system uncertainty $\boldsymbol{\tau}_{F\eta}$ given, respectively, in (21) and (31) not only can be used for the control scheme design of this study but also can be used for the other control schemes design of AUVs such as robust control scheme design, adaptive control scheme design, and so on.

The normal control scheme design for AUVs based on sliding mode methodology usually focuses on designing the control input directly. The control input is a composition of an equivalent control law and a switching term. The equivalent control law is continuous and model based. This control law alone is able to realize the desired dynamics in the absence of the uncertainties and disturbances in the vehicle dynamics. Due to the model uncertainties and external disturbances, the switching term is required to offset the difference between the desired dynamics and real dynamics. This switching term is often designed using a discontinuous sign function, which causes the chattering phenomenon. Different from the normal SMC scheme design for AUVs, this paper starts from designing the time derivative of the control input as in [30]. The time derivative of the control input is composed of an equivalent control law and a switching term. The discontinuous sign function is involved in the time derivative of the control input, the actual control input is thus continuous and chatterless. The detailed control scheme design is as follows.

The time derivative of the control input is designed as

$$\dot{\boldsymbol{\tau}}_\eta = \boldsymbol{\tau}_{\mathrm{eq}} + \boldsymbol{\tau}_{\mathrm{sw}} \tag{32}$$

where $\boldsymbol{\tau}_{\mathrm{eq}}$ denotes the equivalent control law and $\boldsymbol{\tau}_{\mathrm{sw}}$ stands for the switching term.

The equivalent control law $\boldsymbol{\tau}_{\mathrm{eq}}$ can be determined from $\dot{\boldsymbol{s}}_2 = \boldsymbol{0}$ in the absence of the system uncertainty $\boldsymbol{\tau}_{F\eta}$. Therefore, setting $\dot{\boldsymbol{s}}_2$ and $\boldsymbol{\tau}_{F\eta}$ in (29) to zero and then solving (29) for $\boldsymbol{\tau}_{\mathrm{eq}}$ yields the equivalent control law as

$$\begin{aligned}\boldsymbol{\tau}_{\mathrm{eq}} = {}& \hat{\boldsymbol{M}}(\boldsymbol{\eta})\frac{d}{dt}\ddot{\boldsymbol{\eta}}_d + \hat{\boldsymbol{M}}(\boldsymbol{\eta})\boldsymbol{K}_1\ddot{\boldsymbol{\eta}}_d \\ &+ \frac{d}{dt}(\hat{\boldsymbol{C}}(\boldsymbol{\vartheta},\boldsymbol{\eta})\dot{\boldsymbol{\eta}} + \hat{\boldsymbol{D}}(\boldsymbol{\vartheta},\boldsymbol{\eta})\dot{\boldsymbol{\eta}} + \hat{\boldsymbol{G}}(\boldsymbol{\eta})) \\ &- \left(\hat{\boldsymbol{M}}(\boldsymbol{\eta})\boldsymbol{K}_1\hat{\boldsymbol{M}}^{-1}(\boldsymbol{\eta}) + \hat{\boldsymbol{M}}(\boldsymbol{\eta})\dot{\overbrace{\hat{\boldsymbol{M}}^{-1}(\boldsymbol{\eta})}}\right) \\ &\times (\boldsymbol{\tau}_\eta - \hat{\boldsymbol{C}}(\boldsymbol{\vartheta},\boldsymbol{\eta})\dot{\boldsymbol{\eta}} - \hat{\boldsymbol{D}}(\boldsymbol{\vartheta},\boldsymbol{\eta})\dot{\boldsymbol{\eta}} - \hat{\boldsymbol{G}}(\boldsymbol{\eta})) \\ &- \frac{b}{a}\hat{\boldsymbol{M}}(\boldsymbol{\eta})\boldsymbol{K}_3^{-1}\dot{\boldsymbol{s}}_1^{2-a/b} - \frac{bg}{ah}\hat{\boldsymbol{M}}(\boldsymbol{\eta})\boldsymbol{K}_3^{-1} \\ &\times \boldsymbol{K}_2\mathrm{diag}(|\boldsymbol{s}_1|^{g/h-1})\dot{\boldsymbol{s}}_1^{2-a/b}.\end{aligned} \tag{33}$$

The switching term $\boldsymbol{\tau}_{\mathrm{sw}}$ is designed with a discontinuous sign function to suppress the system uncertainty $\boldsymbol{\tau}_{F\eta}$. In practice, the bound parameters λ_i $(i = 0, \ldots, 7)$ of the system uncertainty $\boldsymbol{\tau}_{F\eta}$ are often difficult to obtain. This motivates for the use of adaptive technology to estimate these bound parameters. The estimated bound parameters are then used as controller param-

eters in the switching term to eliminate the effects of the system uncertainty $\boldsymbol{\tau}_{F\eta}$. Thus the switching term is defined as

$$\begin{aligned}\boldsymbol{\tau}_{\rm sw} = -\hat{\boldsymbol{M}}(\boldsymbol{\eta})(&\hat{\lambda}_0 + \hat{\lambda}_1 \|\boldsymbol{\vartheta}\| + \hat{\lambda}_2 \|\dot{\boldsymbol{\eta}}\| + \hat{\lambda}_3 \|\boldsymbol{\vartheta}\| \|\dot{\boldsymbol{\eta}}\| \\ &+ \hat{\lambda}_4 \|\boldsymbol{\vartheta}\|^2 \|\dot{\boldsymbol{\eta}}\| + \hat{\lambda}_5 \|\dot{\boldsymbol{\eta}}\|^2 + \hat{\lambda}_6 \|\boldsymbol{\vartheta}\| \|\dot{\boldsymbol{\eta}}\|^2 \\ &+ \hat{\lambda}_7 \|\dot{\boldsymbol{\eta}}\|^3){\rm sgn}(\boldsymbol{s}_2) \end{aligned} \tag{34}$$

where $\hat{\lambda}_i$ $(i = 0, \ldots, 7)$ are the estimates of λ_i $(i = 0, \ldots, 7)$ and they are updated by the following adaptation laws:

$$\dot{\hat{\lambda}}_0 = \frac{a}{b}\varphi_0 \left\| \boldsymbol{s}_2^T \boldsymbol{K}_3 {\rm diag}(|\dot{\boldsymbol{s}}_1|^{a/b-1}) \right\| \tag{35}$$

$$\dot{\hat{\lambda}}_1 = \frac{a}{b}\varphi_1 \left\| \boldsymbol{s}_2^T \boldsymbol{K}_3 {\rm diag}(|\dot{\boldsymbol{s}}_1|^{a/b-1}) \right\| \|\boldsymbol{\vartheta}\| \tag{36}$$

$$\dot{\hat{\lambda}}_2 = \frac{a}{b}\varphi_2 \left\| \boldsymbol{s}_2^T \boldsymbol{K}_3 {\rm diag}(|\dot{\boldsymbol{s}}_1|^{a/b-1}) \right\| \|\dot{\boldsymbol{\eta}}\| \tag{37}$$

$$\dot{\hat{\lambda}}_3 = \frac{a}{b}\varphi_3 \left\| \boldsymbol{s}_2^T \boldsymbol{K}_3 {\rm diag}(|\dot{\boldsymbol{s}}_1|^{a/b-1}) \right\| \|\boldsymbol{\vartheta}\| \|\dot{\boldsymbol{\eta}}\| \tag{38}$$

$$\dot{\hat{\lambda}}_4 = \frac{a}{b}\varphi_4 \left\| \boldsymbol{s}_2^T \boldsymbol{K}_3 {\rm diag}(|\dot{\boldsymbol{s}}_1|^{a/b-1}) \right\| \|\boldsymbol{\vartheta}\|^2 \|\dot{\boldsymbol{\eta}}\| \tag{39}$$

$$\dot{\hat{\lambda}}_5 = \frac{a}{b}\varphi_5 \left\| \boldsymbol{s}_2^T \boldsymbol{K}_3 {\rm diag}(|\dot{\boldsymbol{s}}_1|^{a/b-1}) \right\| \|\dot{\boldsymbol{\eta}}\|^2 \tag{40}$$

$$\dot{\hat{\lambda}}_6 = \frac{a}{b}\varphi_6 \left\| \boldsymbol{s}_2^T \boldsymbol{K}_3 {\rm diag}(|\dot{\boldsymbol{s}}_1|^{a/b-1}) \right\| \|\boldsymbol{\vartheta}\| \|\dot{\boldsymbol{\eta}}\|^2 \tag{41}$$

$$\dot{\hat{\lambda}}_7 = \frac{a}{b}\varphi_7 \left\| \boldsymbol{s}_2^T \boldsymbol{K}_3 {\rm diag}(|\dot{\boldsymbol{s}}_1|^{a/b-1}) \right\| \|\dot{\boldsymbol{\eta}}\|^3 \tag{42}$$

in which φ_i $(i = 0, \ldots, 7)$ are positive constants that determine the rate of adaptation, and $\hat{\lambda}_i(0) > 0$ for all $i = 0, \ldots, 7$.

The block diagram of the ASOFNTSMC scheme of a fully actuated AUV is shown in Fig. 2.

Remark 8: Since $1 < a/b < 2$ and $g/h > a/b > 1$, we can obtain that $0 < 2 - a/b < 1$, $0 < a/b - 1 < 1$, and $g/h - 1 > 0$. This means that the control law (32)–(42) does not involve any negative fractional power. Thus, the designed ASOFNTSMC scheme is nonsingular.

Remark 9: By using the adaptation laws (35)–(42) to estimate the bound parameters λ_i $(i = 0, \ldots, 7)$ of the system uncertainty $\boldsymbol{\tau}_{F\eta}$, the proposed ASOFNTSMC scheme does not require the prior knowledge of the upper bound of the system uncertainty. Through involving the discontinuous sign function ${\rm sgn}(\boldsymbol{s}_2)$ into the time derivative of the control input $\boldsymbol{\tau}_\eta$, namely, $\dot{\boldsymbol{\tau}}_\eta$, the proposed ASOFNTSMC scheme eliminates the chattering without reducing the tracking precision.

C. Stability Analysis

In this section, the stability of the proposed ASOFNTSMC scheme is analyzed based on the stability analysis of the first adaptive SMC law in [35]. First, a lemma is presented based on Lemma 1 of [35] to guarantee that the adaptively estimated parameters $\hat{\lambda}_i$ $(i = 0, \ldots, 7)$ have upper bounds. Then, based on the presented lemma and [35, Th. 3], a theorem is given to ensure that the sliding modes $\boldsymbol{s}_2 = \boldsymbol{0}$ and $\boldsymbol{s}_1 = \boldsymbol{0}$ are established in turn in finite time, and then the position and attitude tracking errors $\tilde{\boldsymbol{\eta}}$ locally converge to zero exponentially.

Lemma 1: Given the uncertain AUV dynamic system (19) with the sliding variable vector $\boldsymbol{s}_2$ (23) controlled by (32)–(42), the gains $\hat{\lambda}_i$ $(i = 0, \ldots, 7)$ in (34) have upper bounds, i.e., there exist positive constants $\lambda_i^\dagger$ $(i = 0, \ldots, 7)$ such that

$$\hat{\lambda}_i \le \lambda_i^\dagger, \quad i = 0, \ldots, 7. \tag{43}$$

Proof: The proof of this lemma is based on the proof of Lemma 1 in [35]. Suppose that $\dot{\boldsymbol{s}}_1 \neq \boldsymbol{0}$ and $\boldsymbol{s}_2 \neq \boldsymbol{0}$. From the update laws of $\hat{\lambda}_i$ $(i = 0, \ldots, 7)$ expressed in (35)–(42), and given that λ_i $(i = 0, \ldots, 7)$ are bounded, it follows that $\hat{\lambda}_i$ $(i = 0, \ldots, 7)$ are increasing and there exists a time t_1 such that $\hat{\lambda}_i(t_1) > \lambda_i$ for $i = 0, \ldots, 7$. Note that these gains have finite values by the absolute continuity property of $\hat{\lambda}_i$ $(i = 0, \ldots, 7)$. From $t = t_1$, given the update laws of $\hat{\lambda}_i$ $(i = 0, \ldots, 7)$, the gains $\hat{\lambda}_i$ $(i = 0, \ldots, 7)$ are large enough to make the sliding variable vector $\boldsymbol{s}_2$ decreasing. Then, it yields that, in a finite time t_2, $\boldsymbol{s}_2(t_2) = \boldsymbol{0}$ and $\hat{\lambda}_i(t_2)$ $(i = 0, \ldots, 7)$ admit bounded values. It yields that there always exist positive constants $\lambda_i^\dagger$ $(i = 0, \ldots, 7)$ such that $\lambda_i^\dagger \ge \hat{\lambda}_i$. On the other hand, for the case of $\dot{\boldsymbol{s}}_1 = \boldsymbol{0}$ and $\boldsymbol{s}_2 \neq \boldsymbol{0}$, from (29) we have

$$\begin{aligned}\ddot{\boldsymbol{s}}_1 = \hat{\boldsymbol{M}}^{-1}(\boldsymbol{\eta})&\left[\dot{\boldsymbol{\tau}}_\eta - \frac{d}{dt}(\hat{\boldsymbol{C}}(\boldsymbol{\vartheta},\boldsymbol{\eta})\dot{\boldsymbol{\eta}} + \hat{\boldsymbol{D}}(\boldsymbol{\vartheta},\boldsymbol{\eta})\dot{\boldsymbol{\eta}} + \hat{\boldsymbol{G}}(\boldsymbol{\eta}))\right] \\ &+ \left(\dot{\overbrace{\hat{\boldsymbol{M}}^{-1}(\boldsymbol{\eta})}} + \boldsymbol{K}_1 \hat{\boldsymbol{M}}^{-1}(\boldsymbol{\eta})\right) \\ &\times (\boldsymbol{\tau}_\eta - \hat{\boldsymbol{C}}(\boldsymbol{\vartheta},\boldsymbol{\eta})\dot{\boldsymbol{\eta}} - \hat{\boldsymbol{D}}(\boldsymbol{\vartheta},\boldsymbol{\eta})\dot{\boldsymbol{\eta}} - \hat{\boldsymbol{G}}(\boldsymbol{\eta})) \\ &- \frac{d}{dt}\ddot{\boldsymbol{\eta}}_d - \boldsymbol{K}_1 \ddot{\boldsymbol{\eta}}_d + \boldsymbol{\tau}_{F\eta}. \end{aligned} \tag{44}$$

Substituting (32)–(34) into (44) yields

$$\begin{aligned}\ddot{\boldsymbol{s}}_1 = -(&\hat{\lambda}_0 + \hat{\lambda}_1 \|\boldsymbol{\vartheta}\| + \hat{\lambda}_2 \|\dot{\boldsymbol{\eta}}\| + \hat{\lambda}_3 \|\boldsymbol{\vartheta}\| \|\dot{\boldsymbol{\eta}}\| + \hat{\lambda}_4 \|\boldsymbol{\vartheta}\|^2 \|\dot{\boldsymbol{\eta}}\| \\ &+ \hat{\lambda}_5 \|\dot{\boldsymbol{\eta}}\|^2 + \hat{\lambda}_6 \|\boldsymbol{\vartheta}\| \|\dot{\boldsymbol{\eta}}\|^2 + \hat{\lambda}_7 \|\dot{\boldsymbol{\eta}}\|^3){\rm sgn}(\boldsymbol{s}_2) + \boldsymbol{\tau}_{F\eta}. \end{aligned} \tag{45}$$

Assume that $\dot{\boldsymbol{s}}_1 \equiv \boldsymbol{0}$. It follows from (28) and (35)–(42) that $\dot{\boldsymbol{s}}_2 = \dot{\boldsymbol{s}}_1 + (g/h)\boldsymbol{K}_2 {\rm diag}(|\boldsymbol{s}_1|^{g/h-1})\dot{\boldsymbol{s}}_1 + (a/b)\boldsymbol{K}_3 {\rm diag}(|\dot{\boldsymbol{s}}_1|^{a/b-1})\ddot{\boldsymbol{s}}_1 \equiv \boldsymbol{0}$ and $\dot{\hat{\lambda}}_i \equiv 0$ $(i = 0, \ldots, 7)$, which implies that $\boldsymbol{s}_2$ is a constant vector and $\hat{\lambda}_i$ $(i = 0, \ldots, 7)$ are constants. According to (20), (30), and the arbitrariness of the external disturbances $\boldsymbol{\tau}_{d\vartheta}$, we have $\ddot{\boldsymbol{s}}_1 \not\equiv \boldsymbol{0}$. As a result, $\dot{\boldsymbol{s}}_1 \not\equiv \boldsymbol{0}$, which is in contradiction with the initial assumption of $\dot{\boldsymbol{s}}_1 \equiv \boldsymbol{0}$. Therefore, we obtain $\dot{\boldsymbol{s}}_1 \not\equiv \boldsymbol{0}$, showing that $\dot{\boldsymbol{s}}_1 = \boldsymbol{0}$ does not hinder the reachability of the sliding mode manifold $\boldsymbol{s}_2 = \boldsymbol{0}$. The gains $\hat{\lambda}_i$ $(i = 0, \ldots, 7)$ will continue to increase until the sliding variable vector $\boldsymbol{s}_2$ converges to zero. After that, $\hat{\lambda}_i$ $(i = 0, \ldots, 7)$ will admit bounded values. Hence, the boundedness of $\hat{\lambda}_i$ $(i = 0, \ldots, 7)$ is guaranteed, i.e., the inequalities (43) hold for some positive constants $\lambda_i^\dagger$ $(i = 0, \ldots, 7)$. This completes the proof.

Theorem 1: For the AUV dynamic system (19) with the SOFNTSM manifold composed of the PDSM manifold (22) and FNTSM manifold (23), the control law (32)–(42) guarantees that the sliding mode manifolds $\boldsymbol{s}_2 = \boldsymbol{0}$ and $\boldsymbol{s}_1 = \boldsymbol{0}$ are reached in turn in finite time, and then the position and attitude tracking errors $\tilde{\boldsymbol{\eta}}$ locally converge to zero exponentially.

Proof: The proof of this theorem is based on the proof of [35, Th. 3]. From Lemma 1, there always exist positive constants

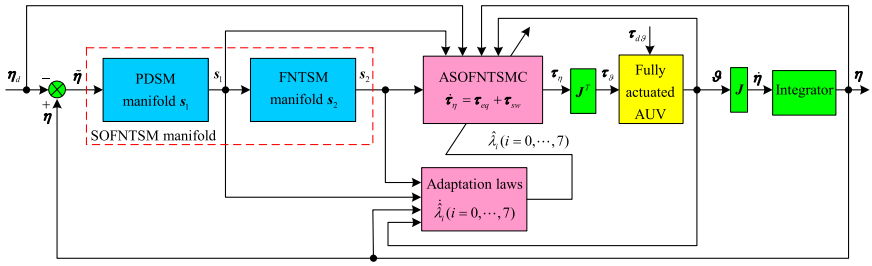

Fig. 2. Block diagram of the ASOFNTSMC scheme of a fully actuated AUV.

λ_i^* $(i=0,\ldots,7)$ such that $\lambda_i^* > \lambda_i$ and $\lambda_i^* > \hat{\lambda}_i$. Defining $\tilde{\lambda}_i = \hat{\lambda}_i - \lambda_i^*$ for $i=0,\ldots,7$, then consider the following Lyapunov candidate

$$V = \frac{1}{2}\boldsymbol{s}_2^T\boldsymbol{s}_2 + \frac{1}{2}\sum_{i=0}^{7}\sigma_i^{-1}\tilde{\lambda}_i^2 \tag{46}$$

in which σ_i $(i=0,\ldots,7)$ are positive constants satisfying $\sigma_i < \varphi_i$.

Differentiating V with respect to time gives

$$\dot{V} = \boldsymbol{s}_2^T\dot{\boldsymbol{s}}_2 + \sum_{i=0}^{7}\sigma_i^{-1}\tilde{\lambda}_i\dot{\tilde{\lambda}}_i. \tag{47}$$

Substituting (29), (32), and (33) into (47) yields

$$\begin{aligned}\dot{V} = {}& \frac{a}{b}\boldsymbol{s}_2^T\boldsymbol{K}_3\mathrm{diag}(|\dot{\boldsymbol{s}}_1|^{a/b-1})(\hat{\boldsymbol{M}}^{-1}(\boldsymbol{\eta})\boldsymbol{\tau}_{sw} + \boldsymbol{\tau}_{F\eta}) \\ & + \sum_{i=0}^{7}\sigma_i^{-1}\tilde{\lambda}_i\dot{\tilde{\lambda}}_i.\end{aligned} \tag{48}$$

Noting that $\dot{\tilde{\lambda}}_i = \dot{\hat{\lambda}}_i$ $(i=0,\ldots,7)$ and then using (34)–(42) into (48) leads to

$$\begin{aligned}\dot{V} = {}& \frac{a}{b}\boldsymbol{s}_2^T\boldsymbol{K}_3\mathrm{diag}\big(|\dot{\boldsymbol{s}}_1|^{a/b-1}\big)\hat{\boldsymbol{M}}^{-1}(\boldsymbol{\eta})\boldsymbol{\tau}_{sw} \\ & + \frac{a}{b}\boldsymbol{s}_2^T\boldsymbol{K}_3\mathrm{diag}\big(|\dot{\boldsymbol{s}}_1|^{a/b-1}\big)\boldsymbol{\tau}_{F\eta} + \sum_{i=0}^{7}\sigma_i^{-1}\tilde{\lambda}_i\dot{\hat{\lambda}}_i \\ \leqslant {}& -\frac{a}{b}\big(\hat{\lambda}_0 + \hat{\lambda}_1\|\boldsymbol{\vartheta}\| + \hat{\lambda}_2\|\dot{\boldsymbol{\eta}}\| + \hat{\lambda}_3\|\boldsymbol{\vartheta}\|\|\dot{\boldsymbol{\eta}}\| + \hat{\lambda}_4\|\boldsymbol{\vartheta}\|^2\|\dot{\boldsymbol{\eta}}\| \\ & + \hat{\lambda}_5\|\dot{\boldsymbol{\eta}}\|^2 + \hat{\lambda}_6\|\boldsymbol{\vartheta}\|\|\dot{\boldsymbol{\eta}}\|^2 + \hat{\lambda}_7\|\dot{\boldsymbol{\eta}}\|^3\big) \\ & \times \sum_{i=1}^{6}k_{3i}|\dot{s}_{1i}|^{a/b-1}|s_{2i}| \\ & + \frac{a}{b}\left\|\boldsymbol{s}_2^T\boldsymbol{K}_3\mathrm{diag}(|\dot{\boldsymbol{s}}_1|^{a/b-1})\right\|\|\boldsymbol{\tau}_{F\eta}\| \\ & + \frac{a}{b}\left\|\boldsymbol{s}_2^T\boldsymbol{K}_3\mathrm{diag}(|\dot{\boldsymbol{s}}_1|^{a/b-1})\right\|[\sigma_0^{-1}\varphi_0(\hat{\lambda}_0 - \lambda_0^*) \\ & + \sigma_1^{-1}\varphi_1(\hat{\lambda}_1 - \lambda_1^*)\|\boldsymbol{\vartheta}\| \\ & + \sigma_2^{-1}\varphi_2(\hat{\lambda}_2 - \lambda_2^*)\|\dot{\boldsymbol{\eta}}\| + \sigma_3^{-1}\varphi_3(\hat{\lambda}_3 - \lambda_3^*)\|\boldsymbol{\vartheta}\|\|\dot{\boldsymbol{\eta}}\| \\ & + \sigma_4^{-1}\varphi_4(\hat{\lambda}_4 - \lambda_4^*)\|\boldsymbol{\vartheta}\|^2\|\dot{\boldsymbol{\eta}}\| + \sigma_5^{-1}\varphi_5(\hat{\lambda}_5 - \lambda_5^*)\|\dot{\boldsymbol{\eta}}\|^2 \\ & + \sigma_6^{-1}\varphi_6(\hat{\lambda}_6 - \lambda_6^*)\|\boldsymbol{\vartheta}\|\|\dot{\boldsymbol{\eta}}\|^2 + \sigma_7^{-1}\varphi_7(\hat{\lambda}_7 - \lambda_7^*)\|\dot{\boldsymbol{\eta}}\|^3] \\ \leqslant {}& -\frac{a}{b}\left\|\boldsymbol{s}_2^T\boldsymbol{K}_3\mathrm{diag}(|\dot{\boldsymbol{s}}_1|^{a/b-1})\right\| \\ & \times (\hat{\lambda}_0 + \hat{\lambda}_1\|\boldsymbol{\vartheta}\| + \hat{\lambda}_2\|\dot{\boldsymbol{\eta}}\| + \hat{\lambda}_3\|\boldsymbol{\vartheta}\|\|\dot{\boldsymbol{\eta}}\| \\ & + \hat{\lambda}_4\|\boldsymbol{\vartheta}\|^2\|\dot{\boldsymbol{\eta}}\| + \hat{\lambda}_5\|\dot{\boldsymbol{\eta}}\|^2 + \hat{\lambda}_6\|\boldsymbol{\vartheta}\|\|\dot{\boldsymbol{\eta}}\|^2 + \hat{\lambda}_7\|\dot{\boldsymbol{\eta}}\|^3) \\ & + \frac{a}{b}\left\|\boldsymbol{s}_2^T\boldsymbol{K}_3\mathrm{diag}(|\dot{\boldsymbol{s}}_1|^{a/b-1})\right\| \\ & \times (\lambda_0 + \lambda_1\|\boldsymbol{\vartheta}\| + \lambda_2\|\dot{\boldsymbol{\eta}}\| + \lambda_3\|\boldsymbol{\vartheta}\|\|\dot{\boldsymbol{\eta}}\| \\ & + \lambda_4\|\boldsymbol{\vartheta}\|^2\|\dot{\boldsymbol{\eta}}\| + \lambda_5\|\dot{\boldsymbol{\eta}}\|^2 + \lambda_6\|\boldsymbol{\vartheta}\|\|\dot{\boldsymbol{\eta}}\|^2 + \lambda_7\|\dot{\boldsymbol{\eta}}\|^3) \\ & + \frac{a}{b}\left\|\boldsymbol{s}_2^T\boldsymbol{K}_3\mathrm{diag}(|\dot{\boldsymbol{s}}_1|^{a/b-1})\right\| \\ & \times (\lambda_0^* + \lambda_1^*\|\boldsymbol{\vartheta}\| + \lambda_2^*\|\dot{\boldsymbol{\eta}}\| + \lambda_3^*\|\boldsymbol{\vartheta}\|\|\dot{\boldsymbol{\eta}}\| \\ & + \lambda_4^*\|\boldsymbol{\vartheta}\|^2\|\dot{\boldsymbol{\eta}}\| + \lambda_5^*\|\dot{\boldsymbol{\eta}}\|^2 + \lambda_6^*\|\boldsymbol{\vartheta}\|\|\dot{\boldsymbol{\eta}}\|^2 + \lambda_7^*\|\dot{\boldsymbol{\eta}}\|^3) \\ & - \frac{a}{b}\left\|\boldsymbol{s}_2^T\boldsymbol{K}_3\mathrm{diag}(|\dot{\boldsymbol{s}}_1|^{a/b-1})\right\| \\ & \times (\lambda_0^* + \lambda_1^*\|\boldsymbol{\vartheta}\| + \lambda_2^*\|\dot{\boldsymbol{\eta}}\| + \lambda_3^*\|\boldsymbol{\vartheta}\|\|\dot{\boldsymbol{\eta}}\| \\ & + \lambda_4^*\|\boldsymbol{\vartheta}\|^2\|\dot{\boldsymbol{\eta}}\| + \lambda_5^*\|\dot{\boldsymbol{\eta}}\|^2 + \lambda_6^*\|\boldsymbol{\vartheta}\|\|\dot{\boldsymbol{\eta}}\|^2 + \lambda_7^*\|\dot{\boldsymbol{\eta}}\|^3) \\ & + \frac{a}{b}\left\|\boldsymbol{s}_2^T\boldsymbol{K}_3\mathrm{diag}(|\dot{\boldsymbol{s}}_1|^{a/b-1})\right\| \\ & \times [\sigma_0^{-1}\varphi_0(\hat{\lambda}_0 - \lambda_0^*) + \sigma_1^{-1}\varphi_1(\hat{\lambda}_1 - \lambda_1^*)\|\boldsymbol{\vartheta}\| \\ & + \sigma_2^{-1}\varphi_2(\hat{\lambda}_2 - \lambda_2^*)\|\dot{\boldsymbol{\eta}}\| + \sigma_3^{-1}\varphi_3(\hat{\lambda}_3 - \lambda_3^*)\|\boldsymbol{\vartheta}\|\|\dot{\boldsymbol{\eta}}\| \\ & + \sigma_4^{-1}\varphi_4(\hat{\lambda}_4 - \lambda_4^*)\|\boldsymbol{\vartheta}\|^2\|\dot{\boldsymbol{\eta}}\| + \sigma_5^{-1}\varphi_5(\hat{\lambda}_5 - \lambda_5^*)\|\dot{\boldsymbol{\eta}}\|^2 \\ & + \sigma_6^{-1}\varphi_6(\hat{\lambda}_6 - \lambda_6^*)\|\boldsymbol{\vartheta}\|\|\dot{\boldsymbol{\eta}}\|^2 + \sigma_7^{-1}\varphi_7(\hat{\lambda}_7 - \lambda_7^*)\|\dot{\boldsymbol{\eta}}\|^3] \\ = {}& -\frac{a}{b}\left\|\boldsymbol{s}_2^T\boldsymbol{K}_3\mathrm{diag}(|\dot{\boldsymbol{s}}_1|^{a/b-1})\right\|[(\lambda_0^* - \lambda_0) + (\lambda_1^* - \lambda_1)\|\boldsymbol{\vartheta}\| \\ & + (\lambda_2^* - \lambda_2)\|\dot{\boldsymbol{\eta}}\| + (\lambda_3^* - \lambda_3)\|\boldsymbol{\vartheta}\|\|\dot{\boldsymbol{\eta}}\| \\ & + (\lambda_4^* - \lambda_4)\|\boldsymbol{\vartheta}\|^2\|\dot{\boldsymbol{\eta}}\| \\ & + (\lambda_5^* - \lambda_5)\|\dot{\boldsymbol{\eta}}\|^2 + (\lambda_6^* - \lambda_6)\|\boldsymbol{\vartheta}\|\|\dot{\boldsymbol{\eta}}\|^2 \\ & + (\lambda_7^* - \lambda_7)\|\dot{\boldsymbol{\eta}}\|^3] - \frac{a}{b}\left\|\boldsymbol{s}_2^T\boldsymbol{K}_3\mathrm{diag}(|\dot{\boldsymbol{s}}_1|^{a/b-1})\right\| \\ & \times [(\sigma_0^{-1}\varphi_0 - 1)(\lambda_0^* - \hat{\lambda}_0) + (\sigma_1^{-1}\varphi_1 - 1)(\lambda_1^* - \hat{\lambda}_1)\|\boldsymbol{\vartheta}\| \\ & + (\sigma_2^{-1}\varphi_2 - 1)(\lambda_2^* - \hat{\lambda}_2)\|\dot{\boldsymbol{\eta}}\| \\ & + (\sigma_3^{-1}\varphi_3 - 1)(\lambda_3^* - \hat{\lambda}_3)\|\boldsymbol{\vartheta}\|\|\dot{\boldsymbol{\eta}}\|\end{aligned}$$

$$
\begin{aligned}
&+(\sigma_4^{-1}\varphi_4-1)(\lambda_4^*-\hat{\lambda}_4)\|\boldsymbol{\vartheta}\|^2\|\dot{\boldsymbol{\eta}}\|\\
&+(\sigma_5^{-1}\varphi_5-1)(\lambda_5^*-\hat{\lambda}_5)\|\dot{\boldsymbol{\eta}}\|^2\\
&+(\sigma_6^{-1}\varphi_6-1)(\lambda_6^*-\hat{\lambda}_6)\|\boldsymbol{\vartheta}\|\|\dot{\boldsymbol{\eta}}\|^2\\
&+(\sigma_7^{-1}\varphi_7-1)(\lambda_7^*-\hat{\lambda}_7)\|\dot{\boldsymbol{\eta}}\|^3]\\
\leqslant&-\frac{a}{b}\lambda_{\min}(\boldsymbol{K}_3)\lambda_{\min}(\mathrm{diag}(|\dot{\boldsymbol{s}}_1|^{a/b-1}))\\
&\times[(\lambda_0^*-\lambda_0)+(\lambda_1^*-\lambda_1)\|\boldsymbol{\vartheta}\|\\
&\quad+(\lambda_2^*-\lambda_2)\|\dot{\boldsymbol{\eta}}\|+(\lambda_3^*-\lambda_3)\|\boldsymbol{\vartheta}\|\|\dot{\boldsymbol{\eta}}\|\\
&\quad+(\lambda_4^*-\lambda_4)\|\boldsymbol{\vartheta}\|^2\|\dot{\boldsymbol{\eta}}\|\\
&\quad+(\lambda_5^*-\lambda_5)\|\dot{\boldsymbol{\eta}}\|^2+(\lambda_6^*-\lambda_6)\|\boldsymbol{\vartheta}\|\|\dot{\boldsymbol{\eta}}\|^2\\
&\quad+(\lambda_7^*-\lambda_7)\|\dot{\boldsymbol{\eta}}\|^3]\|\boldsymbol{s}_2\|\\
&-\frac{a}{b}\left\|\boldsymbol{s}_2^T\boldsymbol{K}_3\mathrm{diag}(|\dot{\boldsymbol{s}}_1|^{a/b-1})\right\|(\sigma_0^{-1}\varphi_0-1)(\lambda_0^*-\hat{\lambda}_0)\\
&-\frac{a}{b}\left\|\boldsymbol{s}_2^T\boldsymbol{K}_3\mathrm{diag}(|\dot{\boldsymbol{s}}_1|^{a/b-1})\right\|(\sigma_1^{-1}\varphi_1-1)\|\boldsymbol{\vartheta}\|(\lambda_1^*-\hat{\lambda}_1)\\
&-\frac{a}{b}\left\|\boldsymbol{s}_2^T\boldsymbol{K}_3\mathrm{diag}(|\dot{\boldsymbol{s}}_1|^{a/b-1})\right\|(\sigma_2^{-1}\varphi_2-1)\|\dot{\boldsymbol{\eta}}\|(\lambda_2^*-\hat{\lambda}_2)\\
&-\frac{a}{b}\left\|\boldsymbol{s}_2^T\boldsymbol{K}_3\mathrm{diag}(|\dot{\boldsymbol{s}}_1|^{a/b-1})\right\|(\sigma_3^{-1}\varphi_3-1)\|\boldsymbol{\vartheta}\|\\
&\times\|\dot{\boldsymbol{\eta}}\|(\lambda_3^*-\hat{\lambda}_3)\\
&-\frac{a}{b}\left\|\boldsymbol{s}_2^T\boldsymbol{K}_3\mathrm{diag}(|\dot{\boldsymbol{s}}_1|^{a/b-1})\right\|(\sigma_4^{-1}\varphi_4-1)\|\boldsymbol{\vartheta}\|^2\\
&\times\|\dot{\boldsymbol{\eta}}\|(\lambda_4^*-\hat{\lambda}_4)\\
&-\frac{a}{b}\left\|\boldsymbol{s}_2^T\boldsymbol{K}_3\mathrm{diag}(|\dot{\boldsymbol{s}}_1|^{a/b-1})\right\|(\sigma_5^{-1}\varphi_5-1)\|\dot{\boldsymbol{\eta}}\|^2(\lambda_5^*-\hat{\lambda}_5)\\
&-\frac{a}{b}\left\|\boldsymbol{s}_2^T\boldsymbol{K}_3\mathrm{diag}(|\dot{\boldsymbol{s}}_1|^{a/b-1})\right\|\\
&\times(\sigma_6^{-1}\varphi_6-1)\|\boldsymbol{\vartheta}\|\|\dot{\boldsymbol{\eta}}\|^2(\lambda_6^*-\hat{\lambda}_6)\\
&-\frac{a}{b}\left\|\boldsymbol{s}_2^T\boldsymbol{K}_3\mathrm{diag}(|\dot{\boldsymbol{s}}_1|^{a/b-1})\right\|(\sigma_7^{-1}\varphi_7-1)\|\dot{\boldsymbol{\eta}}\|^3(\lambda_7^*-\hat{\lambda}_7).
\end{aligned}
\tag{49}
$$

For the case of $\dot{\boldsymbol{s}}_1\neq\boldsymbol{0}$ and $\boldsymbol{s}_2\neq\boldsymbol{0}$, let

$$
\begin{aligned}
\chi_1=&\frac{a}{b}\lambda_{\min}(\boldsymbol{K}_3)\lambda_{\min}(\mathrm{diag}(|\dot{\boldsymbol{s}}_1|^{a/b-1}))\\
&\times[(\lambda_0^*-\lambda_0)+(\lambda_1^*-\lambda_1)\|\boldsymbol{\vartheta}\|+(\lambda_2^*-\lambda_2)\|\dot{\boldsymbol{\eta}}\|\\
&+(\lambda_3^*-\lambda_3)\|\boldsymbol{\vartheta}\|\|\dot{\boldsymbol{\eta}}\|\\
&+(\lambda_4^*-\lambda_4)\|\boldsymbol{\vartheta}\|^2\|\dot{\boldsymbol{\eta}}\|+(\lambda_5^*-\lambda_5)\|\dot{\boldsymbol{\eta}}\|^2\\
&+(\lambda_6^*-\lambda_6)\|\boldsymbol{\vartheta}\|\|\dot{\boldsymbol{\eta}}\|^2+(\lambda_7^*-\lambda_7)\|\dot{\boldsymbol{\eta}}\|^3]\\
\chi_2=&\frac{a}{b}\left\|\boldsymbol{s}_2^T\boldsymbol{K}_3\mathrm{diag}(|\dot{\boldsymbol{s}}_1|^{a/b-1})\right\|(\sigma_0^{-1}\varphi_0-1)\\
\chi_3=&\frac{a}{b}\left\|\boldsymbol{s}_2^T\boldsymbol{K}_3\mathrm{diag}(|\dot{\boldsymbol{s}}_1|^{a/b-1})\right\|(\sigma_1^{-1}\varphi_1-1)\|\boldsymbol{\vartheta}\|\\
\chi_4=&\frac{a}{b}\left\|\boldsymbol{s}_2^T\boldsymbol{K}_3\mathrm{diag}(|\dot{\boldsymbol{s}}_1|^{a/b-1})\right\|(\sigma_2^{-1}\varphi_2-1)\|\dot{\boldsymbol{\eta}}\|\\
\chi_5=&\frac{a}{b}\left\|\boldsymbol{s}_2^T\boldsymbol{K}_3\mathrm{diag}(|\dot{\boldsymbol{s}}_1|^{a/b-1})\right\|(\sigma_3^{-1}\varphi_3-1)\|\boldsymbol{\vartheta}\|\|\dot{\boldsymbol{\eta}}\|\\
\chi_6=&\frac{a}{b}\left\|\boldsymbol{s}_2^T\boldsymbol{K}_3\mathrm{diag}(|\dot{\boldsymbol{s}}_1|^{a/b-1})\right\|(\sigma_4^{-1}\varphi_4-1)\|\boldsymbol{\vartheta}\|^2\|\dot{\boldsymbol{\eta}}\|\\
\chi_7=&\frac{a}{b}\left\|\boldsymbol{s}_2^T\boldsymbol{K}_3\mathrm{diag}(|\dot{\boldsymbol{s}}_1|^{a/b-1})\right\|(\sigma_5^{-1}\varphi_5-1)\|\dot{\boldsymbol{\eta}}\|^2\\
\chi_8=&\frac{a}{b}\left\|\boldsymbol{s}_2^T\boldsymbol{K}_3\mathrm{diag}(|\dot{\boldsymbol{s}}_1|^{a/b-1})\right\|(\sigma_6^{-1}\varphi_6-1)\|\boldsymbol{\vartheta}\|\|\dot{\boldsymbol{\eta}}\|^2\\
\chi_9=&\frac{a}{b}\left\|\boldsymbol{s}_2^T\boldsymbol{K}_3\mathrm{diag}(|\dot{\boldsymbol{s}}_1|^{a/b-1})\right\|(\sigma_7^{-1}\varphi_7-1)\|\dot{\boldsymbol{\eta}}\|^3.
\end{aligned}
\tag{50}
$$

Then, from (46) and (50), inequality (49) can be transformed as

$$
\begin{aligned}
\dot{V}\leq&-\sqrt{2}\chi_1\frac{\sqrt{2}}{2}\|\boldsymbol{s}_2\|-\sqrt{2\sigma_0}\chi_2\frac{\sqrt{2}}{2\sqrt{\sigma_0}}(\lambda_0^*-\hat{\lambda}_0)\\
&-\sqrt{2\sigma_1}\chi_3\frac{\sqrt{2}}{2\sqrt{\sigma_1}}(\lambda_1^*-\hat{\lambda}_1)\\
&-\sqrt{2\sigma_2}\chi_4\frac{\sqrt{2}}{2\sqrt{\sigma_2}}(\lambda_2^*-\hat{\lambda}_2)-\sqrt{2\sigma_3}\chi_5\frac{\sqrt{2}}{2\sqrt{\sigma_3}}(\lambda_3^*-\hat{\lambda}_3)\\
&-\sqrt{2\sigma_4}\chi_6\frac{\sqrt{2}}{2\sqrt{\sigma_4}}(\lambda_4^*-\hat{\lambda}_4)-\sqrt{2\sigma_5}\chi_7\frac{\sqrt{2}}{2\sqrt{\sigma_5}}(\lambda_5^*-\hat{\lambda}_5)\\
&-\sqrt{2\sigma_6}\chi_8\frac{\sqrt{2}}{2\sqrt{\sigma_6}}(\lambda_6^*-\hat{\lambda}_6)-\sqrt{2\sigma_7}\chi_9\frac{\sqrt{2}}{2\sqrt{\sigma_7}}(\lambda_7^*-\hat{\lambda}_7)\\
\leq&-\min(\sqrt{2}\chi_1,\sqrt{2\sigma_0}\chi_2,\sqrt{2\sigma_1}\chi_3,\sqrt{2\sigma_2}\chi_4,\\
&\qquad\sqrt{2\sigma_3}\chi_5,\sqrt{2\sigma_4}\chi_6,\sqrt{2\sigma_5}\chi_7,\sqrt{2\sigma_6}\chi_8,\sqrt{2\sigma_7}\chi_9)\\
&\times\left[\frac{\sqrt{2}}{2}\|\boldsymbol{s}_2\|+\frac{\sqrt{2}}{2\sqrt{\sigma_0}}(\lambda_0^*-\hat{\lambda}_0)+\frac{\sqrt{2}}{2\sqrt{\sigma_1}}(\lambda_1^*-\hat{\lambda}_1)\right.\\
&+\frac{\sqrt{2}}{2\sqrt{\sigma_2}}(\lambda_2^*-\hat{\lambda}_2)+\frac{\sqrt{2}}{2\sqrt{\sigma_3}}(\lambda_3^*-\hat{\lambda}_3)\\
&+\frac{\sqrt{2}}{2\sqrt{\sigma_4}}(\lambda_4^*-\hat{\lambda}_4)+\frac{\sqrt{2}}{2\sqrt{\sigma_5}}(\lambda_5^*-\hat{\lambda}_5)\\
&\left.+\frac{\sqrt{2}}{2\sqrt{\sigma_6}}(\lambda_6^*-\hat{\lambda}_6)+\frac{\sqrt{2}}{2\sqrt{\sigma_7}}(\lambda_7^*-\hat{\lambda}_7)\right]\\
\leq&-\omega V^{1/2}
\end{aligned}
\tag{51}
$$

where

$$
\begin{aligned}
\omega=&\min(\sqrt{2}\chi_1,\sqrt{2\sigma_0}\chi_2,\sqrt{2\sigma_1}\chi_3,\sqrt{2\sigma_2}\chi_4,\sqrt{2\sigma_3}\chi_5,\\
&\sqrt{2\sigma_4}\chi_6,\sqrt{2\sigma_5}\chi_7,\sqrt{2\sigma_6}\chi_8,\sqrt{2\sigma_7}\chi_9)>0.
\end{aligned}
$$

According to [36], the SOFNTSM manifold $\boldsymbol{s}_2=\boldsymbol{0}$ can be reached in the finite time

$$
t_{r1}\leq\frac{2V^{1/2}\big|_{t=0}}{\omega}.
\tag{52}
$$

For the case of $\dot{\boldsymbol{s}}_1=\boldsymbol{0}$ and $\boldsymbol{s}_2\neq\boldsymbol{0}$, it has been shown in the proof of Lemma 1 that $\dot{\boldsymbol{s}}_1=\boldsymbol{0}$ is not an attractor in the reaching phase. Thus, the reachability of the SOFNTSM manifold $\boldsymbol{s}_2=\boldsymbol{0}$ in the finite time (52) is still guaranteed.

When the SOFNTSM manifold $\boldsymbol{s}_2 = \boldsymbol{0}$ is reached, according to the results of Section III-B, the PDSM variable vector $\boldsymbol{s}_1$ will converge to zero in the finite time $t_{r1} + t_s$, where t_s is given in (27), and after the PDSM manifold $\boldsymbol{s}_1 = \boldsymbol{0}$ is reached, the position and attitude tracking errors $\tilde{\boldsymbol{\eta}}$ will converge to zero exponentially.

On the other hand, because only the routine operations and the straight up or down operations using only vertical thrusters for AUVs are considered, i.e., the pitch angle θ is bounded such that $|\theta| \leq \theta_{\max} < \pi/2$, the position and attitude tracking errors $\tilde{\boldsymbol{\eta}}$ are locally stable. This completes the proof.

Remark 10: The ASONTSMC scheme recently proposed in [30] for robotic manipulators can be extended to deal with the trajectory tracking control problem of fully actuated AUVs. The ASONTSMC scheme applied to the trajectory tracking of fully actuated AUVs can be expressed as follows.

The SONTSM manifold, which is composed of a PDSM manifold $\boldsymbol{s}_1$ and a NTSM manifold $\boldsymbol{s}_2$, is defined as

$$\boldsymbol{s}_1 = \dot{\tilde{\boldsymbol{\eta}}} + \boldsymbol{K}_1 \tilde{\boldsymbol{\eta}}, \boldsymbol{s}_2 = \boldsymbol{s}_1 + \boldsymbol{K}_3 \dot{\boldsymbol{s}}_1^{a/b}. \tag{53}$$

The ASONTSMC scheme is given by

$$\dot{\boldsymbol{\tau}}_\eta = \boldsymbol{\tau}_{\rm eq} + \boldsymbol{\tau}_{\rm sw} \tag{54}$$

$$\begin{aligned}\boldsymbol{\tau}_{\rm eq} = {} & \hat{\boldsymbol{M}}(\boldsymbol{\eta})\frac{d}{dt}\ddot{\boldsymbol{\eta}}_d + \hat{\boldsymbol{M}}(\boldsymbol{\eta})\boldsymbol{K}_1\ddot{\boldsymbol{\eta}}_d - \frac{b}{a}\hat{\boldsymbol{M}}(\boldsymbol{\eta})\boldsymbol{K}_3^{-1}\dot{\boldsymbol{s}}_1^{2-a/b} \\ & + \frac{d}{dt}(\hat{\boldsymbol{C}}(\boldsymbol{\vartheta},\boldsymbol{\eta})\dot{\boldsymbol{\eta}} + \hat{\boldsymbol{D}}(\boldsymbol{\vartheta},\boldsymbol{\eta})\dot{\boldsymbol{\eta}} + \hat{\boldsymbol{G}}(\boldsymbol{\eta})) \\ & - \left(\hat{\boldsymbol{M}}(\boldsymbol{\eta})\boldsymbol{K}_1\hat{\boldsymbol{M}}^{-1}(\boldsymbol{\eta}) + \hat{\boldsymbol{M}}(\boldsymbol{\eta})\dot{\hat{\boldsymbol{M}}^{-1}}(\boldsymbol{\eta})\right) \\ & \times (\boldsymbol{\tau}_\eta - \hat{\boldsymbol{C}}(\boldsymbol{\vartheta},\boldsymbol{\eta})\dot{\boldsymbol{\eta}} - \hat{\boldsymbol{D}}(\boldsymbol{\vartheta},\boldsymbol{\eta})\dot{\boldsymbol{\eta}} - \hat{\boldsymbol{G}}(\boldsymbol{\eta}))\end{aligned} \tag{55}$$

$\boldsymbol{\tau}_{\rm sw}$ and the adaptation laws call back (34) and (35)–(42), respectively. The corresponding controller parameters are defined as in the ASOFNTSMC scheme. Similar to the proof of Theorem 1, it can be verified that under this ASONTSMC scheme, the sliding mode manifolds $\boldsymbol{s}_2 = \boldsymbol{0}$ and $\boldsymbol{s}_1 = \boldsymbol{0}$ can be reached in turn in finite time, and then the position and attitude tracking errors $\tilde{\boldsymbol{\eta}}$ can locally converge to zero exponentially. In contrast to this ASONTSMC scheme, the proposed ASOFNTSMC scheme offers a faster convergence rate for the trajectory tracking control of fully actuated AUVs. This is mainly because that the proposed SOFNTSM manifold guarantees a faster convergence rate for the PDSM variable vector $\boldsymbol{s}_1$ than the SONTSM manifold [30] according to the results of Section II. Such superiority of the ASOFNTSMC scheme over the ASONTSMC scheme can also be seen from the simulations in Section IV.

IV. Simulation Studies

In this section, two comparative simulation cases are carried out between the ASOFNTSMC scheme proposed in this study and the ASONTSMC scheme (see Remark 10) presented in [30] to demonstrate the effectiveness and superiority of the ASOFNTSMC scheme. The two simulation cases are performed on two fully actuated AUVs, namely, the URIS AUV [37] and the ODIN AUV [38], respectively. The first simulation case is to command the URIS AUV to track a horizontal circular trajectory. The second simulation case is to command the ODIN AUV to track a 3-D helical trajectory.

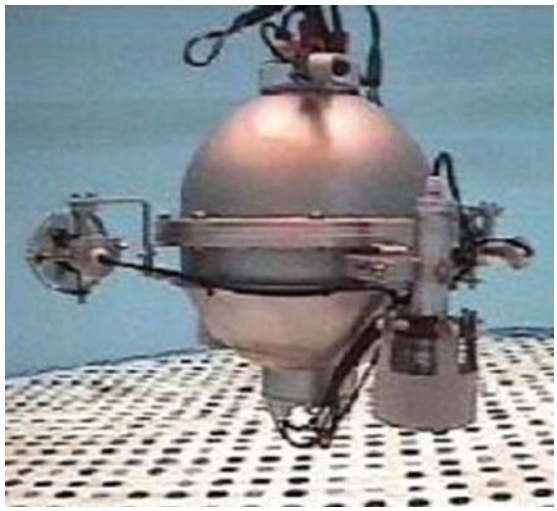

Fig. 3. URIS AUV.

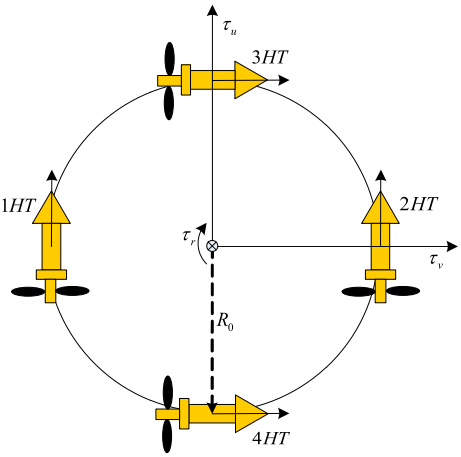

Fig. 4. Thruster layout of the URIS.

A. First Simulation Case

This simulation case is conducted to check the effectiveness and superiority of the proposed ASOFNTSMC scheme for tracking the desired trajectory in horizontal plane. The AUV model used in this case is the URIS built at the University of Girona. URIS is a small sphere shaped AUV. Fig. 3 shows its structure. Here as in [37], the thruster configuration is transformed from the original configuration with two horizontal and two vertical thrusters into a configuration with four horizontal thrusters only, without any vertical thrusters. The horizontal thruster distribution of the vehicle is shown in Fig. 4. The thruster saturation limit for each thruster is taken as ± 75 N. The total vector of thrust forces and moment acting on the URIS can be written

as [37]

$$\underbrace{\begin{bmatrix}\tau_u\\ \tau_v\\ \tau_r\end{bmatrix}}_{\boldsymbol{\tau}_\vartheta} = \underbrace{\begin{bmatrix}1 & 1 & 0 & 0\\ 0 & 0 & 1 & 1\\ R_0 & -R_0 & R_0 & -R_0\end{bmatrix}}_{\boldsymbol{B}_\vartheta} \underbrace{\begin{bmatrix}u_1\\ u_2\\ u_3\\ u_4\end{bmatrix}}_{\boldsymbol{u}_\vartheta} \tag{56}$$

in which $\boldsymbol{\tau}_\vartheta = [\tau_u, \quad \tau_v, \quad \tau_r]^T$ is the vector of total thrust forces and moment, where τ_u, τ_v represent the thrust forces in u and v directions and τ_r represents the moment in r direction, $\boldsymbol{u}_\vartheta = [u_1, \quad u_2, \quad u_3, \quad u_4]^T$ is the vector collecting the individual thrust forces, where u_i represents the force of ith thruster, $i = 1, \ldots, 4$, and $\boldsymbol{B}_\vartheta$ is the thruster distribution matrix where $R_0 = 0.175$ m is the radial distance from the center of the vehicle to the horizontal thruster's center. The force produced by each thruster can be determined by

$$\boldsymbol{u}_\vartheta = \boldsymbol{B}_\vartheta^T (\boldsymbol{B}_\vartheta \boldsymbol{B}_\vartheta^T)^{-1} \boldsymbol{\tau}_\vartheta \tag{57}$$

where $\boldsymbol{B}_\vartheta^T (\boldsymbol{B}_\vartheta \boldsymbol{B}_\vartheta^T)^{-1}$ is the pseudo inverse of matrix $\boldsymbol{B}_\vartheta$.

The dynamic model and related parameter values of the URIS are taken from [39] and are presented as follows:

$$\boldsymbol{M} = \begin{bmatrix} m - X_{\dot{u}} & 0 & 0\\ 0 & m - Y_{\dot{v}} & 0\\ 0 & 0 & I_z - N_{\dot{r}}\end{bmatrix}$$

$$\boldsymbol{D}(\boldsymbol{\vartheta}) = \begin{bmatrix} X_u + X_{u|u|}\,|u| & 0 & 0\\ 0 & Y_v + Y_{v|v|}\,|v| & 0\\ 0 & 0 & N_r + N_{r|r|}\,|r|\end{bmatrix}$$

where $m - X_{\dot{u}} = 54.35$ kg is the mass in u direction, $m - Y_{\dot{v}} = 54.35$ kg is the mass in v direction, $I_z - N_{\dot{r}} = 1.93$ N $\cdot$ ms^2 is the moment of inertia about z direction, $X_u = 17.51$ Ns/m, $Y_v = 17.51$ Ns/m, and $N_r = 2.4$ Nsm are the linear damping terms in u, v, and r directions, respectively, and $X_{u|u|} = 10$ Ns^2/m^2, $Y_{v|v|} = 10$ Ns^2/m^2, and $N_{r|r|} = 2$ Ns^2 are the quadratic damping terms in u, v, and r directions, respectively.

To reflect the uncertainties in the vehicle dynamic model, 20% model inaccuracies are incorporated into both control schemes' dynamic models, that is, the above dynamic parameter values of the vehicle are treated as the actual values, and the nominal dynamic parameter values used in the two control schemes are 80% of the actual values. In addition, the following time-varying external disturbances are considered:

$$\begin{cases}\tau_{d\vartheta 1} = 3 + 2\sin(0.02t) \text{ N}\\ \tau_{d\vartheta 2} = 2 + \sin(0.03t) \text{ N}\\ \tau_{d\vartheta 3} = \cos(0.01t) \text{ N} \cdot \text{m}.\end{cases} \tag{58}$$

The desired horizontal circular trajectory for the URIS is chosen as

$$\begin{cases} x_d(t) = \sin(0.2t) \text{ m}\\ y_d(t) = \cos(0.2t) \text{ m}\\ \psi_d(t) = 0.2t \text{ rad}.\end{cases} \tag{59}$$

TABLE I
CONTROLLER PARAMETERS FOR THE TWO CONTROL SCHEMES

ASONTSMC	$a = 5, b = 3$ $\boldsymbol{K}_1 = \text{diag}(2, 2, 2.5)$ $\boldsymbol{K}_3 = \text{diag}(1.5, 2, 2.3)$ $\varphi_i = 0.02, i = 0, \ldots, 6$
ASOFNTSMC	$g = 11, h = 3, a = 5, b = 3$ $\boldsymbol{K}_1 = \text{diag}(2, 2, 2.5)$ $\boldsymbol{K}_2 = \text{diag}(1, 1, 1)$ $\boldsymbol{K}_3 = \text{diag}(1.5, 2, 2.3)$ $\varphi_i = 0.02, i = 0, \ldots, 6$

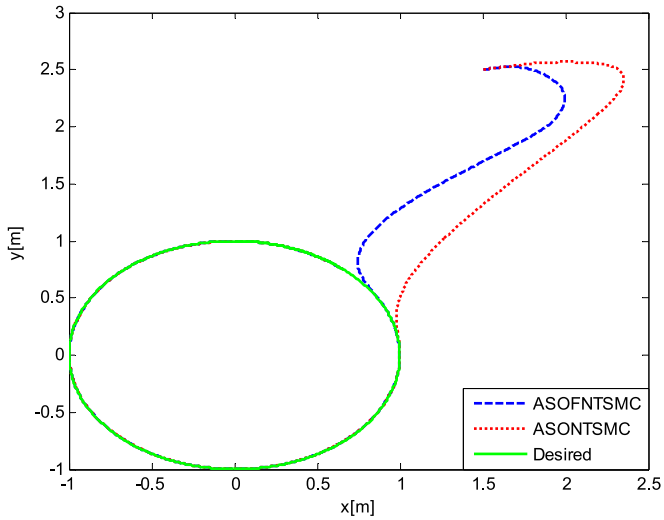

Fig. 5. Horizontal circular trajectory tracking results of the URIS under the ASOFNTSMC and ASONTSMC schemes.

Since the desired trajectory chosen for the vehicle to track requires only the horizontal motion (i.e., surge, sway, and yaw motion) of the vehicle, the kinematic singularity problem does not need to be considered.

For both control schemes, the initial position and attitude of the URIS are set as $x(0) = 1.5$ m, $y(0) = 2.5$ m, $\psi(0) = 1$ rad, the initial velocities of the URIS are defined as zero at the initial time $t = 0$ s, and the initial values of the adaptive parameters $\hat{\lambda}_i$ $(i = 0, \ldots, 6)$ are chosen as $\hat{\lambda}_i(0) = 0.01, i = 0, \ldots, 6$. Note that since the above dynamic model of the URIS does not contain the centripetal and Coriolis term $\boldsymbol{C}(\boldsymbol{\vartheta})$, the expression of the bounding function of the system uncertainty $\boldsymbol{\tau}_{F\eta}$ given in (31) does not contain the term $\|\dot{\boldsymbol{\eta}}\|^3$ here. Consequently, only λ_i $(i = 0, \ldots, 6)$ are needed to be estimated. To make the comparison fair and persuasive, corresponding controller parameters for the two control schemes are selected exactly the same values, as shown in Table I. The response curves of the closed-loop systems under both control schemes are given in Figs. 5–8.

Fig. 5 shows the circular trajectory tracking results of the URIS in xy plane under the ASOFNTSMC and ASONTSMC schemes. The responses of the vehicle position and attitude and their tracking errors are shown in Fig. 6. It can be seen from the two figures that under both control schemes, the URIS accurately tracks the desired trajectories and the tracking errors converge to zero at a fast speed. A clear advantage of the ASOFNTSMC

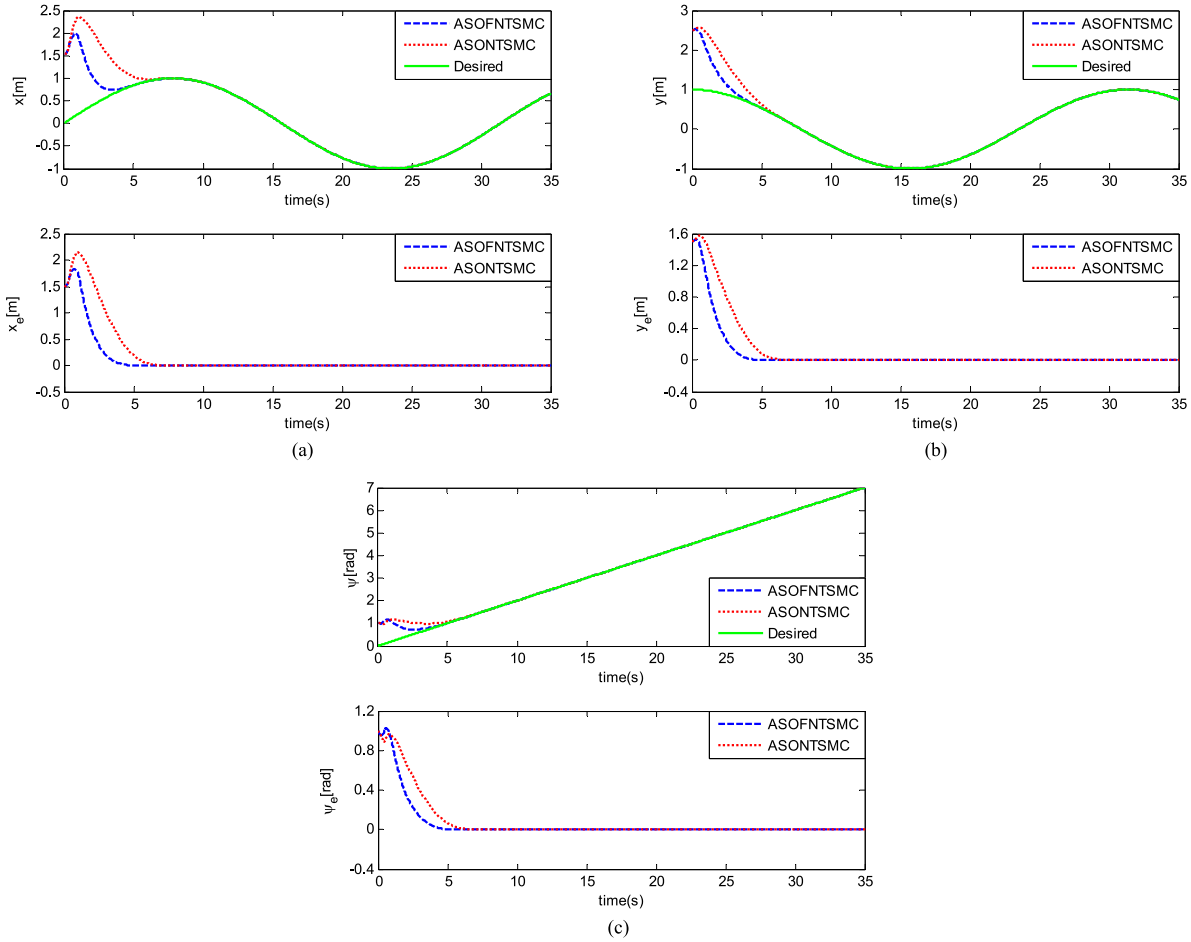

Fig. 6. Tracking results for each state of the URIS under the ASOFNTSMC and ASONTSMC schemes. (a) Tracking response of position x and its tracking error. (b) Tracking response of position y and its tracking error. (c) Tracking response of yaw angle ψ and its tracking error.

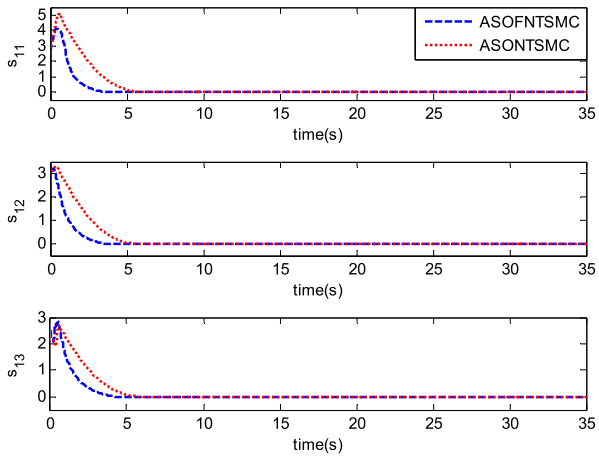

Fig. 7. Responses of the PDSM variable vector $\boldsymbol{s}_1$ under the ASOFNTSMC and ASONTSMC schemes.

scheme demonstrated in the two figures is that it offers a faster convergence rate than the ASONTSMC scheme. Fig. 7 displays the responses of the PDSM variable vector $\boldsymbol{s}_1$ for the two control schemes. It is observed in this figure that the convergence of $\boldsymbol{s}_1$ to zero is faster for the ASOFNTSMC scheme than for the ASONTSMC scheme, which demonstrates the reason why the ASOFNTSMC scheme can offer a faster convergence rate than the ASONTSMC scheme.

Fig. 8 illustrates the thrust force produced by each thruster of the URIS using the ASOFNTSMC and ASONTSMC schemes. It can be observed from this figure that chattering is suppressed effectively for both control schemes. In addition, each thruster only very briefly saturates in the beginning phase, thus inequalities (21) and (31) are valid.

B. Second Simulation Case

This simulation case is conducted to check the effectiveness and superiority of the proposed ASOFNTSMC scheme for tracking the desired trajectory in 3-D space. The AUV model used in this case is the ODIN developed at the University of Hawaii. ODIN is also a sphere shaped AUV. Fig. 9 shows the structure of this vehicle. The propulsion system is made up of four horizontal thrusters and four vertical thrusters. A sketch of the vehicle's thruster distribution is shown in Fig. 10. The thruster saturation limit for each thruster is taken as ± 150 N. The total vector of thrust forces and moments acting on the ODIN can be written from [38] as (60), shown at the bottom of the next page, in which $\boldsymbol{\tau}_\vartheta = [\tau_u, \quad \tau_v, \quad \tau_w, \quad \tau_p, \quad \tau_q, \quad \tau_r]^T$ is the vector of total thrust forces and moments, where τ_u, τ_v,

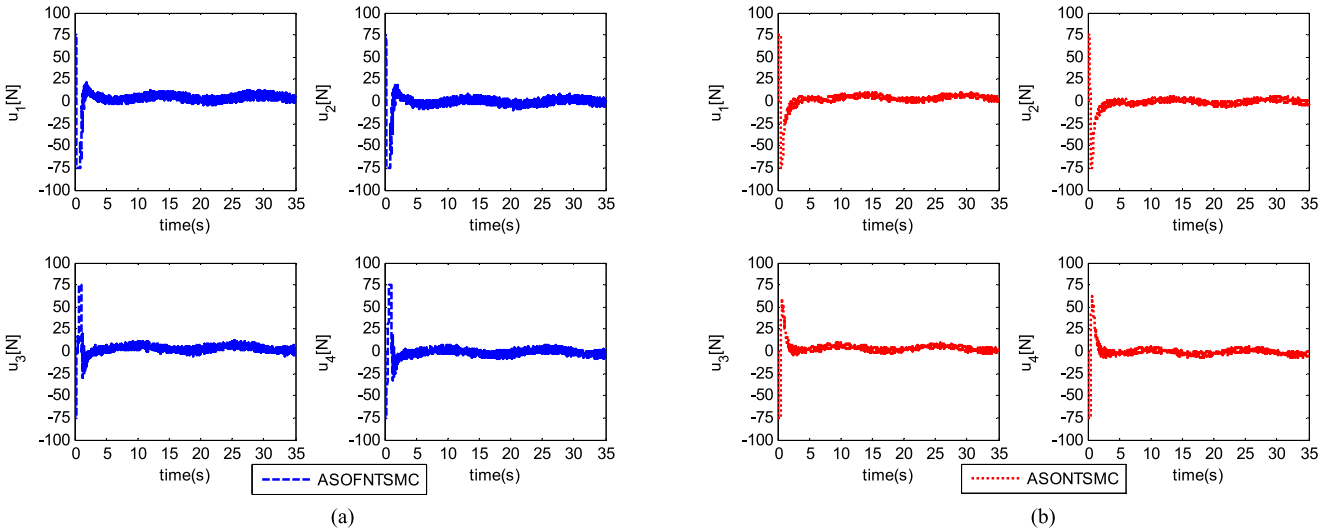

Fig. 8. Force produced by each thruster of the URIS under the ASOFNTSMC and ASONTSMC schemes. (a) Forces produced by horizontal thrusters 1–4 under the ASOFNTSMC scheme. (b) Forces produced by horizontal thrusters 1–4 under the ASONTSMC scheme.

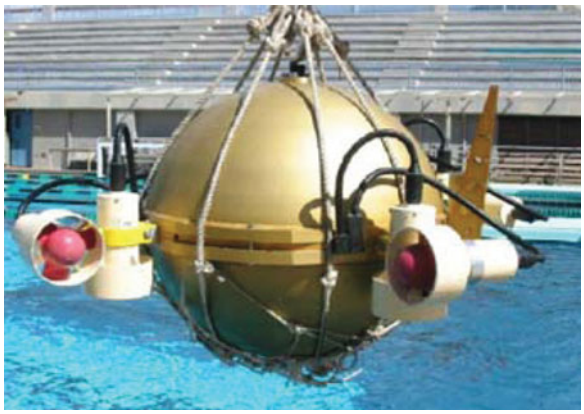

Fig. 9. ODIN AUV.

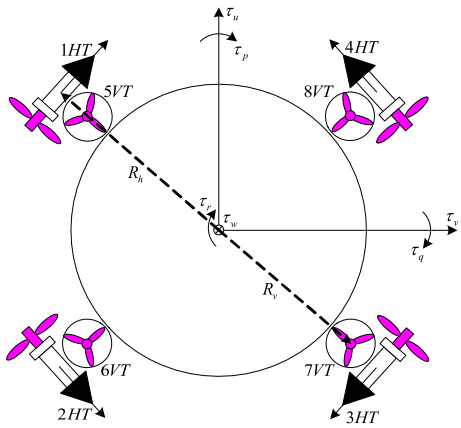

Fig. 10. Thruster layout of the ODIN.

τ_w represent the thrust forces in u, v, and w directions and τ_p, τ_q, τ_r represent the moments in p, q, and r directions, $\boldsymbol{u}_\vartheta = [u_1, \ u_2, \ u_3, \ u_4, \ u_5, \ u_6, \ u_7, \ u_8]^T$ is the vector collecting the individual thrust forces, where u_i represents the force of ith thruster, $i = 1, \ldots, 8$, and $\boldsymbol{B}_\vartheta$ is the thruster distribution matrix where $\xi = \sin(\pi/4)$, $R_v = 0.381$ m is the distance from the center of the vehicle to the vertical thruster's center, and $R_h = 0.508$ m is the radial distance from the center of the vehicle to the horizontal thruster's center. The force produced by each thruster can be determined by

$$\boldsymbol{u}_\vartheta = \boldsymbol{B}_\vartheta^T (\boldsymbol{B}_\vartheta \boldsymbol{B}_\vartheta^T)^{-1} \boldsymbol{\tau}_\vartheta \tag{61}$$

where $\boldsymbol{B}_\vartheta^T (\boldsymbol{B}_\vartheta \boldsymbol{B}_\vartheta^T)^{-1}$ is the pseudo inverse of matrix $\boldsymbol{B}_\vartheta$.

$$\underbrace{\begin{bmatrix} \tau_u \\ \tau_v \\ \tau_w \\ \tau_p \\ \tau_q \\ \tau_r \end{bmatrix}}_{\boldsymbol{\tau}_\vartheta} = \underbrace{\begin{bmatrix} \xi & -\xi & -\xi & \xi & 0 & 0 & 0 & 0 \\ \xi & \xi & -\xi & -\xi & 0 & 0 & 0 & 0 \\ 0 & 0 & 0 & 0 & -1 & -1 & -1 & -1 \\ 0 & 0 & 0 & 0 & R_v\xi & R_v\xi & -R_v\xi & -R_v\xi \\ 0 & 0 & 0 & 0 & R_v\xi & -R_v\xi & -R_v\xi & R_v\xi \\ R_h & -R_h & R_h & -R_h & 0 & 0 & 0 & 0 \end{bmatrix}}_{\boldsymbol{B}_\vartheta} \underbrace{\begin{bmatrix} u_1 \\ u_2 \\ u_3 \\ u_4 \\ u_5 \\ u_6 \\ u_7 \\ u_8 \end{bmatrix}}_{\boldsymbol{u}_\vartheta} \tag{60}$$

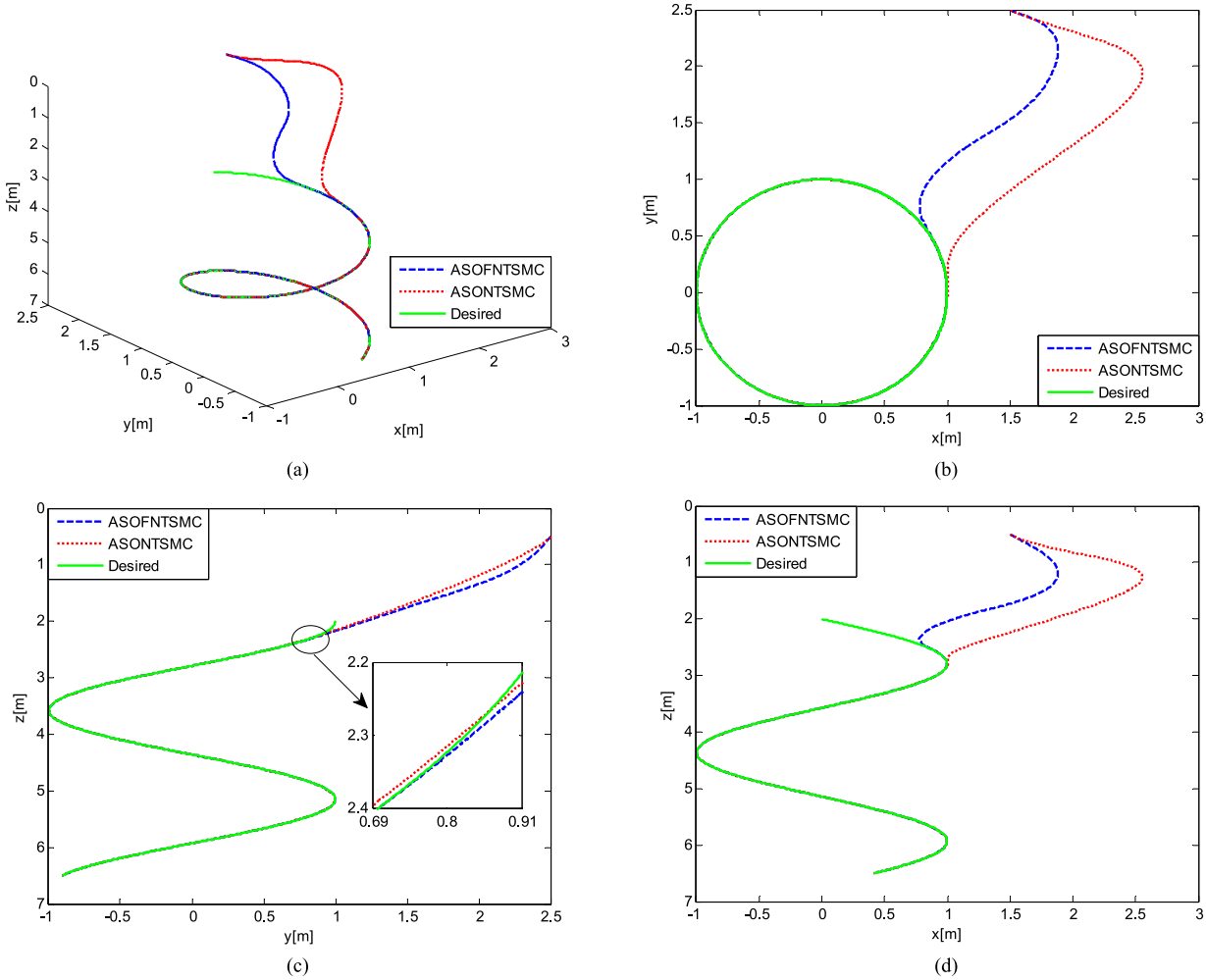

Fig. 11. 3-D helical trajectory tracking results of the ODIN under the ASOFNTSMC and ASONTSMC schemes. (a) xyz plot. (b) xy plot. (c) yz plot. (d) xz plot.

TABLE II
CONTROLLER PARAMETERS FOR THE TWO CONTROL SCHEMES

ASONTSMC	$a = 5, b = 3$
	$\boldsymbol{K}_1 = \text{diag}(2, 2, 2, 4, 3, 3)$
	$\boldsymbol{K}_3 = \text{diag}(1.5, 2, 2, 2.5, 2.5, 2.3)$
	$\varphi_i = 0.01, i = 0, \ldots, 7$
ASOFNTSMC	$g = 11, h = 3, a = 5, b = 3$
	$\boldsymbol{K}_1 = \text{diag}(2, 2, 2, 4, 3, 3)$
	$\boldsymbol{K}_2 = \text{diag}(1, 1, 1, 1, 1, 1)$
	$\boldsymbol{K}_3 = \text{diag}(1.5, 2, 2, 2.5, 2.5, 2.3)$
	$\varphi_i = 0.01, i = 0, \ldots, 7$

The dynamic model and related parameter values of the ODIN are taken from [38] and are presented in the equations at the bottom of the next page, where $I_{xx} = I_{yy} = I_{zz} = I = 8\pi\rho_v r_0^5/15$ are the moments of inertia about the principal axes, $r_0 = 0.31$ m is the radius of the ODIN, $m = 125$ kg is the mass of the ODIN, $z_G = 0.05$ m is the distance of the center of gravity from the geometric center, $\rho = 1000$ kg/m^3 is the density of water, $\rho_v = 965$ kg/m^3 is the average density of the ODIN, $g = 9.81$ m/s^2, $d_{t1} = 148$ Ns^2/m^2 is the translational quadratic damping factor, $d_{t2} = 100$ Ns^2/m^2 is the translational linear damping factor, $d_1 = 280$ Ns^2/m is the angular quadratic damping factor, and $d_2 = 230$ Ns^2/m is the angular linear damping factor.

As with the first simulation case, 20% model inaccuracies are incorporated into both control schemes' dynamic models to reflect the uncertainties in the vehicle dynamic model. In addition, the time-varying external disturbances are given by

$$\begin{cases} \tau_{d\vartheta 1} = 2 + 3\sin(0.02t) \text{ N} \\ \tau_{d\vartheta 2} = 3 + \sin(0.03t) \text{ N} \\ \tau_{d\vartheta 3} = 4\sin(0.01t) \text{ N} \\ \tau_{d\vartheta 4} = 2 + \cos(0.01t) \text{ N} \cdot \text{m} \\ \tau_{d\vartheta 5} = 1 + \cos(0.02t) \text{ N} \cdot \text{m} \\ \tau_{d\vartheta 6} = 2\cos(0.03t) \text{ N} \cdot \text{m}. \end{cases} \tag{62}$$

The desired 3-D helical trajectory for the ODIN is chosen as

$$\begin{cases} x_d(t) = \sin(0.2t) \text{ m} \\ y_d(t) = \cos(0.2t) \text{ m} \\ z_d(t) = 0.1t + 2 \text{ m} \\ \phi_d(t) = 0 \text{ rad} \\ \theta_d(t) = -\arctan(1/2) \text{ rad} \\ \psi_d(t) = 0.2t \text{ rad}. \end{cases} \tag{63}$$

Since the desired trajectory chosen for the vehicle to track remains sufficiently far from pitch angle of $\theta = \pm\pi/2$ rad, possible kinematic singularity is avoided.

For both control schemes, the initial position and attitude of the ODIN are set as $x(0) = 1.5$ m, $y(0) = 2.5$ m, $z(0) = 0.5$ m, $\phi(0) = 1$ rad, $\theta(0) = 0.8$ rad, $\psi(0) = 1.2$ rad, the initial velocities of the ODIN are defined as zero at the initial time $t = 0$ s, and the initial values of the adaptive parameters $\hat{\lambda}_i$ $(i = 0, \ldots, 7)$ are chosen as $\hat{\lambda}_i(0) = 0.01$, $i = 0, \ldots, 7$. As with the first simulation case, corresponding controller parameters for the two control schemes are selected exactly the same values as exhibited in Table II to make the comparison fair and persuasive. The response curves of the closed-loop systems under both control schemes are given in Figs. 11–14.

Fig. 11 illustrates the helical trajectory tracking results including *xyz*, *xy*, *yz*, and *xz* plots of the ODIN under the ASOFNTSMC and ASONTSMC schemes. Fig. 12 shows the responses of the vehicle position and attitude and their tracking errors. From the two figures it can be observed that under both control schemes, the ODIN effectively tracks the desired trajectories and the tracking errors quickly converge to zero. Clearly, the ASOFNTSMC scheme provides a faster convergence rate than the ASONTSMC scheme. Fig. 13 depicts the responses of the PDSM variable vector $\boldsymbol{s}_1$ for the two control schemes. It is obvious that $\boldsymbol{s}_1$ converges to zero faster for the ASOFNTSMC scheme than for the ASONTSMC scheme, which shows the reason why the ASOFNTSMC scheme can provide a faster convergence rate than the ASONTSMC scheme.

Fig. 14 plots the thrust force produced by each thruster of the ODIN adopting the ASOFNTSMC and ASONTSMC schemes. As shown by this figure, chattering is suppressed effectively for both control schemes. Additionally, each thruster only very briefly saturates in the beginning phase, hence inequalities (21) and (31) are valid.

V. Conclusion

In this paper, an ASOFNTSMC scheme is proposed to solve the trajectory tracking control problem of fully actuated AUVs

$$\boldsymbol{M} = \begin{bmatrix} m & 0 & 0 & 0 & mz_G & 0 \\ 0 & m & 0 & -mz_G & 0 & 0 \\ 0 & 0 & m & 0 & 0 & 0 \\ 0 & -mz_G & 0 & I_{xx} & 0 & 0 \\ mz_G & 0 & 0 & 0 & I_{yy} & 0 \\ 0 & 0 & 0 & 0 & 0 & I_{zz} \end{bmatrix} + \begin{bmatrix} 2\pi\rho r_0^3/3 & 0 & 0 & 0 & 0 & 0 \\ 0 & 2\pi\rho r_0^3/3 & 0 & 0 & 0 & 0 \\ 0 & 0 & 2\pi\rho r_0^3/3 & 0 & 0 & 0 \\ 0 & 0 & 0 & 0 & 0 & 0 \\ 0 & 0 & 0 & 0 & 0 & 0 \\ 0 & 0 & 0 & 0 & 0 & 0 \end{bmatrix}$$

$$\boldsymbol{C}(\boldsymbol{\vartheta}) = \begin{bmatrix} 0 & 0 & 0 & mz_G r & 2mw & -2mv \\ 0 & 0 & 0 & -2mw & mz_G r & 2mu \\ 0 & 0 & 0 & 2mv - mz_G p & -2mu - mz_G q & 0 \\ -mz_G r & 2mw & -2mv + mz_G p & 0 & Ir & -Iq \\ -2mw & -mz_G r & 2mu + mz_G q & -Ir & 0 & Ip \\ 2mv & -2mu & 0 & Iq & -Ip & 0 \end{bmatrix}$$

$$\boldsymbol{D}(\boldsymbol{\vartheta}) = \begin{bmatrix} d_{t1}|u| + d_{t2} & 0 & 0 & 0 & 0 & 0 \\ 0 & d_{t1}|v| + d_{t2} & 0 & 0 & 0 & 0 \\ 0 & 0 & d_{t1}|w| + d_{t2} & 0 & 0 & 0 \\ 0 & 0 & 0 & d_1|p| + d_2 & 0 & 0 \\ 0 & 0 & 0 & 0 & d_1|q| + d_2 & 0 \\ 0 & 0 & 0 & 0 & 0 & d_1|r| + d_2 \end{bmatrix}$$

$$\boldsymbol{g}(\boldsymbol{\eta}) = \begin{bmatrix} (mg - 4\pi\rho r_0^3 g/3)\sin(\theta) \\ -(mg - 4\pi\rho r_0^3 g/3)\cos(\theta)\sin(\phi) \\ -(mg - 4\pi\rho r_0^3 g/3)\cos(\theta)\cos(\phi) \\ z_G mg\cos(\theta)\sin(\phi) \\ z_G mg\sin(\theta) \\ 0 \end{bmatrix}$$

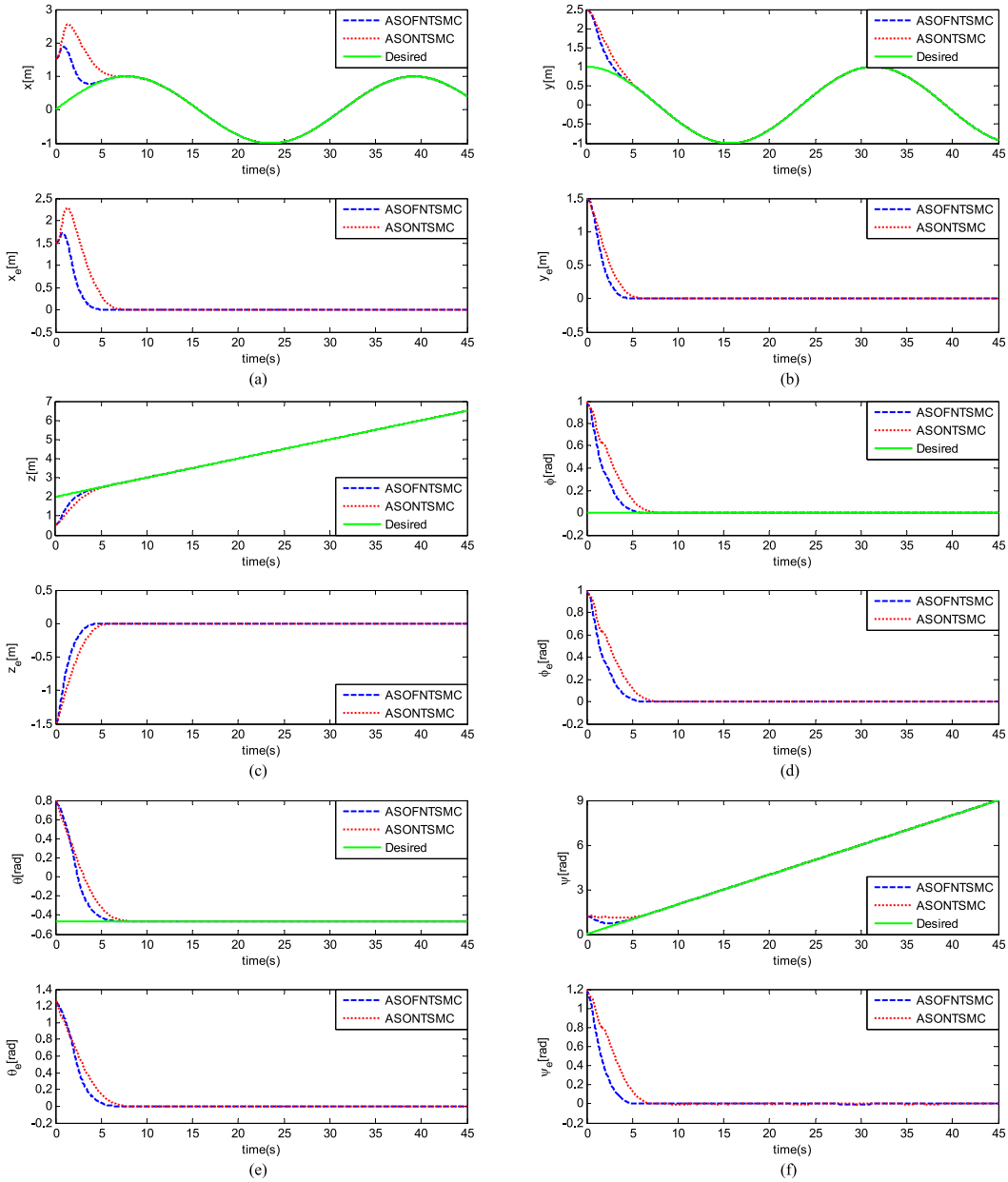

Fig. 12. Tracking results for each state of the ODIN under the ASOFNTSMC and ASONTSMC schemes. (a) Tracking response of position x and its tracking error. (b) Tracking response of position y and its tracking error. (c) Tracking response of position z and its tracking error. (d) Tracking response of roll angle ϕ and its tracking error. (e) Tracking response of pitch angle θ and its tracking error. (f) Tracking response of yaw angle ψ and its tracking error.

with dynamic uncertainties and time-varying external disturbances. A SOFNTSM manifold, which consists of a PDSM manifold and a FNTSM manifold, is first designed to guarantee a faster convergence rate than the SONTSM manifold [30]. Then, by using this SOFNTSM manifold, an ASOFNTSMC scheme is developed for the trajectory tracking of fully actuated AUVs. The designed SOFNTSM manifold ensures that the PDSM variable vector fast converges to zero in finite time and then the position and attitude tracking errors locally converge to zero exponentially, and the developed ASOFNTSMC scheme drives the error trajectories to the SOFNTSM manifold and then keeps them on the manifold to realize the sliding mode motion in spite of dynamic uncertainties and time-varying external disturbances. The expression of the bounding function of the system uncertainty is derived in detail and adaptive tuning laws are used to estimate the unknown parameters of the system uncertainty bounds so that the bound information of the system uncertainty is not required. Meanwhile, the discontinuous sign function is contained in the time derivative of the control input and therefore chattering is eliminated without reducing the tracking precision. In comparison with the ASONTSMC scheme [30], the proposed ASOFNTSMC scheme provides a faster convergence rate for the trajectory tracking control of fully actuated AUVs. Two comparative simulation cases between the ASOFNTSMC scheme and the ASONTSMC scheme are performed on two fully actuated AUVs, respectively. The results show the superiority

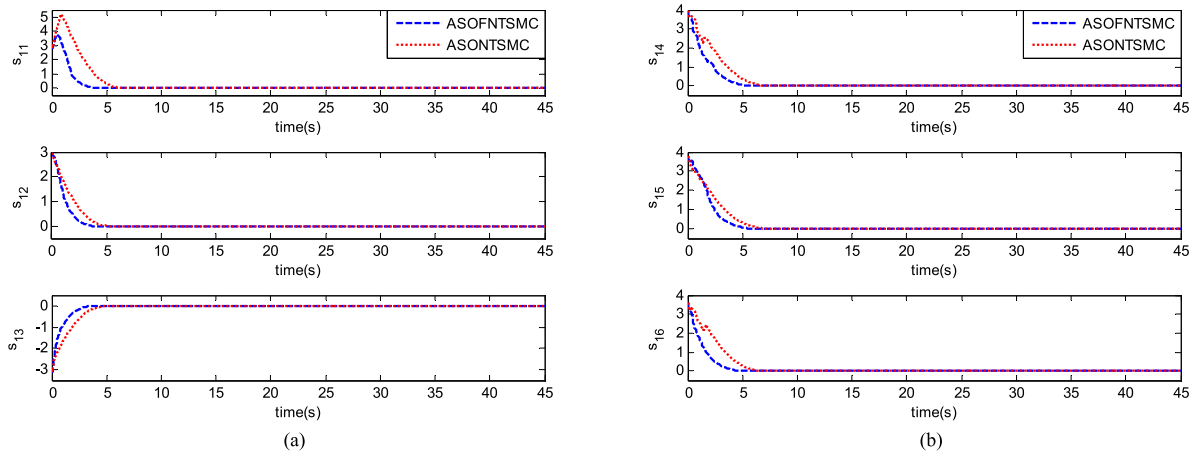

Fig. 13. Responses of the PDSM variable vector $\boldsymbol{s}_1$ under the ASOFNTSMC and ASONTSMC schemes. (a) s_{1i} for $i = 1, 2, 3$. (b) s_{1i} for $i = 4, 5, 6$.

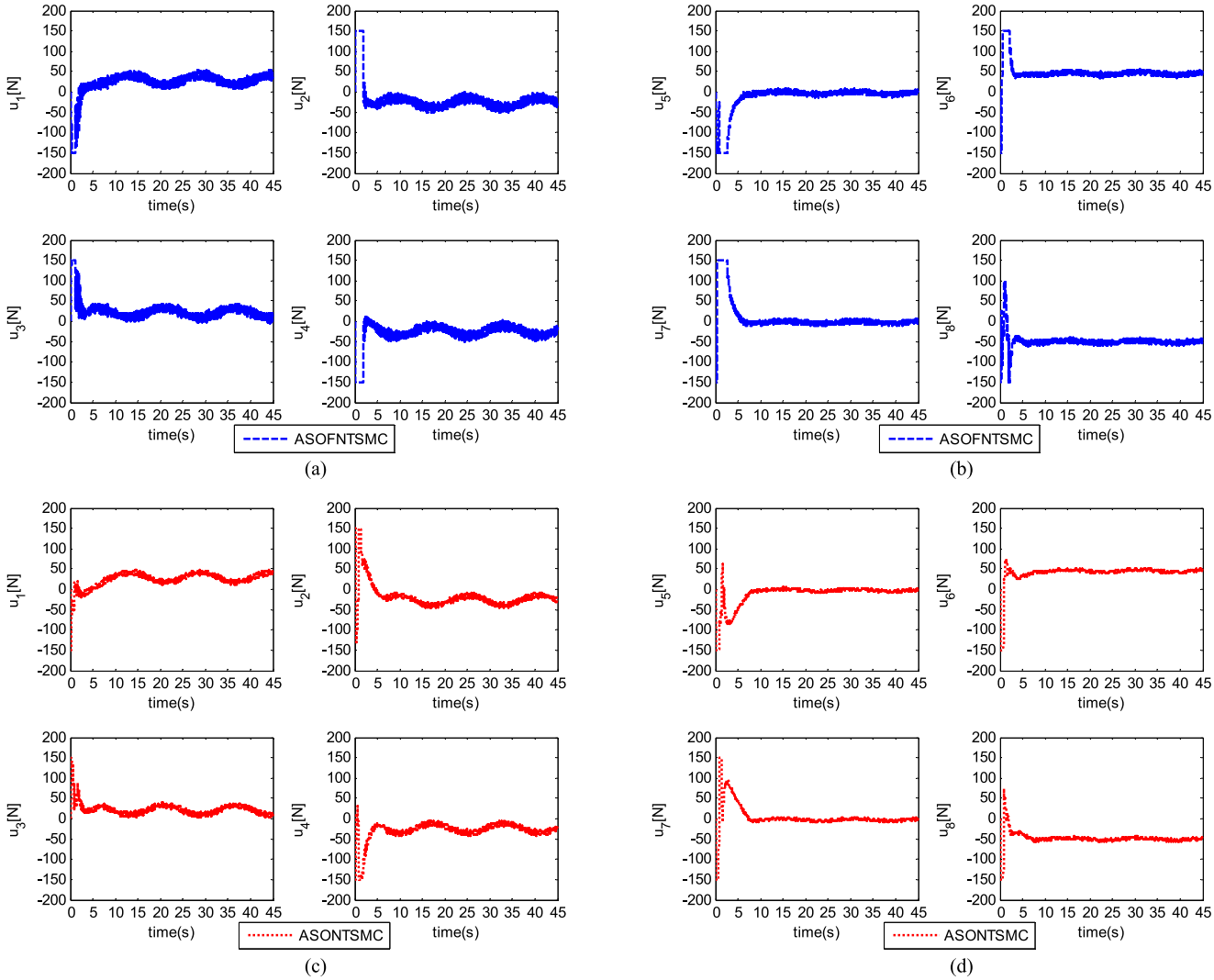

Fig. 14. Force produced by each thruster of the ODIN under the ASOFNTSMC and ASONTSMC schemes. (a) Forces produced by horizontal thrusters 1–4 under the ASOFNTSMC scheme. (b) Forces produced by vertical thrusters 5–8 under the ASOFNTSMC scheme. (c) Forces produced by horizontal thrusters 1–4 under the ASONTSMC scheme. (d) Forces produced by vertical thrusters 5–8 under the ASONTSMC scheme.

of the ASOFNTSMC scheme over the ASONTSMC scheme in terms of convergence rate.

APPENDIX A

Details about Assumption 5

From (19), $\ddot{\boldsymbol{\eta}}$ can be written as

$$\ddot{\boldsymbol{\eta}} = \hat{\boldsymbol{M}}^{-1}(\boldsymbol{\eta})(\boldsymbol{\tau}_{\eta} + \boldsymbol{\tau}_{\rho\eta} - \hat{\boldsymbol{C}}(\boldsymbol{\vartheta},\boldsymbol{\eta})\dot{\boldsymbol{\eta}} - \hat{\boldsymbol{D}}(\boldsymbol{\vartheta},\boldsymbol{\eta})\dot{\boldsymbol{\eta}} - \hat{\boldsymbol{G}}(\boldsymbol{\eta})). \tag{A.1}$$

Using (A.1) in (20), we have

$$\begin{aligned}
\boldsymbol{\tau}_{\rho\eta} =& -\tilde{\boldsymbol{M}}(\boldsymbol{\eta})\hat{\boldsymbol{M}}^{-1}(\boldsymbol{\eta})(\boldsymbol{\tau}_{\eta} + \boldsymbol{\tau}_{\rho\eta} - \hat{\boldsymbol{C}}(\boldsymbol{\vartheta},\boldsymbol{\eta})\dot{\boldsymbol{\eta}} \\
&\qquad - \hat{\boldsymbol{D}}(\boldsymbol{\vartheta},\boldsymbol{\eta})\dot{\boldsymbol{\eta}} - \hat{\boldsymbol{G}}(\boldsymbol{\eta})) \\
&- \tilde{\boldsymbol{C}}(\boldsymbol{\vartheta},\boldsymbol{\eta})\dot{\boldsymbol{\eta}} - \tilde{\boldsymbol{D}}(\boldsymbol{\vartheta},\boldsymbol{\eta})\dot{\boldsymbol{\eta}} - \tilde{\boldsymbol{G}}(\boldsymbol{\eta}) - \boldsymbol{\tau}_{d\eta} \\
=& -(\boldsymbol{M}(\boldsymbol{\eta}) - \hat{\boldsymbol{M}}(\boldsymbol{\eta}))\hat{\boldsymbol{M}}^{-1}(\boldsymbol{\eta}) \\
&\times \left(\boldsymbol{\tau}_{\eta} + \boldsymbol{\tau}_{\rho\eta} - \hat{\boldsymbol{C}}(\boldsymbol{\vartheta},\boldsymbol{\eta})\dot{\boldsymbol{\eta}} - \hat{\boldsymbol{D}}(\boldsymbol{\vartheta},\boldsymbol{\eta})\dot{\boldsymbol{\eta}} - \hat{\boldsymbol{G}}(\boldsymbol{\eta})\right) \\
&- \tilde{\boldsymbol{C}}(\boldsymbol{\vartheta},\boldsymbol{\eta})\dot{\boldsymbol{\eta}} - \tilde{\boldsymbol{D}}(\boldsymbol{\vartheta},\boldsymbol{\eta})\dot{\boldsymbol{\eta}} - \tilde{\boldsymbol{G}}(\boldsymbol{\eta}) - \boldsymbol{\tau}_{d\eta} \\
=& (\boldsymbol{I} - \boldsymbol{M}(\boldsymbol{\eta})\hat{\boldsymbol{M}}^{-1}(\boldsymbol{\eta})) \\
&\times (\boldsymbol{\tau}_{\eta} + \boldsymbol{\tau}_{\rho\eta} - \hat{\boldsymbol{C}}(\boldsymbol{\vartheta},\boldsymbol{\eta})\dot{\boldsymbol{\eta}} - \hat{\boldsymbol{D}}(\boldsymbol{\vartheta},\boldsymbol{\eta})\dot{\boldsymbol{\eta}} - \hat{\boldsymbol{G}}(\boldsymbol{\eta})) \\
&- \tilde{\boldsymbol{C}}(\boldsymbol{\vartheta},\boldsymbol{\eta})\dot{\boldsymbol{\eta}} - \tilde{\boldsymbol{D}}(\boldsymbol{\vartheta},\boldsymbol{\eta})\dot{\boldsymbol{\eta}} - \tilde{\boldsymbol{G}}(\boldsymbol{\eta}) - \boldsymbol{\tau}_{d\eta} \\
=& (\boldsymbol{I} - \boldsymbol{M}(\boldsymbol{\eta})\hat{\boldsymbol{M}}^{-1}(\boldsymbol{\eta}))\boldsymbol{\tau}_{\rho\eta} + (\boldsymbol{I} - \boldsymbol{M}(\boldsymbol{\eta})\hat{\boldsymbol{M}}^{-1}(\boldsymbol{\eta})) \\
&\times (\boldsymbol{\tau}_{\eta} - \hat{\boldsymbol{C}}(\boldsymbol{\vartheta},\boldsymbol{\eta})\dot{\boldsymbol{\eta}} - \hat{\boldsymbol{D}}(\boldsymbol{\vartheta},\boldsymbol{\eta})\dot{\boldsymbol{\eta}} - \hat{\boldsymbol{G}}(\boldsymbol{\eta})) \\
&- \tilde{\boldsymbol{C}}(\boldsymbol{\vartheta},\boldsymbol{\eta})\dot{\boldsymbol{\eta}} - \tilde{\boldsymbol{D}}(\boldsymbol{\vartheta},\boldsymbol{\eta})\dot{\boldsymbol{\eta}} - \tilde{\boldsymbol{G}}(\boldsymbol{\eta}) - \boldsymbol{\tau}_{d\eta}
\end{aligned} \tag{A.2}$$

or

$$\begin{aligned}
\boldsymbol{\tau}_{\rho\eta} =& \hat{\boldsymbol{M}}(\boldsymbol{\eta})\boldsymbol{M}^{-1}(\boldsymbol{\eta})(\boldsymbol{I} - \boldsymbol{M}(\boldsymbol{\eta})\hat{\boldsymbol{M}}^{-1}(\boldsymbol{\eta}))\boldsymbol{\tau}_{\eta} \\
&- \hat{\boldsymbol{M}}(\boldsymbol{\eta})\boldsymbol{M}^{-1}(\boldsymbol{\eta})(\boldsymbol{I} - \boldsymbol{M}(\boldsymbol{\eta})\hat{\boldsymbol{M}}^{-1}(\boldsymbol{\eta})) \\
&\times (\hat{\boldsymbol{C}}(\boldsymbol{\vartheta},\boldsymbol{\eta})\dot{\boldsymbol{\eta}} + \hat{\boldsymbol{D}}(\boldsymbol{\vartheta},\boldsymbol{\eta})\dot{\boldsymbol{\eta}} + \hat{\boldsymbol{G}}(\boldsymbol{\eta})) \\
&- \hat{\boldsymbol{M}}(\boldsymbol{\eta})\boldsymbol{M}^{-1}(\boldsymbol{\eta})(\tilde{\boldsymbol{C}}(\boldsymbol{\vartheta},\boldsymbol{\eta})\dot{\boldsymbol{\eta}} + \tilde{\boldsymbol{D}}(\boldsymbol{\vartheta},\boldsymbol{\eta})\dot{\boldsymbol{\eta}} + \tilde{\boldsymbol{G}}(\boldsymbol{\eta})) \\
&- \hat{\boldsymbol{M}}(\boldsymbol{\eta})\boldsymbol{M}^{-1}(\boldsymbol{\eta})\boldsymbol{\tau}_{d\eta} \\
=& (\hat{\boldsymbol{M}}(\boldsymbol{\eta})\boldsymbol{M}^{-1}(\boldsymbol{\eta}) - \boldsymbol{I})\boldsymbol{\tau}_{\eta} \\
&- (\hat{\boldsymbol{M}}(\boldsymbol{\eta})\boldsymbol{M}^{-1}(\boldsymbol{\eta}) - \boldsymbol{I})(\hat{\boldsymbol{C}}(\boldsymbol{\vartheta},\boldsymbol{\eta})\dot{\boldsymbol{\eta}} \\
&+ \hat{\boldsymbol{D}}(\boldsymbol{\vartheta},\boldsymbol{\eta})\dot{\boldsymbol{\eta}} + \hat{\boldsymbol{G}}(\boldsymbol{\eta})) \\
&- \hat{\boldsymbol{M}}(\boldsymbol{\eta})\boldsymbol{M}^{-1}(\boldsymbol{\eta})(\tilde{\boldsymbol{C}}(\boldsymbol{\vartheta},\boldsymbol{\eta})\dot{\boldsymbol{\eta}} + \tilde{\boldsymbol{D}}(\boldsymbol{\vartheta},\boldsymbol{\eta})\dot{\boldsymbol{\eta}} + \tilde{\boldsymbol{G}}(\boldsymbol{\eta})) \\
&- \hat{\boldsymbol{M}}(\boldsymbol{\eta})\boldsymbol{M}^{-1}(\boldsymbol{\eta})\boldsymbol{\tau}_{d\eta}.
\end{aligned} \tag{A.3}$$

Then

$$\begin{aligned}
\|\boldsymbol{\tau}_{\rho\eta}\| \le& \left\|\hat{\boldsymbol{M}}(\boldsymbol{\eta})\boldsymbol{M}^{-1}(\boldsymbol{\eta}) - \boldsymbol{I}\right\| \|\boldsymbol{\tau}_{\eta}\| \\
&+ \left\|\hat{\boldsymbol{M}}(\boldsymbol{\eta})\boldsymbol{M}^{-1}(\boldsymbol{\eta}) - \boldsymbol{I}\right\| \\
&\times \left\|\hat{\boldsymbol{C}}(\boldsymbol{\vartheta},\boldsymbol{\eta})\dot{\boldsymbol{\eta}} + \hat{\boldsymbol{D}}(\boldsymbol{\vartheta},\boldsymbol{\eta})\dot{\boldsymbol{\eta}} + \hat{\boldsymbol{G}}(\boldsymbol{\eta})\right\| \\
&+ \left\|\hat{\boldsymbol{M}}(\boldsymbol{\eta})\boldsymbol{M}^{-1}(\boldsymbol{\eta})\right\| \\
&\times \left\|\tilde{\boldsymbol{C}}(\boldsymbol{\vartheta},\boldsymbol{\eta})\dot{\boldsymbol{\eta}} + \tilde{\boldsymbol{D}}(\boldsymbol{\vartheta},\boldsymbol{\eta})\dot{\boldsymbol{\eta}} + \tilde{\boldsymbol{G}}(\boldsymbol{\eta})\right\| \\
&+ \left\|\hat{\boldsymbol{M}}(\boldsymbol{\eta})\boldsymbol{M}^{-1}(\boldsymbol{\eta})\right\| \|\boldsymbol{\tau}_{d\eta}\|.
\end{aligned} \tag{A.4}$$

Based on (17), (18), and Assumptions 1–4, we have the following inequalities:

$$\begin{aligned}
&\left\|\hat{\boldsymbol{M}}(\boldsymbol{\eta})\boldsymbol{M}^{-1}(\boldsymbol{\eta}) - \boldsymbol{I}\right\| \le c_1 \\
&\left\|\hat{\boldsymbol{M}}(\boldsymbol{\eta})\boldsymbol{M}^{-1}(\boldsymbol{\eta})\right\| \le c_2 \\
&\left\|\hat{\boldsymbol{C}}(\boldsymbol{\vartheta},\boldsymbol{\eta})\dot{\boldsymbol{\eta}} + \hat{\boldsymbol{D}}(\boldsymbol{\vartheta},\boldsymbol{\eta})\dot{\boldsymbol{\eta}} + \hat{\boldsymbol{G}}(\boldsymbol{\eta})\right\| \le c_3 \\
&\quad + c_4\|\dot{\boldsymbol{\eta}}\| + c_5\|\boldsymbol{\vartheta}\|\|\dot{\boldsymbol{\eta}}\| + c_6\|\dot{\boldsymbol{\eta}}\|^2 \\
&\left\|\tilde{\boldsymbol{C}}(\boldsymbol{\vartheta},\boldsymbol{\eta})\dot{\boldsymbol{\eta}} + \tilde{\boldsymbol{D}}(\boldsymbol{\vartheta},\boldsymbol{\eta})\dot{\boldsymbol{\eta}} + \tilde{\boldsymbol{G}}(\boldsymbol{\eta})\right\| \le c_7 \\
&\quad + c_8\|\dot{\boldsymbol{\eta}}\| + c_9\|\boldsymbol{\vartheta}\|\|\dot{\boldsymbol{\eta}}\| + c_{10}\|\dot{\boldsymbol{\eta}}\|^2 \\
&\|\boldsymbol{\tau}_{d\eta}\| = \left\|\boldsymbol{J}^{-T}\boldsymbol{\tau}_{d\vartheta}\right\| \le \left\|\boldsymbol{J}^{-T}\right\| \|\boldsymbol{\tau}_{d\vartheta}\| \le \bar{J}_1\alpha_0
\end{aligned} \tag{A.5}$$

where c_i $(i = 1, 2, 7, \ldots, 10)$ are unknown positive constants, c_i $(i = 3, \ldots, 6)$ are known positive constants, and $\bar{J}_1$, α_0 are defined in Assumptions 1 and 3, respectively.

Using (A.5) in (A.4), we get

$$\begin{aligned}
\|\boldsymbol{\tau}_{\rho\eta}\| \le& c_1\|\boldsymbol{\tau}_{\eta}\| + (c_1c_3 + c_2c_7 + c_2\bar{J}_1\alpha_0) \\
&+ (c_1c_4 + c_2c_8)\|\dot{\boldsymbol{\eta}}\| + (c_1c_5 + c_2c_9)\|\boldsymbol{\vartheta}\|\|\dot{\boldsymbol{\eta}}\| \\
&+ (c_1c_6 + c_2c_{10})\|\dot{\boldsymbol{\eta}}\|^2.
\end{aligned} \tag{A.6}$$

Equation (A.6) implies that the upper bound of the lumped uncertainty $\boldsymbol{\tau}_{\rho\eta}$ is input related. However, according to [26], if the thrust saturation effect is not serious, the control input $\boldsymbol{\tau}_{\vartheta}$ can be bounded by a known positive constant. As a result, $\boldsymbol{\tau}_{\eta}$ can be bounded such that $\|\boldsymbol{\tau}_{\eta}\| = \|\boldsymbol{J}^{-T}\boldsymbol{\tau}_{\vartheta}\| \le c_{11}$, where c_{11} is a known positive constant. Therefore, let $\beta_0 = c_1c_{11} + c_1c_3 + c_2c_7 + c_2\bar{J}_1\alpha_0$, $\beta_1 = c_1c_4 + c_2c_8$, $\beta_2 = c_1c_5 + c_2c_9$, and $\beta_3 = c_1c_6 + c_2c_{10}$, then the inequality (21) given in Assumption 5 is satisfied.

APPENDIX B

Details about Assumption 7

From (17) and Assumptions 1, 2, and 4, there exist known positive constants d_0 and d_1 such that the following inequality

holds

$$\begin{aligned}&\left\|\dot{\widehat{\boldsymbol{M}^{-1}(\boldsymbol{\eta})}}+\boldsymbol{K}_1\hat{\boldsymbol{M}}^{-1}(\boldsymbol{\eta})\right\|\\&\quad=\left\|\dot{\boldsymbol{J}}\hat{\boldsymbol{M}}^{-1}\boldsymbol{J}^T+\boldsymbol{J}\hat{\boldsymbol{M}}^{-1}\dot{\boldsymbol{J}}^T+\boldsymbol{K}_1\hat{\boldsymbol{M}}^{-1}(\boldsymbol{\eta})\right\|\\&\quad\le d_0+d_1\left\|\dot{\boldsymbol{\eta}}\right\|.\end{aligned}\tag{B.1}$$

Then, it follows from (B.1) and Assumption 5 that

$$\begin{aligned}&\left\|(\dot{\widehat{\boldsymbol{M}^{-1}(\boldsymbol{\eta})}}+\boldsymbol{K}_1\hat{\boldsymbol{M}}^{-1}(\boldsymbol{\eta}))\boldsymbol{\tau}_{\rho\eta}\right\|\\&\le\left\|\dot{\widehat{\boldsymbol{M}^{-1}(\boldsymbol{\eta})}}+\boldsymbol{K}_1\hat{\boldsymbol{M}}^{-1}(\boldsymbol{\eta})\right\|\|\boldsymbol{\tau}_{\rho\eta}\|\\&\le d_0\beta_0+(d_0\beta_1+d_1\beta_0)\|\dot{\boldsymbol{\eta}}\|+d_0\beta_2\|\boldsymbol{\vartheta}\|\|\dot{\boldsymbol{\eta}}\|\\&\quad+(d_0\beta_3+d_1\beta_1)\|\dot{\boldsymbol{\eta}}\|^2+d_1\beta_2\|\boldsymbol{\vartheta}\|\|\dot{\boldsymbol{\eta}}\|^2+d_1\beta_3\|\dot{\boldsymbol{\eta}}\|^3.\end{aligned}\tag{B.2}$$

From (A.1) and (A.3), it can be obtained that

$$\begin{aligned}\dot{\boldsymbol{\tau}}_{\rho\eta}=&\dot{\widehat{(\hat{\boldsymbol{M}}(\boldsymbol{\eta})\boldsymbol{M}^{-1}(\boldsymbol{\eta})-\boldsymbol{I})}}\boldsymbol{\tau}_\eta+(\hat{\boldsymbol{M}}(\boldsymbol{\eta})\boldsymbol{M}^{-1}(\boldsymbol{\eta})-\boldsymbol{I})\dot{\boldsymbol{\tau}}_\eta\\&-\dot{\widehat{(\hat{\boldsymbol{M}}(\boldsymbol{\eta})\boldsymbol{M}^{-1}(\boldsymbol{\eta})-\boldsymbol{I})}}\\&\times(\hat{\boldsymbol{C}}(\boldsymbol{\vartheta},\boldsymbol{\eta})\dot{\boldsymbol{\eta}}+\hat{\boldsymbol{D}}(\boldsymbol{\vartheta},\boldsymbol{\eta})\dot{\boldsymbol{\eta}}+\hat{\boldsymbol{G}}(\boldsymbol{\eta}))\\&-(\hat{\boldsymbol{M}}(\boldsymbol{\eta})\boldsymbol{M}^{-1}(\boldsymbol{\eta})-\boldsymbol{I})\\&\times\dot{\widehat{(\hat{\boldsymbol{C}}(\boldsymbol{\vartheta},\boldsymbol{\eta})\dot{\boldsymbol{\eta}}+\hat{\boldsymbol{D}}(\boldsymbol{\vartheta},\boldsymbol{\eta})\dot{\boldsymbol{\eta}}+\hat{\boldsymbol{G}}(\boldsymbol{\eta}))}}\\&-\dot{\widehat{\hat{\boldsymbol{M}}(\boldsymbol{\eta})\boldsymbol{M}^{-1}(\boldsymbol{\eta})}}(\tilde{\boldsymbol{C}}(\boldsymbol{\vartheta},\boldsymbol{\eta})\dot{\boldsymbol{\eta}}+\tilde{\boldsymbol{D}}(\boldsymbol{\vartheta},\boldsymbol{\eta})\dot{\boldsymbol{\eta}}+\tilde{\boldsymbol{G}}(\boldsymbol{\eta}))\\&-\hat{\boldsymbol{M}}(\boldsymbol{\eta})\boldsymbol{M}^{-1}(\boldsymbol{\eta})\dot{\widehat{(\tilde{\boldsymbol{C}}(\boldsymbol{\vartheta},\boldsymbol{\eta})\dot{\boldsymbol{\eta}}+\tilde{\boldsymbol{D}}(\boldsymbol{\vartheta},\boldsymbol{\eta})\dot{\boldsymbol{\eta}}+\tilde{\boldsymbol{G}}(\boldsymbol{\eta}))}}\\&-\dot{\widehat{\hat{\boldsymbol{M}}(\boldsymbol{\eta})\boldsymbol{M}^{-1}(\boldsymbol{\eta})}}\boldsymbol{\tau}_{d\eta}-\hat{\boldsymbol{M}}(\boldsymbol{\eta})\boldsymbol{M}^{-1}(\boldsymbol{\eta})\dot{\boldsymbol{\tau}}_{d\eta}\\=&(\dot{\hat{\boldsymbol{M}}}(\boldsymbol{\eta})\boldsymbol{M}^{-1}(\boldsymbol{\eta})+\hat{\boldsymbol{M}}(\boldsymbol{\eta})\dot{\widehat{\boldsymbol{M}^{-1}(\boldsymbol{\eta})}})\boldsymbol{\tau}_\eta\\&+(\hat{\boldsymbol{M}}(\boldsymbol{\eta})\boldsymbol{M}^{-1}(\boldsymbol{\eta})-\boldsymbol{I})\dot{\boldsymbol{\tau}}_\eta\\&-(\dot{\hat{\boldsymbol{M}}}(\boldsymbol{\eta})\boldsymbol{M}^{-1}(\boldsymbol{\eta})+\hat{\boldsymbol{M}}(\boldsymbol{\eta})\dot{\widehat{\boldsymbol{M}^{-1}(\boldsymbol{\eta})}})\\&\times(\hat{\boldsymbol{C}}(\boldsymbol{\vartheta},\boldsymbol{\eta})\dot{\boldsymbol{\eta}}+\hat{\boldsymbol{D}}(\boldsymbol{\vartheta},\boldsymbol{\eta})\dot{\boldsymbol{\eta}}+\hat{\boldsymbol{G}}(\boldsymbol{\eta}))\\&-(\hat{\boldsymbol{M}}(\boldsymbol{\eta})\boldsymbol{M}^{-1}(\boldsymbol{\eta})-\boldsymbol{I})(\dot{\hat{\boldsymbol{C}}}(\boldsymbol{\vartheta},\boldsymbol{\eta})\dot{\boldsymbol{\eta}}\\&+\dot{\hat{\boldsymbol{D}}}(\boldsymbol{\vartheta},\boldsymbol{\eta})\dot{\boldsymbol{\eta}}+\dot{\hat{\boldsymbol{G}}}(\boldsymbol{\eta}))\\&-(\dot{\hat{\boldsymbol{M}}}(\boldsymbol{\eta})\boldsymbol{M}^{-1}(\boldsymbol{\eta})+\hat{\boldsymbol{M}}(\boldsymbol{\eta})\dot{\widehat{\boldsymbol{M}^{-1}(\boldsymbol{\eta})}})\\&\times(\tilde{\boldsymbol{C}}(\boldsymbol{\vartheta},\boldsymbol{\eta})\dot{\boldsymbol{\eta}}+\tilde{\boldsymbol{D}}(\boldsymbol{\vartheta},\boldsymbol{\eta})\dot{\boldsymbol{\eta}}+\tilde{\boldsymbol{G}}(\boldsymbol{\eta}))\\&-\hat{\boldsymbol{M}}(\boldsymbol{\eta})\boldsymbol{M}^{-1}(\boldsymbol{\eta})(\dot{\tilde{\boldsymbol{C}}}(\boldsymbol{\vartheta},\boldsymbol{\eta})\dot{\boldsymbol{\eta}}+\dot{\tilde{\boldsymbol{D}}}(\boldsymbol{\vartheta},\boldsymbol{\eta})\dot{\boldsymbol{\eta}}+\dot{\tilde{\boldsymbol{G}}}(\boldsymbol{\eta}))\\&-(\hat{\boldsymbol{M}}(\boldsymbol{\eta})\boldsymbol{M}^{-1}(\boldsymbol{\eta})-\boldsymbol{I})(\hat{\boldsymbol{C}}(\boldsymbol{\vartheta},\boldsymbol{\eta})+\hat{\boldsymbol{D}}(\boldsymbol{\vartheta},\boldsymbol{\eta}))\\&\times\hat{\boldsymbol{M}}^{-1}(\boldsymbol{\eta})(\boldsymbol{\tau}_\eta+\boldsymbol{\tau}_{\rho\eta}-\hat{\boldsymbol{C}}(\boldsymbol{\vartheta},\boldsymbol{\eta})\dot{\boldsymbol{\eta}}-\hat{\boldsymbol{D}}(\boldsymbol{\vartheta},\boldsymbol{\eta})\dot{\boldsymbol{\eta}}-\hat{\boldsymbol{G}}(\boldsymbol{\eta}))\\&-\hat{\boldsymbol{M}}(\boldsymbol{\eta})\boldsymbol{M}^{-1}(\boldsymbol{\eta})(\tilde{\boldsymbol{C}}(\boldsymbol{\vartheta},\boldsymbol{\eta})+\tilde{\boldsymbol{D}}(\boldsymbol{\vartheta},\boldsymbol{\eta}))\\&\times\hat{\boldsymbol{M}}^{-1}(\boldsymbol{\eta})(\boldsymbol{\tau}_\eta+\boldsymbol{\tau}_{\rho\eta}-\hat{\boldsymbol{C}}(\boldsymbol{\vartheta},\boldsymbol{\eta})\dot{\boldsymbol{\eta}}-\hat{\boldsymbol{D}}(\boldsymbol{\vartheta},\boldsymbol{\eta})\dot{\boldsymbol{\eta}}-\hat{\boldsymbol{G}}(\boldsymbol{\eta}))\\&-(\dot{\hat{\boldsymbol{M}}}(\boldsymbol{\eta})\boldsymbol{M}^{-1}(\boldsymbol{\eta})+\hat{\boldsymbol{M}}(\boldsymbol{\eta})\dot{\widehat{\boldsymbol{M}^{-1}(\boldsymbol{\eta})}})\boldsymbol{\tau}_{d\eta}\\&-\hat{\boldsymbol{M}}(\boldsymbol{\eta})\boldsymbol{M}^{-1}(\boldsymbol{\eta})\dot{\boldsymbol{\tau}}_{d\eta}\\=&\{\dot{\hat{\boldsymbol{M}}}(\boldsymbol{\eta})\boldsymbol{M}^{-1}(\boldsymbol{\eta})+\hat{\boldsymbol{M}}(\boldsymbol{\eta})\dot{\widehat{\boldsymbol{M}^{-1}(\boldsymbol{\eta})}}\\&-[(\hat{\boldsymbol{M}}(\boldsymbol{\eta})\boldsymbol{M}^{-1}(\boldsymbol{\eta})-\boldsymbol{I})\\&\quad\times(\hat{\boldsymbol{C}}(\boldsymbol{\vartheta},\boldsymbol{\eta})+\hat{\boldsymbol{D}}(\boldsymbol{\vartheta},\boldsymbol{\eta}))+\hat{\boldsymbol{M}}(\boldsymbol{\eta})\boldsymbol{M}^{-1}(\boldsymbol{\eta})\\&\quad\times(\tilde{\boldsymbol{C}}(\boldsymbol{\vartheta},\boldsymbol{\eta})+\tilde{\boldsymbol{D}}(\boldsymbol{\vartheta},\boldsymbol{\eta}))]\hat{\boldsymbol{M}}^{-1}(\boldsymbol{\eta})\}\boldsymbol{\tau}_\eta\\&+(\hat{\boldsymbol{M}}(\boldsymbol{\eta})\boldsymbol{M}^{-1}(\boldsymbol{\eta})-\boldsymbol{I})\dot{\boldsymbol{\tau}}_\eta\\&-[(\hat{\boldsymbol{M}}(\boldsymbol{\eta})\boldsymbol{M}^{-1}(\boldsymbol{\eta})-\boldsymbol{I})(\hat{\boldsymbol{C}}(\boldsymbol{\vartheta},\boldsymbol{\eta})+\hat{\boldsymbol{D}}(\boldsymbol{\vartheta},\boldsymbol{\eta}))\\&\quad+\hat{\boldsymbol{M}}(\boldsymbol{\eta})\boldsymbol{M}^{-1}(\boldsymbol{\eta})(\tilde{\boldsymbol{C}}(\boldsymbol{\vartheta},\boldsymbol{\eta})+\tilde{\boldsymbol{D}}(\boldsymbol{\vartheta},\boldsymbol{\eta}))]\hat{\boldsymbol{M}}^{-1}(\boldsymbol{\eta})\boldsymbol{\tau}_{\rho\eta}\\&-\{\dot{\hat{\boldsymbol{M}}}(\boldsymbol{\eta})\boldsymbol{M}^{-1}(\boldsymbol{\eta})+\hat{\boldsymbol{M}}(\boldsymbol{\eta})\dot{\widehat{\boldsymbol{M}^{-1}(\boldsymbol{\eta})}}\\&\quad-[(\hat{\boldsymbol{M}}(\boldsymbol{\eta})\boldsymbol{M}^{-1}(\boldsymbol{\eta})-\boldsymbol{I})\\&\quad\times(\hat{\boldsymbol{C}}(\boldsymbol{\vartheta},\boldsymbol{\eta})+\hat{\boldsymbol{D}}(\boldsymbol{\vartheta},\boldsymbol{\eta}))+\hat{\boldsymbol{M}}(\boldsymbol{\eta})\boldsymbol{M}^{-1}(\boldsymbol{\eta})\\&\quad\times(\tilde{\boldsymbol{C}}(\boldsymbol{\vartheta},\boldsymbol{\eta})+\tilde{\boldsymbol{D}}(\boldsymbol{\vartheta},\boldsymbol{\eta}))]\hat{\boldsymbol{M}}^{-1}(\boldsymbol{\eta})\}\\&\times(\hat{\boldsymbol{C}}(\boldsymbol{\vartheta},\boldsymbol{\eta})\dot{\boldsymbol{\eta}}+\hat{\boldsymbol{D}}(\boldsymbol{\vartheta},\boldsymbol{\eta})\dot{\boldsymbol{\eta}}+\hat{\boldsymbol{G}}(\boldsymbol{\eta}))\\&-(\dot{\hat{\boldsymbol{M}}}(\boldsymbol{\eta})\boldsymbol{M}^{-1}(\boldsymbol{\eta})+\hat{\boldsymbol{M}}(\boldsymbol{\eta})\dot{\widehat{\boldsymbol{M}^{-1}(\boldsymbol{\eta})}})\\&\times(\tilde{\boldsymbol{C}}(\boldsymbol{\vartheta},\boldsymbol{\eta})\dot{\boldsymbol{\eta}}+\tilde{\boldsymbol{D}}(\boldsymbol{\vartheta},\boldsymbol{\eta})\dot{\boldsymbol{\eta}}+\tilde{\boldsymbol{G}}(\boldsymbol{\eta}))\\&-(\hat{\boldsymbol{M}}(\boldsymbol{\eta})\boldsymbol{M}^{-1}(\boldsymbol{\eta})-\boldsymbol{I})\\&\times(\dot{\hat{\boldsymbol{C}}}(\boldsymbol{\vartheta},\boldsymbol{\eta})\dot{\boldsymbol{\eta}}+\dot{\hat{\boldsymbol{D}}}(\boldsymbol{\vartheta},\boldsymbol{\eta})\dot{\boldsymbol{\eta}}+\dot{\hat{\boldsymbol{G}}}(\boldsymbol{\eta}))\\&-\hat{\boldsymbol{M}}(\boldsymbol{\eta})\boldsymbol{M}^{-1}(\boldsymbol{\eta})(\dot{\tilde{\boldsymbol{C}}}(\boldsymbol{\vartheta},\boldsymbol{\eta})\dot{\boldsymbol{\eta}}+\dot{\tilde{\boldsymbol{D}}}(\boldsymbol{\vartheta},\boldsymbol{\eta})\dot{\boldsymbol{\eta}}+\dot{\tilde{\boldsymbol{G}}}(\boldsymbol{\eta}))\\&-(\dot{\hat{\boldsymbol{M}}}(\boldsymbol{\eta})\boldsymbol{M}^{-1}(\boldsymbol{\eta})+\hat{\boldsymbol{M}}(\boldsymbol{\eta})\dot{\widehat{\boldsymbol{M}^{-1}(\boldsymbol{\eta})}})\boldsymbol{\tau}_{d\eta}\\&-\hat{\boldsymbol{M}}(\boldsymbol{\eta})\boldsymbol{M}^{-1}(\boldsymbol{\eta})\dot{\boldsymbol{\tau}}_{d\eta}.\end{aligned}\tag{B.3}$$

Then

$$\begin{aligned}
\|\dot{\boldsymbol{\tau}}_{\rho\eta}\| \leq & \left(\left\| \dot{\hat{\boldsymbol{M}}}(\boldsymbol{\eta})\boldsymbol{M}^{-1}(\boldsymbol{\eta}) + \hat{\boldsymbol{M}}(\boldsymbol{\eta})\dot{\overbrace{\boldsymbol{M}^{-1}(\boldsymbol{\eta})}} \right\| \right. \\
& + \left\| [(\hat{\boldsymbol{M}}(\boldsymbol{\eta})\boldsymbol{M}^{-1}(\boldsymbol{\eta}) - \boldsymbol{I})(\hat{\boldsymbol{C}}(\boldsymbol{\vartheta},\boldsymbol{\eta}) + \hat{\boldsymbol{D}}(\boldsymbol{\vartheta},\boldsymbol{\eta})) \right. \\
& + \hat{\boldsymbol{M}}(\boldsymbol{\eta})\boldsymbol{M}^{-1}(\boldsymbol{\eta})(\tilde{\boldsymbol{C}}(\boldsymbol{\vartheta},\boldsymbol{\eta}) \\
& \left. \left. + \tilde{\boldsymbol{D}}(\boldsymbol{\vartheta},\boldsymbol{\eta}))]\hat{\boldsymbol{M}}^{-1}(\boldsymbol{\eta}) \right\| \right) \|\boldsymbol{\tau}_{\eta}\| \\
& + \left\| \hat{\boldsymbol{M}}(\boldsymbol{\eta})\boldsymbol{M}^{-1}(\boldsymbol{\eta}) - \boldsymbol{I} \right\| \|\dot{\boldsymbol{\tau}}_{\eta}\| \\
& + \left\| [(\hat{\boldsymbol{M}}(\boldsymbol{\eta})\boldsymbol{M}^{-1}(\boldsymbol{\eta}) - \boldsymbol{I})(\hat{\boldsymbol{C}}(\boldsymbol{\vartheta},\boldsymbol{\eta}) + \hat{\boldsymbol{D}}(\boldsymbol{\vartheta},\boldsymbol{\eta})) \right. \\
& \left. + \hat{\boldsymbol{M}}(\boldsymbol{\eta})\boldsymbol{M}^{-1}(\boldsymbol{\eta})(\tilde{\boldsymbol{C}}(\boldsymbol{\vartheta},\boldsymbol{\eta}) + \tilde{\boldsymbol{D}}(\boldsymbol{\vartheta},\boldsymbol{\eta}))]\hat{\boldsymbol{M}}^{-1}(\boldsymbol{\eta}) \right\| \|\boldsymbol{\tau}_{\rho\eta}\| \\
& + \left(\left\| \dot{\hat{\boldsymbol{M}}}(\boldsymbol{\eta})\boldsymbol{M}^{-1}(\boldsymbol{\eta}) + \hat{\boldsymbol{M}}(\boldsymbol{\eta})\dot{\overbrace{\boldsymbol{M}^{-1}(\boldsymbol{\eta})}} \right\| \right. \\
& + \left\| [(\hat{\boldsymbol{M}}(\boldsymbol{\eta})\boldsymbol{M}^{-1}(\boldsymbol{\eta}) - \boldsymbol{I})(\hat{\boldsymbol{C}}(\boldsymbol{\vartheta},\boldsymbol{\eta}) + \hat{\boldsymbol{D}}(\boldsymbol{\vartheta},\boldsymbol{\eta})) \right. \\
& \left. \left. + \hat{\boldsymbol{M}}(\boldsymbol{\eta})\boldsymbol{M}^{-1}(\boldsymbol{\eta})(\tilde{\boldsymbol{C}}(\boldsymbol{\vartheta},\boldsymbol{\eta}) + \tilde{\boldsymbol{D}}(\boldsymbol{\vartheta},\boldsymbol{\eta}))]\hat{\boldsymbol{M}}^{-1}(\boldsymbol{\eta}) \right\| \right) \\
& \times \left\| \hat{\boldsymbol{C}}(\boldsymbol{\vartheta},\boldsymbol{\eta})\dot{\boldsymbol{\eta}} + \hat{\boldsymbol{D}}(\boldsymbol{\vartheta},\boldsymbol{\eta})\dot{\boldsymbol{\eta}} + \hat{\boldsymbol{G}}(\boldsymbol{\eta}) \right\| \\
& + \left\| \dot{\hat{\boldsymbol{M}}}(\boldsymbol{\eta})\boldsymbol{M}^{-1}(\boldsymbol{\eta}) + \hat{\boldsymbol{M}}(\boldsymbol{\eta})\dot{\overbrace{\boldsymbol{M}^{-1}(\boldsymbol{\eta})}} \right\| \\
& \quad \times \left\| \tilde{\boldsymbol{C}}(\boldsymbol{\vartheta},\boldsymbol{\eta})\dot{\boldsymbol{\eta}} + \tilde{\boldsymbol{D}}(\boldsymbol{\vartheta},\boldsymbol{\eta})\dot{\boldsymbol{\eta}} + \tilde{\boldsymbol{G}}(\boldsymbol{\eta}) \right\| \\
& + \left\| \hat{\boldsymbol{M}}(\boldsymbol{\eta})\boldsymbol{M}^{-1}(\boldsymbol{\eta}) - \boldsymbol{I} \right\| \left\| \dot{\hat{\boldsymbol{C}}}(\boldsymbol{\vartheta},\boldsymbol{\eta})\dot{\boldsymbol{\eta}} + \dot{\hat{\boldsymbol{D}}}(\boldsymbol{\vartheta},\boldsymbol{\eta})\dot{\boldsymbol{\eta}} + \dot{\hat{\boldsymbol{G}}}(\boldsymbol{\eta}) \right\| \\
& + \left\| \hat{\boldsymbol{M}}(\boldsymbol{\eta})\boldsymbol{M}^{-1}(\boldsymbol{\eta}) \right\| \left\| \dot{\tilde{\boldsymbol{C}}}(\boldsymbol{\vartheta},\boldsymbol{\eta})\dot{\boldsymbol{\eta}} + \dot{\tilde{\boldsymbol{D}}}(\boldsymbol{\vartheta},\boldsymbol{\eta})\dot{\boldsymbol{\eta}} + \dot{\tilde{\boldsymbol{G}}}(\boldsymbol{\eta}) \right\| \\
& + \left\| \dot{\hat{\boldsymbol{M}}}(\boldsymbol{\eta})\boldsymbol{M}^{-1}(\boldsymbol{\eta}) + \hat{\boldsymbol{M}}(\boldsymbol{\eta})\dot{\overbrace{\boldsymbol{M}^{-1}(\boldsymbol{\eta})}} \right\| \\
& \quad \times \|\boldsymbol{\tau}_{d\eta}\| + \left\| \hat{\boldsymbol{M}}(\boldsymbol{\eta})\boldsymbol{M}^{-1}(\boldsymbol{\eta}) \right\| \|\dot{\boldsymbol{\tau}}_{d\eta}\| . \qquad \text{(B.4)}
\end{aligned}$$

According to (17), (18), Assumptions 1–4, and the knowledge of the AUV dynamics given in [33], we have the following inequalities:

$$\begin{aligned}
& \left\| \dot{\hat{\boldsymbol{M}}}(\boldsymbol{\eta})\boldsymbol{M}^{-1}(\boldsymbol{\eta}) + \hat{\boldsymbol{M}}(\boldsymbol{\eta})\dot{\overbrace{\boldsymbol{M}^{-1}(\boldsymbol{\eta})}} \right\| \\
& \quad = \left\| (\dot{\overbrace{\boldsymbol{J}^{-T}}}\hat{\boldsymbol{M}}\boldsymbol{J}^{-1} + \boldsymbol{J}^{-T}\hat{\boldsymbol{M}}\dot{\overbrace{\boldsymbol{J}^{-1}}})\boldsymbol{M}^{-1}(\boldsymbol{\eta}) \right. \\
& \qquad \left. + \hat{\boldsymbol{M}}(\boldsymbol{\eta})(\dot{\boldsymbol{J}}\boldsymbol{M}^{-1}\boldsymbol{J}^{T} + \boldsymbol{J}\boldsymbol{M}^{-1}\dot{\boldsymbol{J}}^{T}) \right\| \\
& \quad \leq l_1 \|\dot{\boldsymbol{\eta}}\| \\
& \left\| [(\hat{\boldsymbol{M}}(\boldsymbol{\eta})\boldsymbol{M}^{-1}(\boldsymbol{\eta}) - \boldsymbol{I})(\hat{\boldsymbol{C}}(\boldsymbol{\vartheta},\boldsymbol{\eta}) + \hat{\boldsymbol{D}}(\boldsymbol{\vartheta},\boldsymbol{\eta})) \right. \\
& \quad \left. + \hat{\boldsymbol{M}}(\boldsymbol{\eta})\boldsymbol{M}^{-1}(\boldsymbol{\eta})(\tilde{\boldsymbol{C}}(\boldsymbol{\vartheta},\boldsymbol{\eta}) + \tilde{\boldsymbol{D}}(\boldsymbol{\vartheta},\boldsymbol{\eta}))]\hat{\boldsymbol{M}}^{-1}(\boldsymbol{\eta}) \right\| \\
& \quad \leq l_2 + l_3 \|\boldsymbol{\vartheta}\| + l_4 \|\dot{\boldsymbol{\eta}}\| \\
& \left\| \dot{\hat{\boldsymbol{C}}}(\boldsymbol{\vartheta},\boldsymbol{\eta})\dot{\boldsymbol{\eta}} + \dot{\hat{\boldsymbol{D}}}(\boldsymbol{\vartheta},\boldsymbol{\eta})\dot{\boldsymbol{\eta}} + \dot{\hat{\boldsymbol{G}}}(\boldsymbol{\eta}) \right\| \\
& \quad = \left\| [\dot{\overbrace{\boldsymbol{J}^{-T}}}(\hat{\boldsymbol{C}}(\boldsymbol{\vartheta}) - \hat{\boldsymbol{M}}\boldsymbol{J}^{-1}\dot{\boldsymbol{J}})\boldsymbol{J}^{-1} + \boldsymbol{J}^{-T}(\dot{\hat{\boldsymbol{C}}}(\boldsymbol{\vartheta}) - \hat{\boldsymbol{M}}\dot{\overbrace{\boldsymbol{J}^{-1}}}\dot{\boldsymbol{J}} \right. \\
& \qquad - \hat{\boldsymbol{M}}\boldsymbol{J}^{-1}\ddot{\boldsymbol{J}})\boldsymbol{J}^{-1} + \boldsymbol{J}^{-T}(\hat{\boldsymbol{C}}(\boldsymbol{\vartheta}) - \hat{\boldsymbol{M}}\boldsymbol{J}^{-1}\dot{\boldsymbol{J}})\dot{\overbrace{\boldsymbol{J}^{-1}}}]\dot{\boldsymbol{\eta}} \\
& \qquad + (\dot{\overbrace{\boldsymbol{J}^{-T}}}\hat{\boldsymbol{D}}(\boldsymbol{\vartheta})\boldsymbol{J}^{-1} + \boldsymbol{J}^{-T}\dot{\hat{\boldsymbol{D}}}(\boldsymbol{\vartheta})\boldsymbol{J}^{-1} \\
& \qquad \left. + \boldsymbol{J}^{-T}\hat{\boldsymbol{D}}(\boldsymbol{\vartheta})\dot{\overbrace{\boldsymbol{J}^{-1}}})\dot{\boldsymbol{\eta}} + \dot{\overbrace{\boldsymbol{J}^{-T}}}\hat{\boldsymbol{g}}(\boldsymbol{\eta}) + \boldsymbol{J}^{-T}\dot{\hat{\boldsymbol{g}}}(\boldsymbol{\eta}) \right\| \\
& \quad \leq l_5 \|\dot{\boldsymbol{\eta}}\| + l_6\|\dot{\boldsymbol{\eta}}\|^2 + l_7 \|\boldsymbol{\vartheta}\| \|\dot{\boldsymbol{\eta}}\|^2 + l_8\|\dot{\boldsymbol{\eta}}\|^3 \\
& \left\| \dot{\tilde{\boldsymbol{C}}}(\boldsymbol{\vartheta},\boldsymbol{\eta})\dot{\boldsymbol{\eta}} + \dot{\tilde{\boldsymbol{D}}}(\boldsymbol{\vartheta},\boldsymbol{\eta})\dot{\boldsymbol{\eta}} + \dot{\tilde{\boldsymbol{G}}}(\boldsymbol{\eta}) \right\| \\
& \quad = \left\| [\dot{\overbrace{\boldsymbol{J}^{-T}}}(\tilde{\boldsymbol{C}}(\boldsymbol{\vartheta}) - \tilde{\boldsymbol{M}}\boldsymbol{J}^{-1}\dot{\boldsymbol{J}})\boldsymbol{J}^{-1} + \boldsymbol{J}^{-T}(\dot{\tilde{\boldsymbol{C}}}(\boldsymbol{\vartheta}) - \tilde{\boldsymbol{M}}\dot{\overbrace{\boldsymbol{J}^{-1}}}\dot{\boldsymbol{J}} \right. \\
& \qquad - \tilde{\boldsymbol{M}}\boldsymbol{J}^{-1}\ddot{\boldsymbol{J}})\boldsymbol{J}^{-1} + \boldsymbol{J}^{-T}(\tilde{\boldsymbol{C}}(\boldsymbol{\vartheta}) - \tilde{\boldsymbol{M}}\boldsymbol{J}^{-1}\dot{\boldsymbol{J}})\dot{\overbrace{\boldsymbol{J}^{-1}}}]\dot{\boldsymbol{\eta}} \\
& \qquad + (\dot{\overbrace{\boldsymbol{J}^{-T}}}\tilde{\boldsymbol{D}}(\boldsymbol{\vartheta})\boldsymbol{J}^{-1} + \boldsymbol{J}^{-T}\dot{\tilde{\boldsymbol{D}}}(\boldsymbol{\vartheta})\boldsymbol{J}^{-1} + \boldsymbol{J}^{-T}\tilde{\boldsymbol{D}}(\boldsymbol{\vartheta})\dot{\overbrace{\boldsymbol{J}^{-1}}})\dot{\boldsymbol{\eta}} \\
& \qquad \left. + \dot{\overbrace{\boldsymbol{J}^{-T}}}\tilde{\boldsymbol{g}}(\boldsymbol{\eta}) + \boldsymbol{J}^{-T}\dot{\tilde{\boldsymbol{g}}}(\boldsymbol{\eta}) \right\| \\
& \quad \leq l_9 \|\dot{\boldsymbol{\eta}}\| + l_{10}\|\dot{\boldsymbol{\eta}}\|^2 + l_{11} \|\boldsymbol{\vartheta}\| \|\dot{\boldsymbol{\eta}}\|^2 + l_{12}\|\dot{\boldsymbol{\eta}}\|^3 \\
& \|\dot{\boldsymbol{\tau}}_{d\eta}\| = \left\| \dot{\overbrace{\boldsymbol{J}^{-T}}}\boldsymbol{\tau}_{d\vartheta} + \boldsymbol{J}^{-T}\dot{\boldsymbol{\tau}}_{d\vartheta} \right\| \leq \left\| \dot{\overbrace{\boldsymbol{J}^{-T}}} \right\| \|\boldsymbol{\tau}_{d\vartheta}\| \\
& \qquad + \left\| \boldsymbol{J}^{-T} \right\| \|\dot{\boldsymbol{\tau}}_{d\vartheta}\| \leq \bar{J}_1\alpha_1 + \bar{J}_2\alpha_0 \|\dot{\boldsymbol{\eta}}\| \qquad \text{(B.5)}
\end{aligned}$$

where l_i ($i = 1, \ldots, 12$) are unknown positive constants, $\bar{J}_1$, $\bar{J}_2$ call back Assumption 1, and α_0, α_1 call back Assumption 3.

If the thrust saturation effect is not serious, the control input $\boldsymbol{\tau}_{\vartheta}$ and its derivative $\dot{\boldsymbol{\tau}}_{\vartheta}$ can be bounded by known positive constants. As a result, $\boldsymbol{\tau}_{\eta}$ can be bounded such that $\|\boldsymbol{\tau}_{\eta}\| = \|\boldsymbol{J}^{-T}\boldsymbol{\tau}_{\vartheta}\| \leq c_{11}$, where c_{11} is defined in Appendix A and $\dot{\boldsymbol{\tau}}_{\eta}$ can be bounded such that $\|\dot{\boldsymbol{\tau}}_{\eta}\| = \|\dot{\overbrace{\boldsymbol{J}^{-T}}}\boldsymbol{\tau}_{\vartheta} + \boldsymbol{J}^{-T}\dot{\boldsymbol{\tau}}_{\vartheta}\| \leq l_{13} + l_{14}\|\dot{\boldsymbol{\eta}}\|$, where l_{13} and l_{14} are known positive constants. Then using (A.5), (B.5), Assumption 5, $\|\boldsymbol{\tau}_{\eta}\| \leq c_{11}$, and

$\|\dot{\boldsymbol{\tau}}_\eta\| \le l_{13} + l_{14}\|\dot{\boldsymbol{\eta}}\|$ in (B.4), we get

$$\begin{aligned}\|\dot{\boldsymbol{\tau}}_{\rho\eta}\| \le\ & (l_2c_{11} + c_1l_{13} + l_2\beta_0 + l_2c_3 + c_2\bar{J}_1\alpha_1) \\ & + (l_3c_{11} + l_3\beta_0 + l_3c_3)\,\|\boldsymbol{\vartheta}\| \\ & + [c_{11}(l_1 + l_4) + c_1l_{14} + l_2\beta_1 + l_4\beta_0 \\ & \quad + l_2c_4 + c_3(l_1 + l_4) \\ & \quad + l_1c_7 + c_1l_5 + c_2l_9 + l_1\bar{J}_1\alpha_0 + c_2\bar{J}_2\alpha_0]\,\|\dot{\boldsymbol{\eta}}\| \\ & + (l_2\beta_2 + l_3\beta_1 + l_2c_5 + l_3c_4)\,\|\boldsymbol{\vartheta}\|\,\|\dot{\boldsymbol{\eta}}\| \\ & + (l_3\beta_2 + l_3c_5)\|\boldsymbol{\vartheta}\|^2\,\|\dot{\boldsymbol{\eta}}\| \\ & + [l_2\beta_3 + l_4\beta_1 + l_2c_6 + c_4(l_1 + l_4) + l_1c_8 \\ & \quad + c_1l_6 + c_2l_{10}]\|\dot{\boldsymbol{\eta}}\|^2 \\ & + [l_3\beta_3 + l_4\beta_2 + l_3c_6 + c_5(l_1 + l_4) \\ & \quad + l_1c_9 + c_1l_7 + c_2l_{11}]\,\|\boldsymbol{\vartheta}\|\,\|\dot{\boldsymbol{\eta}}\|^2 \\ & + [l_4\beta_3 + c_6(l_1 + l_4) + l_1c_{10} + c_1l_8 + c_2l_{12}]\|\dot{\boldsymbol{\eta}}\|^3. \end{aligned} \tag{B.6}$$

From (17) and Assumptions 1 and 2, $\hat{\boldsymbol{M}}^{-1}(\boldsymbol{\eta})$ can be bounded such that $\|\hat{\boldsymbol{M}}^{-1}(\boldsymbol{\eta})\| \le l_{15}$, where l_{15} is a known positive constant. Therefore, from the above analysis, we can obtain that

$$\begin{aligned}\|\boldsymbol{\tau}_{F\eta}\| =\ & \left\| (\dot{\hat{\boldsymbol{M}}^{-1}}(\boldsymbol{\eta}) + \boldsymbol{K}_1\hat{\boldsymbol{M}}^{-1}(\boldsymbol{\eta}))\boldsymbol{\tau}_{\rho\eta} + \hat{\boldsymbol{M}}^{-1}(\boldsymbol{\eta})\dot{\boldsymbol{\tau}}_{\rho\eta} \right\| \\ \le\ & \left\| \dot{\hat{\boldsymbol{M}}^{-1}}(\boldsymbol{\eta}) + \boldsymbol{K}_1\hat{\boldsymbol{M}}^{-1}(\boldsymbol{\eta}) \right\| \\ & \times \|\boldsymbol{\tau}_{\rho\eta}\| + \left\|\hat{\boldsymbol{M}}^{-1}(\boldsymbol{\eta})\right\|\|\dot{\boldsymbol{\tau}}_{\rho\eta}\| \\ \le\ & [l_{15}(l_2c_{11} + c_1l_{13} + l_2\beta_0 + l_2c_3 + c_2\bar{J}_1\alpha_1) + d_0\beta_0] \\ & + l_{15}(l_3c_{11} + l_3\beta_0 + l_3c_3)\,\|\boldsymbol{\vartheta}\| \\ & + \{l_{15}[c_{11}(l_1 + l_4) + c_1l_{14} + l_2\beta_1 \\ & \quad + l_4\beta_0 + l_2c_4 + c_3(l_1 + l_4) \\ & \quad + l_1c_7 + c_1l_5 + c_2l_9 + l_1\bar{J}_1\alpha_0 \\ & \quad + c_2\bar{J}_2\alpha_0] + d_0\beta_1 + d_1\beta_0\}\,\|\dot{\boldsymbol{\eta}}\| \\ & + [l_{15}(l_2\beta_2 + l_3\beta_1 + l_2c_5 + l_3c_4) + d_0\beta_2]\,\|\boldsymbol{\vartheta}\|\,\|\dot{\boldsymbol{\eta}}\| \\ & + l_{15}(l_3\beta_2 + l_3c_5)\|\boldsymbol{\vartheta}\|^2\,\|\dot{\boldsymbol{\eta}}\| \\ & + \{l_{15}[l_2\beta_3 + l_4\beta_1 + l_2c_6 + c_4(l_1 + l_4) + l_1c_8 \\ & \quad + c_1l_6 + c_2l_{10}] + d_0\beta_3 + d_1\beta_1\}\|\dot{\boldsymbol{\eta}}\|^2 \\ & + \{l_{15}[l_3\beta_3 + l_4\beta_2 + l_3c_6 + c_5(l_1 + l_4) \\ & \quad + l_1c_9 + c_1l_7 + c_2l_{11}] + d_1\beta_2\}\,\|\boldsymbol{\vartheta}\|\,\|\dot{\boldsymbol{\eta}}\|^2 \\ & + \{l_{15}[l_4\beta_3 + c_6(l_1 + l_4) + l_1c_{10} \\ & \quad + c_1l_8 + c_2l_{12}] + d_1\beta_3\}\|\dot{\boldsymbol{\eta}}\|^3. \end{aligned} \tag{B.7}$$

Thus, let $\lambda_0 = l_{15}(l_2c_{11} + c_1l_{13} + l_2\beta_0 + l_2c_3 + c_2\bar{J}_1\alpha_1) + d_0\beta_0$, $\lambda_1 = l_{15}(l_3c_{11} + l_3\beta_0 + l_3c_3)$, $\lambda_2 = l_{15}[c_{11}(l_1 + l_4) + c_1l_{14} + l_2\beta_1 + l_4\beta_0 + l_2c_4 + c_3(l_1 + l_4) + l_1c_7 + c_1l_5 + c_2l_9 + l_1\bar{J}_1\alpha_0 + c_2\bar{J}_2\alpha_0] + d_0\beta_1 + d_1\beta_0$, $\lambda_3 = l_{15}(l_2\beta_2 + l_3\beta_1 + l_2c_5 + l_3c_4) + d_0\beta_2$, $\lambda_4 = l_{15}(l_3\beta_2 + l_3c_5)$, $\lambda_5 = l_{15}[l_2\beta_3 + l_4\beta_1 + l_2c_6 + c_4(l_1 + l_4) + l_1c_8 + c_1l_6 + c_2l_{10}] + d_0\beta_3 + d_1\beta_1$, $\lambda_6 = l_{15}[l_3\beta_3 + l_4\beta_2 + l_3c_6 + c_5(l_1 + l_4) + l_1c_9 + c_1l_7 + c_2l_{11}] + d_1\beta_2$, and $\lambda_7 = l_{15}[l_4\beta_3 + c_6(l_1 + l_4) + l_1c_{10} + c_1l_8 + c_2l_{12}] + d_1\beta_3$, then the inequality (31) given in Assumption 7 is satisfied.

REFERENCES

[1] J. Yuh, "Design and control of autonomous underwater robots: a survey," *Auton. Robots*, vol. 8, no. 1, pp. 7–24, Jan. 2000.

[2] L. Paull, S. Saeedi, M. Seto, and H. Li, "AUV navigation and localization: a review," *IEEE J. Ocean. Eng.*, vol. 39, no. 1, pp. 131–149, Jan. 2014.

[3] X. Xiang, L. Lapierre, and B. Jouvencel, "Smooth transition of AUV motion control: from fully actuated to under-actuated configuration," *Robot. Auton. Syst.*, vol. 67, pp. 14–22, May 2015.

[4] H. Li and W. Yan, "Model predictive stabilization of constrained underactuated autonomous underwater vehicles with guaranteed feasibility and stability," *IEEE/ASME Trans. Mechatronics*, vol. 22, no. 3, pp. 1185–1194, Jun. 2017.

[5] S. Li, X. Wang, and L. Zhang, "Finite-time output feedback tracking control for autonomous underwater vehicles," *IEEE J. Ocean. Eng.*, vol. 40, no. 3, pp. 727–751, Jul. 2015.

[6] M. Santhakumar and T. Asokan, "Power efficient dynamic station keeping control of a flat-fish type autonomous underwater vehicle through design modifications of thruster configuration," *Ocean Eng.*, vol. 58, pp. 11–21, Jan. 2013.

[7] Z. Yan, H. Yu, W. Zhang, B. Li, and J. Zhou, "Globally finite-time stable tracking control of underactuated UUVs," *Ocean Eng.*, vol. 107, pp. 132–146, Aug. 2015.

[8] J. Xu, M. Wang, and L. Qiao, "Dynamical sliding mode control for the trajectory tracking of underactuated unmanned underwater vehicles," *Ocean Eng.*, vol. 105, pp. 54–63, Jul. 2015.

[9] L. Qiao and W. Zhang, "Adaptive non-singular integral terminal sliding mode tracking control for autonomous underwater vehicles," *IET Control Theory Appl.*, vol. 11, no. 8, pp. 1293–1306, May 2017.

[10] V. I. Utkin, *Sliding Modes in Control and Optimization*. Berlin, Germany: Springer, 1992.

[11] F. Gao, C. Pan, and Y. Han, "Design and analysis of a new AUV's sliding control system based on dynamic boundary layer," *Chin. J. Mech. Eng.*, vol. 26, no. 1, pp. 35–45, Jan. 2013.

[12] M. Zhang and Z. Chu, "Adaptive sliding mode control based on local recurrent neural networks for underwater robot," *Ocean Eng.*, vol. 45, pp. 56–62, May 2012.

[13] M. Kim, H. Joe, J. Kim, and S. Yu, "Integral sliding mode controller for precise maneuvering of autonomous underwater vehicle in the presence of unknown environmental disturbances," *Int. J. Control*, vol. 88, no. 10, pp. 2055–2065, Oct. 2015.

[14] Y. Wang, M. Zhang, P. A. Wilson, and X. Liu, "Adaptive neural network-based backstepping fault tolerant control for underwater vehicles with thruster fault," *Ocean Eng.*, vol. 110, pp. 15–24, Dec. 2015.

[15] E. Zakeri, S. Farahat, S. A. Moezi, and A. Zare, "Robust sliding mode control of a mini unmanned underwater vehicle equipped with a new arrangement of water jet propulsions: Simulation and experimental study," *Appl. Ocean Res.*, vol. 59, pp. 521–542, Sep. 2016.

[16] R. Cui, X. Zhang, and D. Cui, "Adaptive sliding-mode attitude control for autonomous underwater vehicles with input nonlinearities," *Ocean Eng.*, vol. 123, pp. 45–54, Sep. 2016.

[17] L. Qiao and W. Zhang, "Double-loop chattering-free adaptive integral sliding mode control for underwater vehicles," in *Proc. MTS/IEEE OCEANS Conf.*, Shanghai, China, Apr. 10–13, 2016, pp. 1–6.

[18] M. Zak, "Terminal attractors for addressable memory in neural networks," *Phys. Lett. A*, vol. 133, no. 1–2, pp. 18–22, Oct. 1988.

[19] M. Zhihong and X. Yu, "Terminal sliding mode control of MIMO linear systems," *IEEE Trans. Circuits Syst. I, Fundam. Theory Appl.*, vol. 44, no. 11, pp. 1065–1070, Nov. 1997.

[20] M. Zhihong, A. P. Paplinski, and H. R. Wu, "A robust MIMO terminal sliding mode control scheme for rigid robotic manipulators," *IEEE Trans. Autom. Control*, vol. 39, no. 12, pp. 2464–2469, Dec. 1994.
[21] X. Yu and M. Zhihong, "Fast terminal sliding-mode control design for nonlinear dynamical systems," *IEEE Trans. Circuits Syst. I, Fundam. Theory Appl.*, vol. 49, no. 2, pp. 261–264, Feb. 2002.
[22] T. Elmokadem, M. Zribi, and K. Youcef-Toumi, "Terminal sliding mode control for the trajectory tracking of underactuated autonomous underwater vehicles," *Ocean Eng.*, vol. 129, pp. 613–625, Jan. 2017.
[23] Y. Feng, X. Yu, and M. Zhihong, "Non-singular terminal sliding mode control of rigid manipulators," *Automatica*, vol. 38, no. 12, pp. 2159–2167, Dec. 2002.
[24] S. Yu, X. Yu, B. Shirinzadeh, and M. Zhihong, "Continuous finite-time control for robotic manipulators with terminal sliding mode," *Automatica*, vol. 41, no. 11, pp. 1957–1964, Nov. 2005.
[25] Y. Wang, L. Gu, M. Gao, and K. Zhu, "Multivariable output feedback adaptive terminal sliding mode control for underwater vehicles," *Asian J. Control*, vol. 18, no. 1, pp. 247–265, Jan. 2016.
[26] M. Zhang, X. Liu, B. Yin, and W. Liu, "Adaptive terminal sliding mode based thruster fault tolerant control for underwater vehicle in time-varying ocean currents," *J. Franklin Inst.*, vol. 352, no. 11, pp. 4935–4961, Nov. 2015.
[27] A. Levant, "Sliding order and sliding accuracy in sliding mode control," *Int. J. Control*, vol. 58, no. 6, pp. 1247–1263, Dec. 1993.
[28] M. K. Khan and S. K. Spurgeon, "Robust MIMO water level control in interconnected twin-tanks using second order sliding mode control," *Control Eng. Pract.*, vol. 14, no. 4, pp. 375–386, Apr. 2006.
[29] Y. Feng, X. Han, Y. Wang, and X. Yu, "Second-order terminal sliding mode control of uncertain multivariable systems," *Int. J. Control*, vol. 80, no. 6, pp. 856–862, Jun. 2007.
[30] S. Mondal and C. Mahanta, "Adaptive second order terminal sliding mode controller for robotic manipulators," *J. Franklin Inst.*, vol. 351, no. 4, pp. 2356–2377, Apr. 2014.
[31] S. Li, K. Li, J. Wang, and F. Gao, "Nonsingular and fast terminal sliding mode control method," *Inf. Control*, vol. 38, no. 1, pp. 1–8, Feb. 2009.
[32] M. Abramowitz and I. A. Stegun, *Handbook of Mathematical Functions: With Formulas, Graphs, and Mathematical Tables*. New York, USA.: Dover, 1972.
[33] T. I. Fossen, *Handbook of Marine Craft Hydrodynamics and Motion Control*. New York, NY, USA: Wiley, 2011.
[34] N. Fischer, D. Hughes, P. Walters, E. M. Schwartz, and W. E. Dixon, "Nonlinear RISE-based control of an autonomous underwater vehicle," *IEEE Trans. Robot.*, vol. 30, no. 4, pp. 845–852, Aug. 2014.
[35] F. Plestan, Y. Shtessel, V. Bregeault, and A. Poznyak, "New methodologies for adaptive sliding mode control," *Int. J. Control*, vol. 83, no. 9, pp. 1907–1919, Sep. 2010.
[36] V. I. Utkin and A. S. Poznyak, "Adaptive sliding mode control with application to super-twist algorithm: equivalent control method," *Automatica*, vol. 49, no. 1, pp. 39–47, Jan. 2013.
[37] E. Omerdic and G. Roberts, "Thruster fault diagnosis and accommodation for open-frame underwater vehicles," *Control Eng. Pract.*, vol. 12, no. 12, pp. 1575–1598, Dec. 2004.
[38] T. K. Podder and N. Sarkar, "Fault-tolerant control of an autonomous underwater vehicle under thruster redundancy," *Robot. Auton. Syst.*, vol. 34, no. 1, pp. 39–52, Jan. 2001.
[39] B. Sun, D. Zhu, F. Ding, and S. X. Yang, "A novel tracking control approach for unmanned underwater vehicles based on bio-inspired neurodynamics," *J. Mar. Sci. Technol.*, vol. 18, no. 1, pp. 63–74, Mar. 2013.

Lei Qiao received the B.S. degree in automation and the M.Eng. degree in control engineering from the College of Automation, Harbin Engineering University, Harbin, China, in 2012 and 2014, respectively. He is currently working toward the Ph.D. degree in control science and engineering at the Department of Automation, Shanghai Jiao Tong University, Shanghai, China.

Since 2017, he has been a Visiting Research Scholar at the Department of Electrical and Computer Engineering, Ohio State University, Columbus, OH, USA. His research interests include sliding mode and adaptive control, robust control, machine learning, and their applications to marine vehicles and robots.

Weidong Zhang (M'99–SM'17) received the B.S. degree in measurement technology and instruments, the M.S. degree in applied electronic technology, and the Ph.D. degree in control theory and its application from Zhejiang University, Hangzhou, China, in 1990, 1993, and 1996, respectively.

He joined Shanghai Jiao Tong University, Shanghai, China, where he was a Postdoctoral Fellow, and in 1998 he became an Associate Professor, and since 1999, he has been a Full Professor. From 2003 to 2004, he was an Alexander von Humboldt Fellow with the University of Stuttgart, Stuttgart, Germany. In 2011, he became the Chair Professor with Shanghai Jiao Tong University. He is currently the Director of the Engineering Research Center of Marine Automation, Shanghai Municipal Education Commission, Shanghai, China, and the Deputy Dean of the Department of Automation, Shanghai Jiao Tong University. He has authored more than 300 refereed papers and a book, and holds 32 patents. His research interests include control theory and its applications in industry and ocean engineering.

Prof. Zhang was a recipient of the National Science Fund for Distinguished Young Scholars of China.